

INTRUDER DETECTION USING SEISMIC  
SENSOR NETWORK

By  
Gökhan Koç

Submitted to the Institute of Graduate Studies in  
Science and Engineering in partial fulfillment of  
the requirements for the degree of  
Master of Science  
in  
Electrical and Electronics Engineering

Yeditepe University  
2013



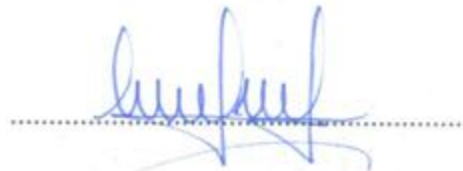
INTRUDER DETECTION USING SEISMIC  
SENSOR NETWORK

APPROVED BY:

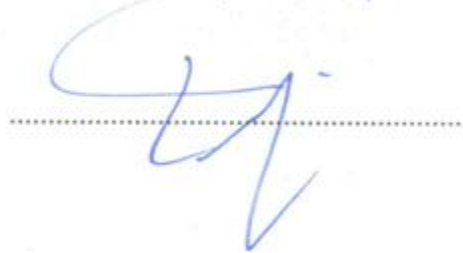
Assoc. Prof. Dr. Korkut Yeğin  
(Supervisor)



Assoc. Prof. Dr. Duygun E. Barkana



Assist. Prof. Dr. Engin Maşazade



DATE OF APPROVAL: .../.../...

*To my soul mate and to my family...*

## **ABSTRACT**

### **INTRUDER DETECTION USING SEISMIC SENSOR NETWORK**

A low-power seismic detector and classifier system with two different alarm transmitting method was designed and implemented which was able to detect footsteps of human and vehicle. One of these alarm transmitting methods called WCA (Wireless Communication Application) is a typical wireless sensor network application in which geophone sensor is used. The other one is called SAA (Stand-Alone Application) is an application in which alarms are transmitted with the change in power consumption. The features of these applications such as; alarm triggering, high-gain amplification, noise cancellation and power conversion are designed and manufactured on a single sensor board. After the productions of sensor board, varieties of data are collected from the fields to use in classify the intruders. A signal processing algorithm which is suitable for wireless sensor network theory is designed and the performance of the algorithm is measured.

## ÖZET

### SİSMİK SENSÖRLÜ AĞLARDAN FAYDALANARAK TEHDİT ALGILAMA

İnsan-araç algılaması ve sınıflandırması yapabilen, düşük güçlü tüketimine sahip sismik detektör ve sınıflandırma sistemi, iki farklı alarm iletme yöntemiyle tasarlanmıştır. Bu alarm iletme yöntemlerinden biri; içinde geophone sensörü kullanılan WCA isimli tipik bir kablosuz sensör ağı uygulamasıdır. Diğeri ise SAA olarak adlandırılan ve alarmların güç tüketimindeki değişimle iletildiği bir uygulamadır. Uygulamaların; alarm tetikleme, yüksek kazançlı kuvvetlendirme, gürültü filtreleme ve güç çevrimi gibi özellikleri, tek bir sensör kartı üzerinde konumlanacak şekilde tasarlanmıştır. Sensör kartın üretiminden sonra, sınıflandırma ile alakalı çalışmalarda kullanmak üzere, sahadan bol miktarda veri toplanmıştır. Ayrıca, kablosuz sensör ağı teorisine uygun bir sinyal işleme algoritması tasarlanıp bu algoritmanın performans ölçümleri yapılmıştır.

## TABLE OF CONTENTS

ABSTRACT .....	v
ÖZET .....	vi
TABLE OF CONTENTS .....	vii
LIST OF FIGURES .....	ix
LIST OF TABLES .....	xvi
1. INTRODUCTION .....	1
2. SENSOR BOARD REQUIREMENTS .....	6
2.1. AMPLIFICATION .....	6
2.2. FILTERING AND NOISE CANCELLATION .....	8
2.3. SENSOR .....	8
2.4. ALARM TRIGGERING BLOCK FOR SAA ARCHITECTURE .....	9
2.5. SYSTEM SPECIFICATIONS .....	9
3. HARDWARE DESIGN .....	11
3.1. SYSTEM ARCHITECTURE .....	11
3.1.1. SAA .....	12
3.1.2. WCA .....	13
3.2. SENSOR BOARD CIRCUIT AND SIMULATIONS .....	14
3.2.1. Filter-1 Analyses .....	17
3.2.2. Filter-2 Analyses .....	18
3.2.3. Filter-4 Analyses .....	20
3.2.4. Power Filter Analyses .....	22
3.2.5. Combined Analyses .....	23
3.2.6. Total Power Consumption .....	25
3.3. DETAILS OF SAA ARCHITECTURE .....	25
3.3.1. Normal Mode Current Consumption .....	26
3.3.2. Single Alarm Mode Current Consumption .....	30
3.3.3. Double Alarm Mode Current Consumption .....	32
3.4. PROTOTYPES .....	34
3.5. SENSOR BOARD AMPLIFICATION ANALYSES AFTER PRODUCTION.	40
3.6. GEOPHONE SENSOR EQUIVALENT CIRCUIT .....	44

4. WIRELESS COMMUNICATION UNIT .....	46
4.1. DESCRIPTION OF THE COMMUNICATION .....	46
4.2. HARDWARE .....	48
5. SIGNAL PROCESSING ALGORITHM .....	54
5.1. ALGORITHM .....	54
6. SYSTEM EVALUATION .....	60
6.1. PERFORMANCE OF SIGNAL PROCESSING ALGORITHM .....	60
6.1.1. Noise Performance of The Signal Processing Algorithm .....	60
6.1.2. Footstep Detection Performance of The Signal Processing Algorithm ...	61
6.1.3. Vehicle Detection Performance of The Signal Processing Algorithm .....	65
6.1.4. Rain Detection Performance of The Signal Processing Algorithm .....	69
6.1.5. Combined Detection Performance of Signal Processing Algorithm .....	73
6.2. PERFORMANCE OF STAND ALONE APPLICATION .....	75
6.3. MEASURES OF KURTOSIS EQUATION .....	77
7. PROBABILITY OF DETECTION AND FALSE ALARM .....	83
7.1. NOISE ANALYSES .....	85
7.2. FOOTSTEP ANALYSES .....	86
7.3. VEHICLE ANALYSES .....	95
7.4. VEHICLE AND FOOTSTEP COMBINED ANALYSES .....	98
7.5. QAT AND SAT ANALYSES .....	100
7.6. COMPARISON WITH SIMILAR PRODUCTS .....	107
8. CONCLUSION .....	109
8.1. FUTURE WORKS .....	109
REFERENCES .....	111



## LIST OF FIGURES

Figure 2.1. Footstep amplitude loss depending on different distance (3KGain).....	6
Figure 2.2. Ambient noise voltage with different gain values.....	7
Figure 3.1. System Illustration, a) WCA, b) SAA .....	11
Figure 3.2. Sensor Board block diagram .....	14
Figure 3.3. Sensor Board schematic .....	15
Figure 3.4. Filter-1 simulation circuit .....	17
Figure 3.5. Frequency and current analyses of Filter-1 .....	18
Figure 3.6. Filter-2 simulation circuit .....	19
Figure 3.7. Frequency and current analyses of Filter-2 (Forward) .....	19
Figure 3.8. Frequency and current analyses of Filter-2 (Reverse) .....	20
Figure 3.9. Filter-4 simulation circuit .....	21
Figure 3.10. Frequency and current analyses of Filter-3 (Forward) .....	21
Figure 3.11. Frequency and current analyses of Filter-4 (Reverse) .....	22
Figure 3.12. Power Filter simulation circuit .....	22
Figure 3.13. Frequency and current analyses of Power Filter .....	23

Figure 3.14. Gain analyses of complete Sensor Board at V (To_ADC) .....	24
Figure 3.15. Current consumption model of the sensor nodes system .....	26
Figure 3.16. RN_Min and RN_Max analyses of normal mode .....	27
Figure 3.17. Noise_Ratio analyses of normal mode .....	28
Figure 3.18. RT_Load analyses of normal mode .....	29
Figure 3.19. Total currents of sensor nodes at single alarm mode RA=200 .....	30
Figure 3.20. Total currents of sensor nodes at single alarm mode (RA=1000) .....	31
Figure 3.21. Total currents of sensor nodes at double alarm mode .....	33
Figure 3.22. Final node voltage of sensor nodes at double alarm mode .....	33
Figure 3.23. Screen capture of sensor board schemantic (Altium) .....	34
Figure 3.24. Screen capture of top view sensor board pcb (Altium) .....	35
Figure 3.25. Screen capture of bottom view sensor board pcb (Altium) .....	36
Figure 3.26. Top view of sensor board .....	37
Figure 3.27. Bottom view of sensor board .....	37
Figure 3.28. Sensor board and NodeRFV2.1 connected .....	38
Figure 3.29. Inside view of node box .....	38
Figure 3.30. Outside view of node box .....	39

Figure 3.31. SAA connection photo .....	39
Figure 3.32. Block diagram of amplification line .....	40
Figure 3.33. Amplifier-1 input stage .....	40
Figure 3.34. Amplifier-1 output stage .....	41
Figure 3.35. Amplifier-2 input stage .....	41
Figure 3.36. Amplifier-2 output stage .....	42
Figure 3.37. ADC input stage .....	42
Figure 3.38. Equivalent circuits at low frequencies .....	44
Figure 3.39. Equivalent circuits at high frequencies .....	45
Figure 4.1. Nodes communication paths .....	47
Figure 4.2. NodeRFV2.1 photos, a) Top view, b) Bottom view .....	48
Figure 5.1. Main parts of the signal processing algorithm .....	55
Figure 5.2. Signal processing algorithm flow chart .....	56
Figure 5.3. Definitions on signal duration sizes .....	57
Figure 6.1. Thresholds and original signal for noise only recording.....	60
Figure 6.2. Duration, filtered duration and alarm results due to noise.....	61
Figure 6.3. Physical test details.....	61

Figure 6.4. Original footstep signals with 3K gain (Test-1).....	62
Figure 6.5. QAT and SAT of original footstep signals with 3K gain (Test-1) .....	62
Figure 6.6. Duration, Filtered Duration and Alarm result of footstep signal (Test-1)..	62
Figure 6.7. Original footstep signals with 5.5K gain (Test-2) .....	63
Figure 6.8. QAT and SAT of original footstep signals with 5.5K gain (Test-2) .....	64
Figure 6.9. Duration, Filtered Duration and Alarm result of footstep signal (Test-2)..	64
Figure 6.10. Physical test details.....	65
Figure 6.11. Original vehicle vibration signal with 10 Km/h speed (Test-1) .....	66
Figure 6.12. QAT and SAT of original vehicle signals with 5K gain (Test-1).....	66
Figure 6.13. Duration, Filtered Duration and Alarm result of vehicle signal (Test-1) ...	67
Figure 6.14. Original vehicle vibration signal with 30 Km/h speed (Test-2) .....	67
Figure 6.15. QAT and SAT of original vehicle signals with 5K gain (Test-2) .....	68
Figure 6.16. Duration, Filtered Duration and Alarm result of vehicle signal (Test-2) ...	68
Figure 6.17. Original rain listening signal with 10K gain (Test-1) .....	69
Figure 6.18. QAT and SAT of rain listening signal with 10K gain (Test-1) .....	70
Figure 6.19. Duration, filtered duration and alarm result of rain listening signal .....	70
Figure 6.20. Original rain listening signal with 10K Gain (Test-2) .....	71

Figure 6.21. QAT and SAT of rain listening signal with 10K gain (Test-2) .....	71
Figure 6.22. Duration, Filtered Duration and Alarm result of rain listening signal .....	72
Figure 6.23. Classification results of combined test .....	74
Figure 6.24. Additional parallel resistor to R-Switch .....	75
Figure 6.25. Combined alarm test current graphic .....	76
Figure 6.26. Single alarm test current graphics .....	76
Figure 6.27. Kurtosis values of noise data with different interval sizes .....	78
Figure 6.28. Kurtosis values of footstep data with different interval sizes .....	79
Figure 6.29. Kurtosis values of vehicle data with different interval sizes .....	80
Figure 6.30. Kurtosis values of vehicle data with different interval sizes .....	81
Figure 7.1. Detection rate calculation criteria .....	84
Figure 7.2. Footstep test paths .....	86
Figure 7.3. True footstep detection rate with different gain values (Person A) .....	87
Figure 7.4. False footstep detection rate with different gain values (Person A) .....	88
Figure 7.5. Missed footstep detection rate with different gain values (Person A) .....	88
Figure 7.6. True footstep detection rate with different gain values (Person B) .....	89
Figure 7.7. False footstep detection rate with different gain values (Person B) .....	89

Figure 7.8. Missed footstep detection rate with different gain values (Person B) .....	90
Figure 7.9. True classification rates of footsteps with different gain values .....	93
Figure 7.10. False classification rates of footsteps with different gain values .....	93
Figure 7.11. Missed classification rates of footsteps with different gain values .....	94
Figure 7.12. Vehicle test paths .....	95
Figure 7.13. True classification rates of vehicle with different gain and range values ..	97
Figure 7.14. False classification rates of vehicle with different gain and range values..	97
Figure 7.15. Missed classification rates of vehicle with different gain values .....	97
Figure 7.16. Vehicle and footstep together test paths .....	98
Figure 7.17. True footstep detection rate with different QAT memory (Person B) .....	100
Figure 7.18. True footstep detection rate with different QAT memory (Person A) .....	101
Figure 7.19. False footstep detection rate with different QAT memory (Person B) .....	101
Figure 7.20. False footstep detection rate with different QAT memory (Person A) .....	102
Figure 7.21. Missed footstep detection rate with different QAT memory (Person B) ...	102
Figure 7.22. Missed footstep detection rate with different QAT memory (Person A) ...	103
Figure 7.23. True footstep detection rate with different SAT memory (Person B) .....	103
Figure 7.24. True footstep detection rate with different SAT memory (Person A) .....	104

Figure 7.25. False footstep detection rate with different SAT memory (Person B) ..... 104

Figure 7.26. False footstep detection rate with different SAT memory (Person A) ..... 105

Figure 7.27. Missed footstep detection rate with different SAT memory (Person B) .... 105

Figure 7.28. Missed footstep detection rate with different SAT memory (Person A) ... 106

Figure 7.29. Test area photos-1 ..... 106

Figure 7.30. Test area photos-2 ..... 107

## LIST OF TABLES

Table 2.1.	Geophone SM-24 technical specifications .....	8
Table 2.2.	WCA based system specifications .....	9
Table 2.3.	SAA based system specifications .....	10
Table 3.1.	Hardware blocks of the node.....	12
Table 3.2.	Hardware blocks of the gateway.....	12
Table 3.3.	Results of RN_Min and RN_Max analyses at normal mode.....	27
Table 3.4.	Results of Noise_Ration analyses at normal mode.....	28
Table 3.5.	Results of RT_Load analyses at normal mode.....	29
Table 3.6.	Results of Node_Number_At_System analyses at normal mode.....	29
Table 3.7.	Results of total currents of sensor nodes at S.A. mode RA=200.....	31
Table 3.8.	Results of total currents of sensor nodes at S.A. mode (RA=1000).....	32
Table 4.1.	NodeRFV2.1 Technical Specifications.....	49
Table 4.2.	MSP430F1611 technical specifications.....	50
Table 4.3.	ST M25P80 technical specifications.....	50
Table 4.4.	Output power configuration of CC2420.....	51



Table 4.5.	CC2420 technical specifications.....	51
Table 4.6.	CC2591 technical specifications.....	52
Table 4.7.	NodeRFV2.1 power specifications.....	53
Table 5.1.	Definitions of used constants in signal processing algorithm.....	59
Table 6.1.	Footstep detection tests performance.....	65
Table 6.2.	Vehicle detection tests performance .....	69
Table 6.3.	Rain Listening test performance .....	72
Table 6.4.	Combined signals test definations.....	73
Table 7.1.	General test properties .....	83
Table 7.2.	General detection performance criteria .....	83
Table 7.3.	General classification performance criteria .....	83
Table 7.4.	Noise performance of signal processing code in field .....	85
Table 7.5.	Footstep test pool .....	87
Table 7.6.	Classification performance criteria of footstep tests .....	91
Table 7.7.	Footstep classification results with 1k gain value .....	91
Table 7.8.	Footstep classification results with 2.5k gain value .....	91
Table 7.9.	Footstep classification results with 5k gain value .....	92

Table 7.10. Footstep classification results with 7.5k gain value .....	92
Table 7.11. Vehicle test pool .....	95
Table 7.12. Classification performance criteria of vehicle tests .....	96
Table 7.13. Vehicle classification results with different test parameters .....	96
Table 7.14. Vehicle and footstep together test pool .....	98
Table 7.15. Classification performance criteria of vehicle tests .....	99
Table 7.16. Vehicle and footstep together classification results .....	99
Table 7.17. Technical specifications of similar products .....	108

## 1. INTRODUCTION

Intruder detection is an important and mostly, integral part of any security system. In building and perimeter of the building are two essential components of such security systems. In building or immediate vicinity of the structure can be monitored with cameras or security personnel, but perimeter of the building, especially wide open area security systems require sensors for intruder detection. Those sensors can be of many different forms ranging from passive and/or active infrared, thermal, seismic, ultrasound, microphone to electromechanical film (EMFi). Visually obscured sensors are definitely desired, which makes seismic or acoustic sensors preferable over other sensors. In this study, we used seismic sensors to detect vibrations in the ground soil to identify and classify human, rain or vehicle presence in certain range of the sensor. Although seismic sensor based detection systems date back mid 1970's, recent advances in the wireless communication technologies and signal processing hardware enabled system performance to a much greater extent.

Human body produces radiation in the infrared range and that radiation could be detected by passive infrared (PIR) sensors. Also, these type of sensors could be used as an aid to another sensor [1]. Another widely used sensors are microphones. Walking loudly, talking and vehicle engines can generate different acoustic signals so that microphones can be used to detect these type of intrusions [2]. However , acoustic signals can be easily contaminated with wind sounds, human voices, or unexpected airplane engine sounds [3]. Seismic and PIR sensors, on the other hand, have relatively clean response. Ultrasonic sensors are also used for object detection in short distances with high performances [4, 5]. Another sensor type is electromechanical film (EMFi) sensor which is a thin, flexible, low price electret material that consists of cellular, biaxially oriented polypropylene film coated with metal electrodes [6]. Although EMFi offers good localization and tracking accuracy, they have the disadvantage of high constructional cost which limits its usage. To achieve higher detection performance, some sensors can be used together such as geophone-microphone, accelerometer-microphone, geophone-piezoelectric [3, 7, 8].

Human activities on the ground generate vibrations from the point of contact as seismic waves. Seventy percent of those seismic vibrations are transmitted by Rayleigh waves which spread on the surface of the world. The remaining part of that energy is moved by body waves which spreads perpendicular to the Rayleigh waves [9, 10]. In order to detect human and vehicles, Rayleigh waves can be very useful because of the transmission direction. Those vibrations also have frequency dependent attenuation characteristics [11]. Most part of footstep vibration energy is distributed in the band of 10 to 100 Hz [10]. Thus, filters for the amplification of the signal must be of low pass filter type. Ambient environment also plays a crucial role in footstep and vehicle detection. For example, because of the increased seismic noise levels, detection distances are lowered during daytimes [12]. The relationship between the noise level and footstep detection distance is examined in [13]. Another important parameter of the ambient environment is the vibration transmission filter of the ground. Vibration speed in the ground vary depending on the vibration frequency [14]. Footstep and vehicle vibration vary considerably according to these additional properties of environment and intruders [1]. According to [15, 16], some important parameters of detection are footstep size and speed, shoes of the intruder, seismic noise at the background, unwanted targets, presence of residential buildings, generators, guns, type of ground surface, air condition, geology and soil conditions. Geophone sensors have several advantages in detecting footsteps and vehicle vibrations such as being less sensitive to Doppler effects of the environment variations than acoustic sensors, ability to work with no power (passive) and higher detection ranges relative to other sensors [1, 3, 17].

In intruder detection systems, generally two types of geophone sensors are used: single-axis and three axis geophones. High bearing estimation error is usually the bottleneck of three-axis geophones [18] . Also path tracking and bearing estimations in critical areas is more difficult by three-axis geophones than triangulation of single-axis geophones because single-axis geophones sensitivity is divided along all other axis [18].

Wireless communication of sensors with gateway is the backbone of the wireless sensor systems. One of the most important aspect of wireless sensor networks (WSN) is its power management. For example, in [19], 7.5 Watt NI-PCI-6033E is used to detect footsteps with 16AH-5V battery which would work only for 2 days. Extending systems lifetime without

battery replacement is one of the targets of any WSN. Battery replacement can be very difficult when the system consists of thousands of nodes. Several research works in WSN focusing on power efficiency were reported in [20, 21]. In [22], Analog Devices Sharc DSP, which works under 0.1 W is used to analyse vibrations on ground. However, low power processor is very expensive (in excess 20 USD) which precludes its usage in a WSN application. In [19, 23, 24], NI Data Acquisition Boards were used without any wireless communication unit. In [25], wireless communication modules are used to transmit sensor data and alarm conditions to the control center.

Detection and classification of intruder type is also an integral part of these systems. The study of seismic vibrations has a rich history involving a variety techniques based on trial-and-error but, the majority of the seismic signal processing research focuses on earthquakes and well-logging [14]. One of the most accepted method of footstep and vehicle detection is "kurtosis" which measures extreme deviations from the mean signal [26]. Kurtosis is also used in other research works [17, 27, 28]. However, detecting intruder movements with kurtosis does not produce clear successful results because vibration of some noises could easily generate deviations similar to human steps [27]. One of the other popular intruder detection methods is based on "Copula" theory. Gaussian Copula, archimedean copulas, empirical copulas, montecarlo integration for copulas models are the main members of copula theory. Copulas are in essence full measures of statistical dependence among random variables [29]. However, understanding and quantifying dependence is a challenging task in multivariate statistical modeling. Copula is also used to detect footsteps and vehicle movements [23, 29, 30]. Markov Models are also used in detection of footsteps [19, 1].

The most popular footstep and vehicle detection method is analyzing spectrum of the intruder vibration signals. There is only two types of spectrum analyses methods exist for the intruder detection: narrow band and wide band spectrum analyses. Wide band spectrum analyses methods are focusing on a single footstep and vehicle vibration. However, vehicle and footstep vibrations may have frequency components at the same frequency. In several researches, this method has been used to detect intruder and classification [31, 26]. Narrow band spectrum analyses methods are focusing on a several footsteps and vehicle components [32, 33]. However, narrow and wide band spectrum analyses require FFT

algorithms. Because of the limited memory and power, FFT algorithm usage is not preferred in wireless sensor network devices. Although FFT may provide promising traffic detection, an alternate analog signal processing design is still necessary due to the required power to run FFT performing digital circuits. For a very-low power seismic sensor network, the power draw is a significant design constraint such that an analog system is not a preference but a requirement [24]. In addition, efficacy of these systems is often limited by high false alarm rates because the onboard data processing algorithms may not be able to correctly discriminate different types of targets (e.g., humans from animals) [34]. Power-efficient sensing modalities, low-power signal processing algorithms, and efficient methods for exchanging information between the sensor nodes are still needed [1, 35].

Signal filtering is also an important issue in intruder detection algorithms. Filtering can be done with analog circuits [16, 25] because of the limited memory and power. Wavelets, which are one of the famous digital noise reduction algorithms, have been used in [13, 27]. It was claimed in [13] that wavelet analysis of footstep seismic signal had a lot of advantages because of its un-stationary and random nature. Also digital band pass filters could be implemented in noise cancellation [35].

In our study, we utilized two different forms of intruder detection: one using wired communication through sensors and the other using wireless communication between the sensors and the terminal (gateway). In wired communication all sensors despite sensor itself is passive, the electronics requires electrical power) are fed through a common power line and current draw from the main power supply unit which is located at the gateway, is used to determine the location of sensor that provides the alarm. On the other hand, the system that utilizes wireless communication among sensors are standalone units and each unit has its own power supply (battery) to operate. All sensor boards are equipped with a wireless unit operating at 2.4 GHz to enable two-way (half duplex) communication between the sensor and the gateway unit. The advantages and disadvantages of these two configurations are detailed along with the signal processing algorithms employed for each configuration.

The sensor network generally consists of five different units: power supply, sensor, sensor driver circuit, control-communication circuit, antenna and signal processing algorithm. As

it is well known, seismic signals have very low amplitude voltage levels, thus one of the most important features of the sensor board design is high gain amplification without distorting the signal and adding electronic noise already noisy seismic electrical signal. Almost all electronic components are acting as a source of noise, and noise can be easily amplified in high gain stages. Therefore, second most important feature of sensor board is its noise cancellation and/or minimization ability. Due to the presence of wireless communication and battery supply, different type of filtering are needed. One of the other hardware blocks is the alarm transmitting circuit based on power consumption in wired-communication architecture of sensor nodes. Last and perhaps the most important feature of sensor board is its power consumption which must be under 1 mA with 3VDC supply. With that feature, system can operate more than two months with two AA size min 1500 mAh alkaline batteries. This feature is one of the most basic requirements for wireless products.

In seismic detection systems, most widely used seismic sensor is the geophone due to its sensitivity and accuracy as a passive sensor. Although it is bulky, it's been number one choice for many human and foot-step detection systems. CMOS based small sensors are also available but their response range is very limited and require much larger vibrations to produce electrically meaningful signals

Detection also requires signal processing algorithm where human and vehicle classification can be done. Signal processing algorithm is only used on the data obtained by the wireless sensor network. The algorithm is designed to eliminate the effects of soil type, environment changes and ambient noise. Design details of the algorithm are explained in Chapter 5. In addition, typical scenarios for all types of threats are analyzed for performance evaluation which are presented in Chapter 6.

## 2. SENSOR BOARD REQUIREMENTS

Two different power structures are used for two different applications; in wireless sensor architecture (WSA) where sensors are supplied with their batteries, and the other is stand alone architecture (SAA) where sensors are connected in parallel to a power cable that has 12 VDC.

### 2.1. AMPLIFICATION

Geophone sensor generates ultra-low amplitude response (in micro volts) for human steps and vehicle movements. For signal processing hardware, the amplitude of geophone sensor signal should be amplified with a gain in the order of 1000. Low-level amplifications require high resolution ADC and low electronics induced added-noise levels. In this application, resolution of ADC and added noise play key roles in the selection of amplification gain which is chosen as 1000.

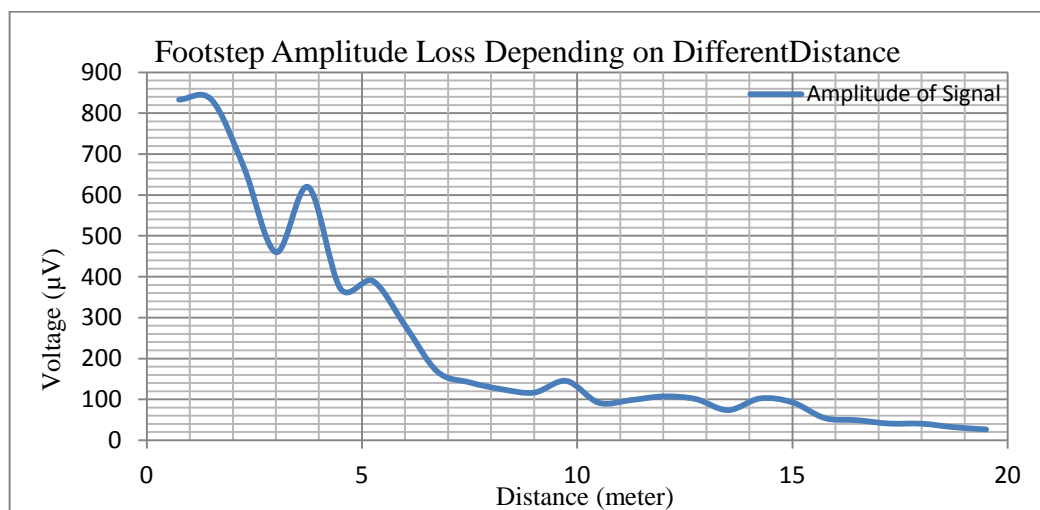


Figure 2.1. Footstep amplitude loss depending on different distance (normalized after 3K Gain)

To determine the exact amplitudes that geophone responds to a footstep, a footstep test is done and data are collected. The results are shown in the Figure 2.1. The amplitude of a



footstep signal, as shown in the Figure 2.1., can be as low as  $30\mu\text{V}$  at 15-20 meter distance. In addition, maximum reference voltage of 12-bit ADC (TI-MSP430F1611) is 2.5 V so the resolution of the ADC is  $610\mu\text{V}$ . The difference between the signal and noise must be as large as possible so that the highest possible number of bits of ADC can be used for better results in signal processing. By just considering this aspect would be erroneous as ambient noise plays a critical role.

Ambient noise level is changing with the gain value because of the added noise in the amplifier electronics. Figure 2.2. shows that the ambient noise voltage is increasing with the gain while minimizing the signal amplitude range. Different gain values than 1K is also used in this study for representation purposes but, 1K is the ultimate gain value as it's been found the most suitable value. Also the presence of natural noise on the ground and noisy environments gives rise to increased noise level higher gain values are used.

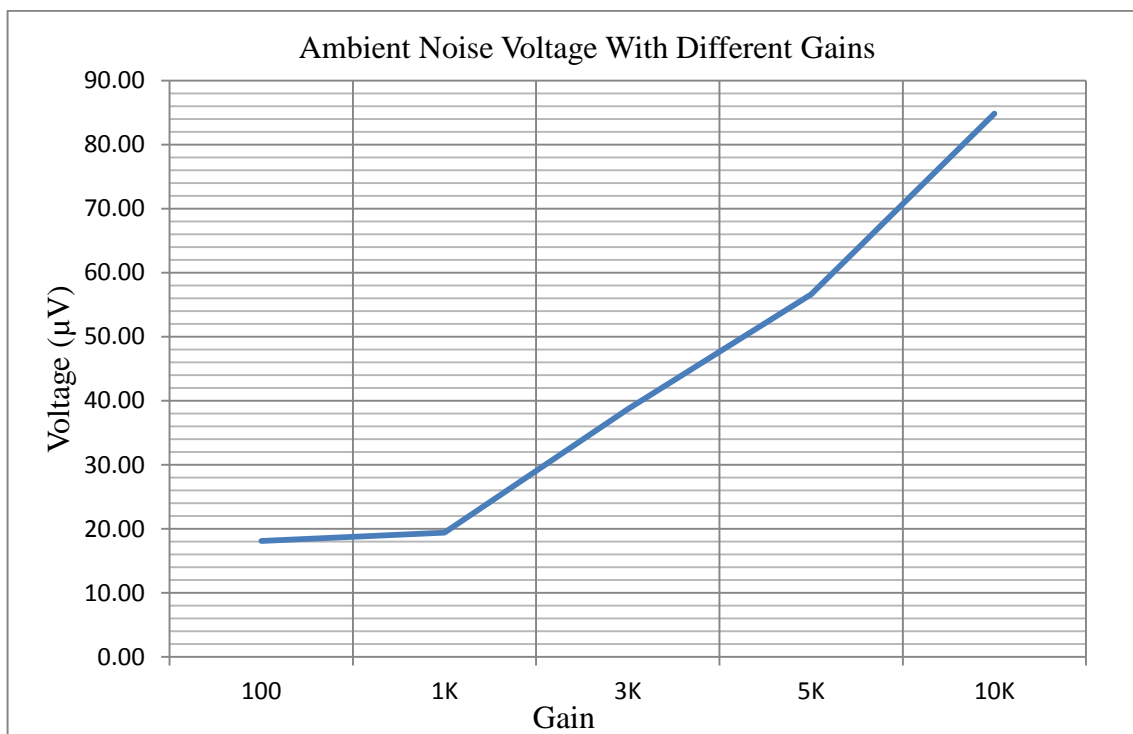


Figure 2.2. Ambient noise voltage with different gain values

Cascade amplifiers with two Op-Amps are used to reduce wireless communication induced noise. With single Op-Amp, 1000 gain requires high resistor values (feedback gain

proportional to  $1 + R_1/R_2$ ) like  $R_1=100 \text{ KOhm}$  and  $R_2=1 \text{ KOhm}$ . By using 2 Op-Amps in a cascade topology, gain is shared between the two Op-Amps and same gain level is reached by lower resistor values such as  $R_1=33\text{K}$ ,  $R_2=1\text{K}$ . Lower resistance values may lead to higher power consumption but, the ability of noise rejection increases. Proper choice of current resistance values is important for power consumption and noise rejection.

## 2.2. FILTERING AND NOISE CANCELLATION

Geophone sensor generates low frequency signal responses on human steps and vehicle movements which do not necessitate the use of high frequency Op-Amps. Geophone sensor generates low frequency signals between 10-200 Hz. In addition, the main noise source will be the 2.4 GHz RF communication. Therefore, filters should be low pass filters with low cut-off frequency. RF based noises could affect the amplifier at any point on the circuit. Therefore, filters should be placed before and after the amplifiers and buffers. Because the amplifiers are of feedback type, noises at the output of the op-amps are amplified, therefore T type filters should be chosen. Passive filters components should be chosen according to Op-Amp input and output resistance. In addition, power consumption of these filters should be minimized by choosing higher resistance values as possible. Buffer circuits are required before the ADC.

## 2.3. SENSOR

Geophone sensor SM-24 is used as the sensor in this study. Technical specifications of this device is shown in Table 2.1.

Table 2.1. Geophone SM-24 technical specifications [37]

<b>Frequency</b>	<b>Values</b>
Natural frequency	10 Hz
Tolerance	$\pm 2.5\%$
Maximum tilt angle for specified Fn	$10^\circ$
Typical spurious frequency	$>240 \text{ Hz}$
<b>Distortion</b>	<b>Values</b>
Distortion measurement frequency	12 Hz

Table 2.1. Geophone SM-24 technical specifications (Continue)

<b>Damping</b>	<b>Values</b>
Open circuit (typical)	0.25
Damping calibration - shunt resistance	1.339 Ohm
Tolerance with calibration shunt	5%
<b>Sensitivity</b>	<b>Values</b>
Sensitivity	28.8 V/m/s (0.73 V/in/s)
Tolerance	± 2.5 %

#### **2.4. ALARM TRIGGERING BLOCK FOR STAND-ALONE ARCHITECTURE**

To implement alarm situations with change in power consumption, a triggering circuit which shorts the 12VDC to ground with a serial resistance is required. Along the 12 VDC power line, voltage will decrease because of the nodes' power consumptions. This circuit block should detect alarms with a comparator that compares signal with a threshold voltage which could be implemented with voltage divider. According to this comparison, a digital switch can be activated and shorts the power line to ground with a specific resistance value. By this way, power consumption will be changed when the seismic signal is over the threshold. To implement these functions, the bouncing on the common power line should be as low as possible. In stand-alone architecture, none of the digital signal processing functions are executed.

#### **2.5. SYSTEM SPECIFICATIONS**

Required system level specifications are shown in Tables 2.2 and 2.3.

Table 2.2. WCA based system specifications

Power Source for the node	3VDC Battery with min 1500 mAh
Current draw on the geophone sensor circuit	< 500 $\mu$ A
Current draw on the wireless unit (average)	< 5 mA
False Alarm Rate	< 5 %

Table 2.2. WCA based system specifications (Continue)

Detection Rate	> 99 %
Classification Rate	> 90 %
Detection Range	> 6 m

Table 2.3 SAA based system specifications

Power Source for the node	12VDC Line external
Current draw on the geophone sensor circuit	< 500 $\mu$ A
Current draw in the presence of alarm (single node)	< 20 mA
Current draw in the absence of alarm (single node)	< 10 mA
False Alarm Rate	< 5 %
Detection Rate	> 99 %
Classification Rate	> 90 %
Detection Range	> 6 m

### 3. HARDWARE DESIGN

#### 3.1. SYSTEM ARCHITECTURES

The design that is realized in this study can accommodate hardware configuration in two different working modes. The working modes are described as Wireless Communication Architecture (WCA) and Stand Alone Architecture (SAA). In WCS mode, seismic sensor data are transmitted using a wireless link at 2.4 GHz. In SAA mode, sensors are connected via power line and critical data were inferred from DC current pull of each sensor node. These are illustrated in Fig. 3.1. Hardware blocks in WCA and SAA are summarized in Table 3.1 and 3.2.

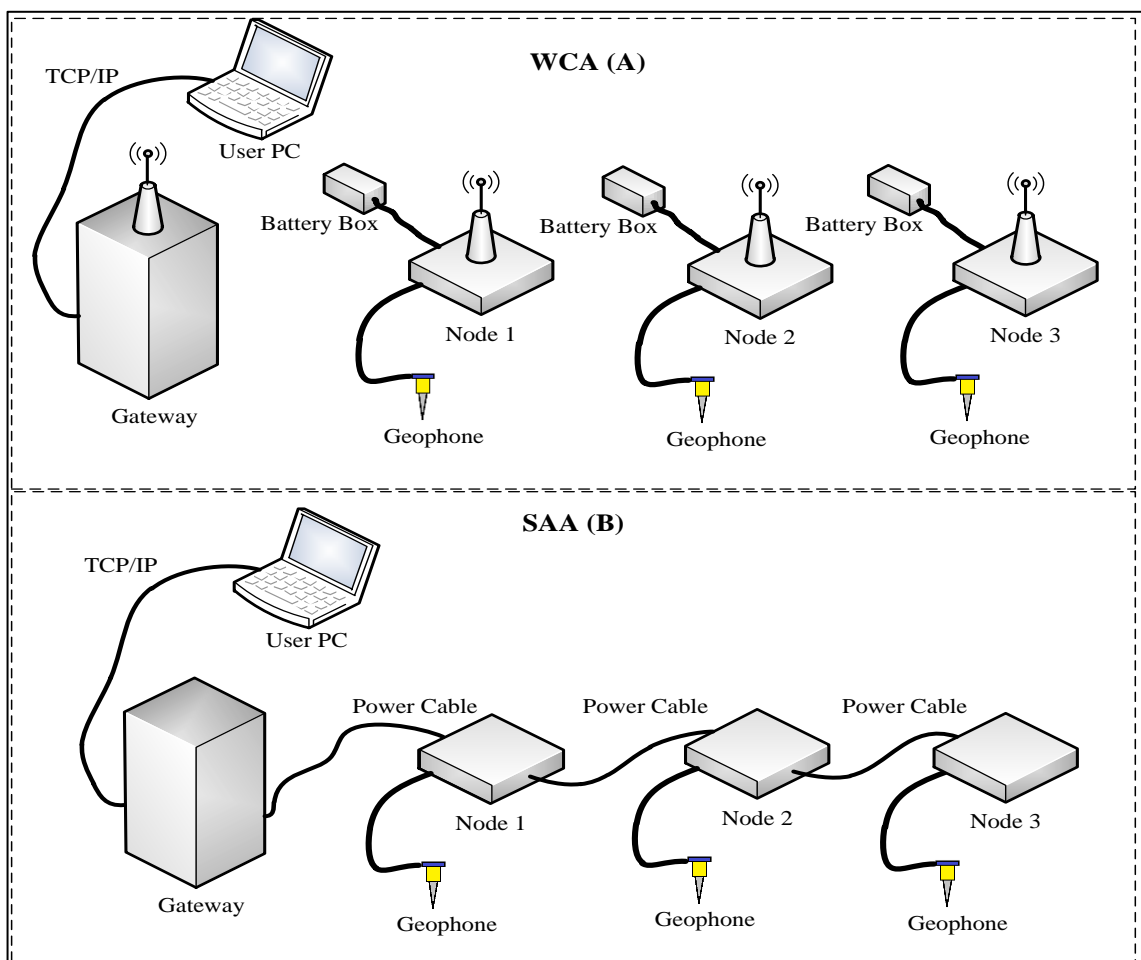


Figure 3.1. System illustration, a) WCA, b) SAA.

Table 3.1. Hardware blocks of the sensor node

Location	Hardware Block (Node)	Standalone Arch.	Wireless Communication Arch.
Sensor Board	Alarm Triggering	+	-
Sensor Board	Amplifier Block	+	+
Sensor Board	Power Converter	+	+
NodeRF	Antenna	-	+
NodeRF	RF Communicator	-	+
NodeRF	MCU	-	+
External	Battery Box	-	+
External	Seismic Sensor	+	+
External	Power Cable	-	-

Table 3.2. Hardware blocks of the gateway

Location	Hardware Block (Gateway)	Standalone Arch.	Wireless Communication Arch.
In Panel	Antenna	-	+
In Panel	RF Communicator	-	+
In Panel	MCU	+	+
In Panel	TCP/IP Communication	+	+
In Panel	Current Reader	+	-
In Panel	Power Supply	+	+

### 3.1.1. SAA

SAA is an architecture of one gateway and multiple sensor nodes. Sensor nodes include the sensor board and sensor itself. They are connected to each other through 12 V power line and the circuits are biased with this power. Alarm information is inferred from current pull from the power line, and notification of alarm is performed at the gateway. In SAA, there is no wireless communication and there is no extra cable for data communication. All sensor blocks are used, and all blocks in the gateway except the antenna and the RF communication block are active.

In SAA;

- There is no two-way communication.
- The signal processing is realized at the gateway.
- Gateway infers vibration durations through constant monitoring of current pull from sensor nodes and makes a decision on signaling an alarm.
- There is no need for a separate battery.
- Production cost is much smaller than WCA.
- In sensor nodes, there is no need for a microcontroller or communication protocols.

### **3.1.2. WCA**

WCA includes sensor nodes and one gateway but gateways can be increased depending on the coverage area of the wireless network. There are sensor board, sensor itself, Battery Box, NodeRF V2.1 and 2.4 GHz antenna in each sensor node. There is no cable to connect the sensor nodes. They need a Battery Box for power. They make an alarm decision at the node and send only alarm information to gateway via wireless communication. The signal processing is performed at the node and but signal processing parameters such as duration thresholds, threshold memory sizes, adjustable gain values at Op-Amps can be modified remotely through wireless communication link. The hardware blocks are shown in Table 3.1..

In the Wireless Communication Architecture;

- There is two-way communication so that the parameters of communication and signal processing can be controlled by remote access.
- The communication traffic is at minimum since signal processing is performed mostly at the gateway.
- Gateway only receives alarm information; the vibration signal is kept in the sensor nodes.
- There is no need for alarm trigger block which is used in SAA for current-pull monitoring..
- There is no need for 12 V supply cable or separate communication cable.

- All blocks are used in gateway except Current reader block.
- The production costs of WCA sensor nodes are much higher than those of SAA sensor nodes.
- Software development cost is higher due to wireless communication protocols and associated operating system.
- There is a unique ID for every product so that two products in overall system cannot be simply interchanged.

### 3.2. SENSOR BOARD CIRCUIT AND SIMULATIONS

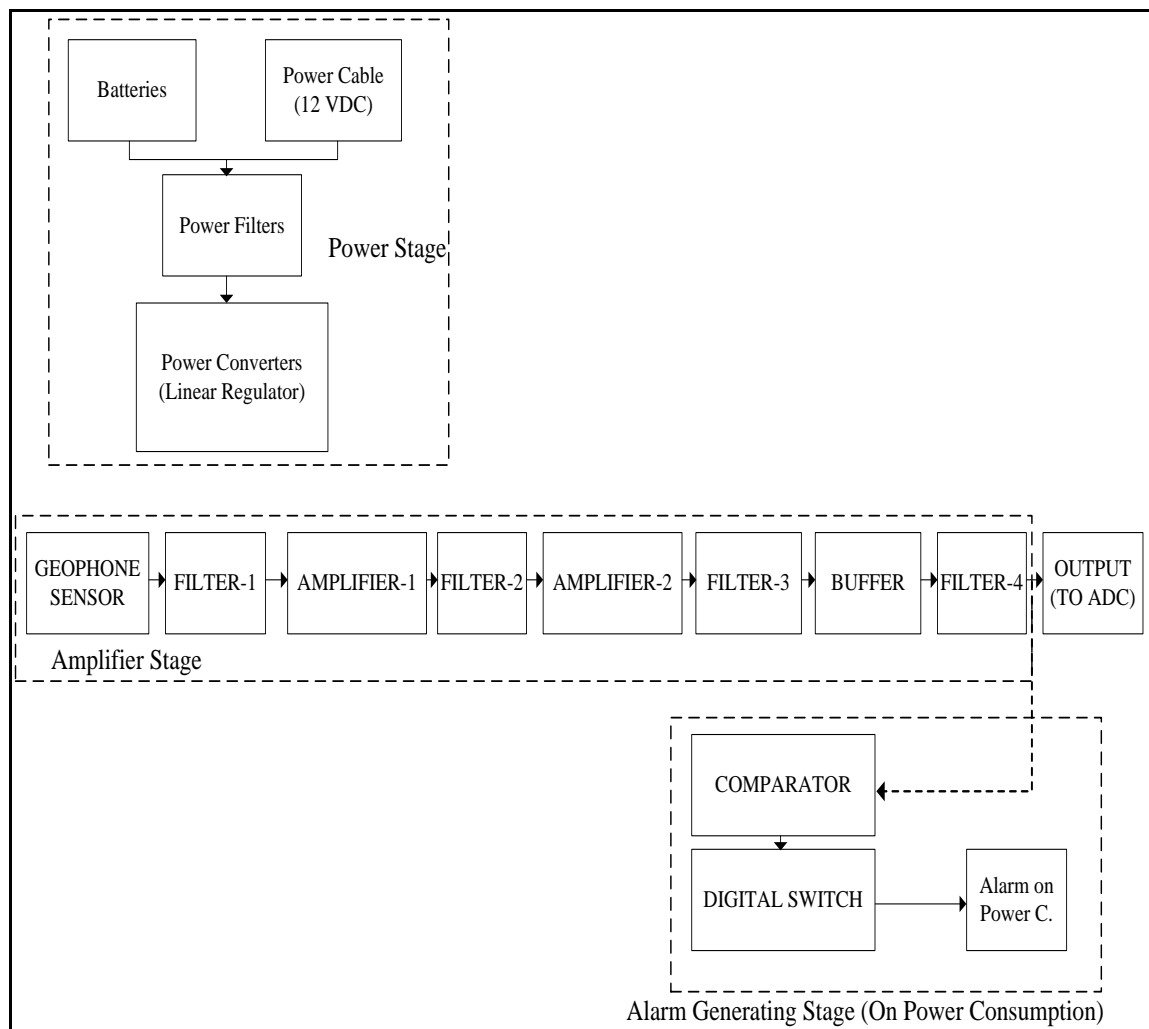


Figure 3.2. Sensor board block diagram



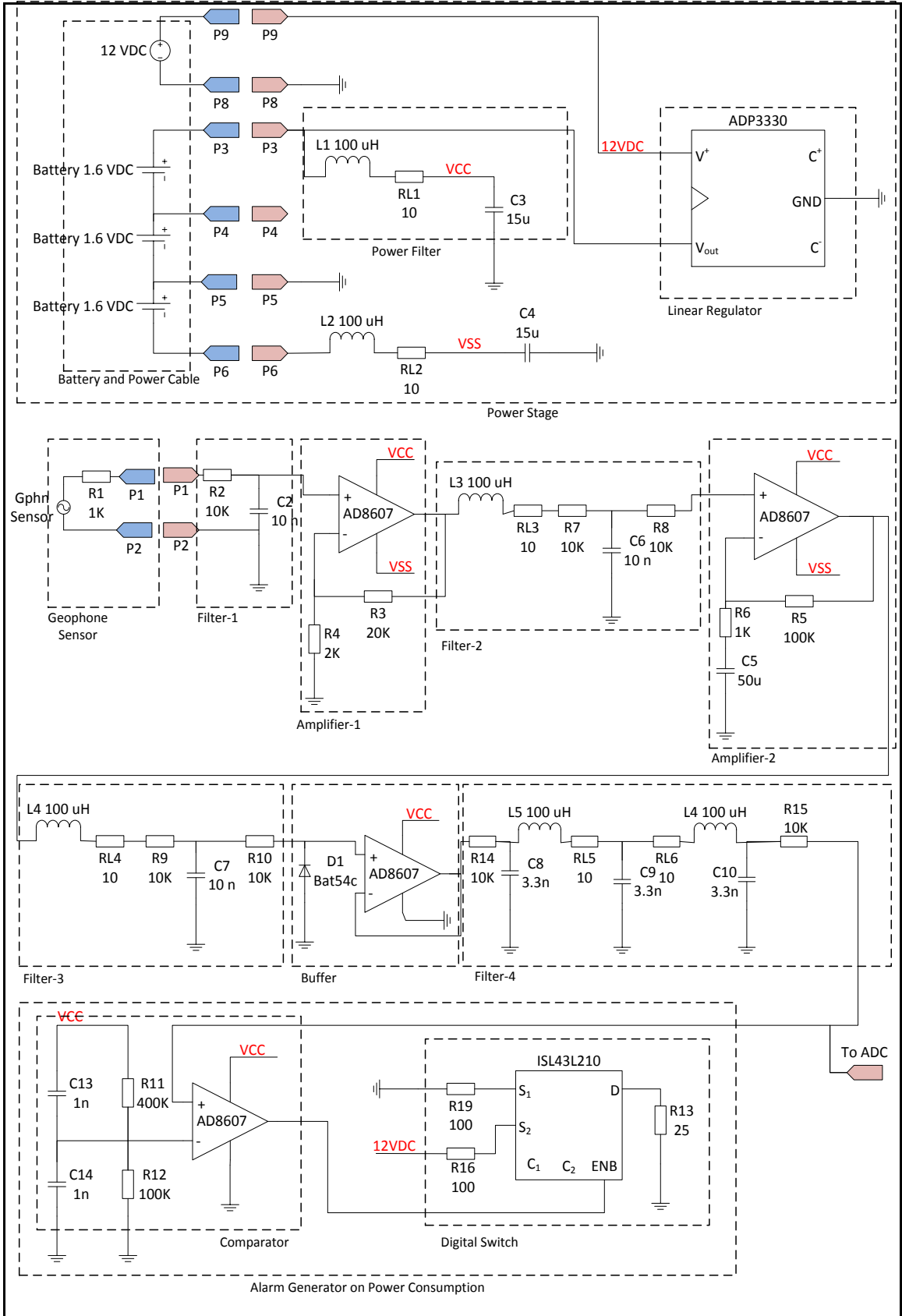


Figure 3.3. Sensor board schematic

As shown in Figure 3.2., first, the data obtained from the sensor is filtered with filter-1 and after this initial filtering, 10-gain amplification is operated on the seismic data. Two-stage amplification has the advantage that same total gain value can be obtained with low-value resistors. Thus, noise from resistors are decreased, and signal-noise ratio is increased with filters between amplifiers.

As shown in Figure 3.3., C5 capacitor removes unwanted offset value that may occur by the Op-Amps. Another important point of this design is its dual-supply compatibility with wireless unit, NodeRF. ADC input can be easily corrupted due to dual power supply and to prevent this, D1 diode is used before the buffer block. So, the negative side of the amplified seismic signal is not transmitted to ADC input. At the bottom of the Figure 3.3., alarm generator from power consumption circuit, which is triggered by the amplitude of the signal, is placed.

In high gain amplifier circuits, sometimes sensor signals leak to offset voltage which is generated by voltage reference integrated circuits or voltage dividers. If supply voltage has a DC bouncing or high frequency noises, all offsets would be affected. Because of this, signal from the sensor can be corrupted. Also this is not just a problem for signal processing, any digital or analog circuits could be affected by that DC voltage bouncing. However, it is not be so easy to eliminate DC bouncing on power lines which is generated by current consuming components.

Filters on signal line are used to eliminate high frequency noises, so clean signal processing can be done. According to SM-24 geophone sensor, signal frequencies from natural activities would be under 100 Hz. Also wireless communication in this work is implemented at 2.4 GHz. There is a huge frequency difference between signal and the wireless communication frequency. Elimination of high frequency noise is not difficult because there is large separation between the noise frequency and DC power.

As mentioned above, sharp filtering is not necessary for this application. However, considering other possible noise sources, cut-off frequencies should be selected as close as to sensor signal considering at least Nyquist sampling criteria. By looking at the frequencies, it is obvious that low pass filters must be used on signal lines. These passive

filters' component properties will be the most important parameter on power consumption. Filters should be used between the opamp circuit blocks so that they do not drive any load. Also high input impedance will reduce power consumption. However, higher filter input impedance will affect the total gain value indirectly.

As mentioned above, RFI and EMI kind of noise sources are not stable in the circuits. They can enter into system at any point. Also high gain amplifiers has feedback architecture, but feedback architecture will not only increase the desired signals, all input and output noises will be increased by these amplifiers.

Directional filters would be more appropriate but difficult to implement. T-type filters, which has same cut of frequencies in both directions of the signal line provide good isolation between input and output.

### 3.2.1. Filter-1 Analysis

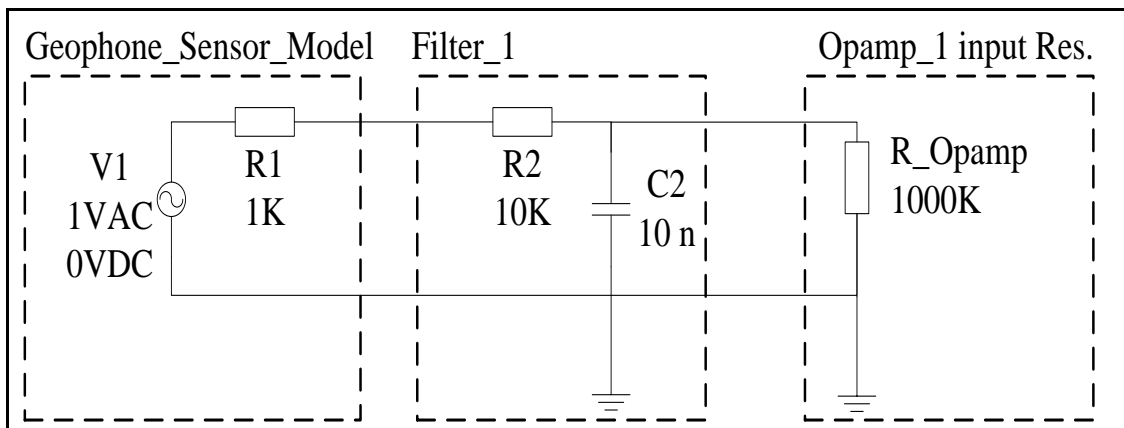


Figure 3.4. Filter-1 simulation circuit

Filter-1 operates only in the forward direction, because any noise transmitted from circuit to sensor is not amplified at that block. Filter-1 is connected directly to op-amp input and power consumption is not important. 1.5 KHz cut-off frequency is selected to support high-order FFT functions for possible future applications.

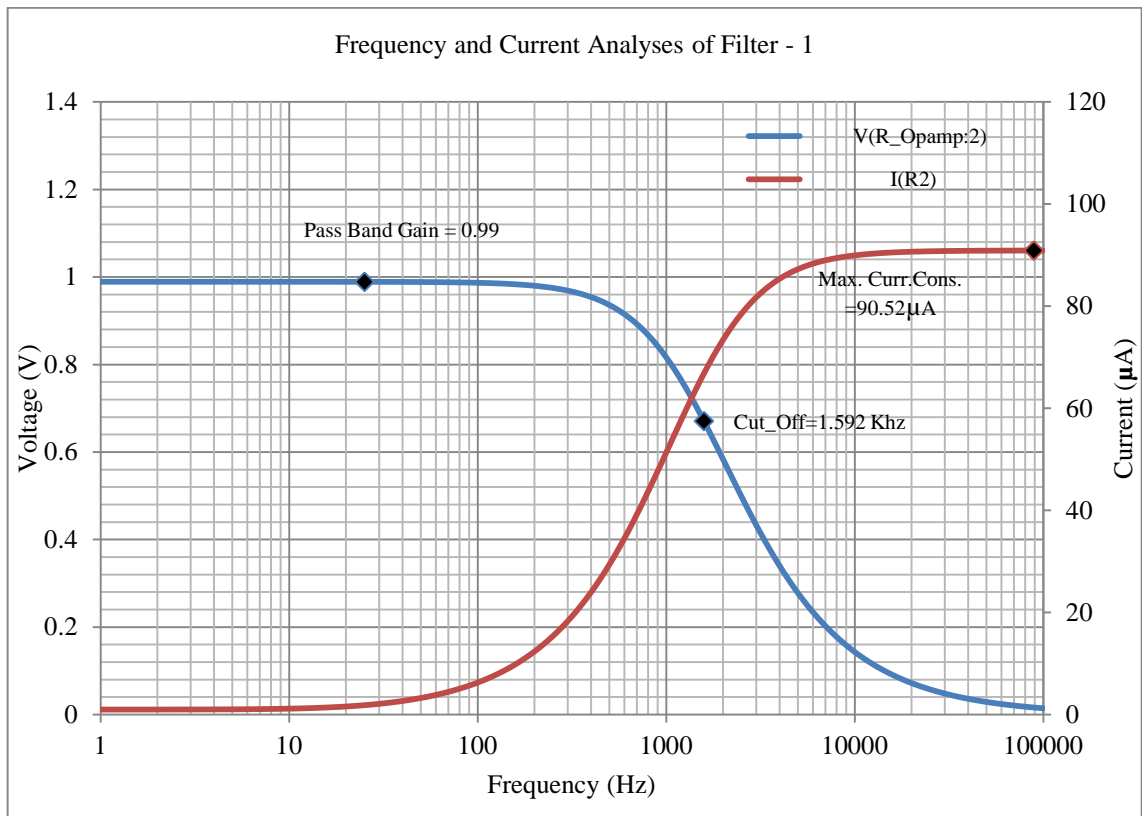


Figure 3.5. Frequency and current analyses of Filter-1

### 3.2.2. Filter-2 Analysis

Filter-2 and Filter-3 has the same circuit blocks so Filter-3 analyses will not presented. Filter-2 is a T-Type filter that is used in both directions to prevent noise amplification. As seen in Figure 3.6., forward filtering is supported with an inductor because of the amplification gains. As a result of that, forward cut-off frequency is better than reverse cut-off frequency.

Power consumption of filter-2 is important in forward mode because the power source of forward mode is the output of Amplifier-1. However, in reverse mode, power source can only be parasitic noise. Increasing R7 and R8 values reduces the pass band gain and reducing the R7 and R8 values increases filter's current consumption. The other relevant circuit blocks such as amplification resistances are included in the simulations.

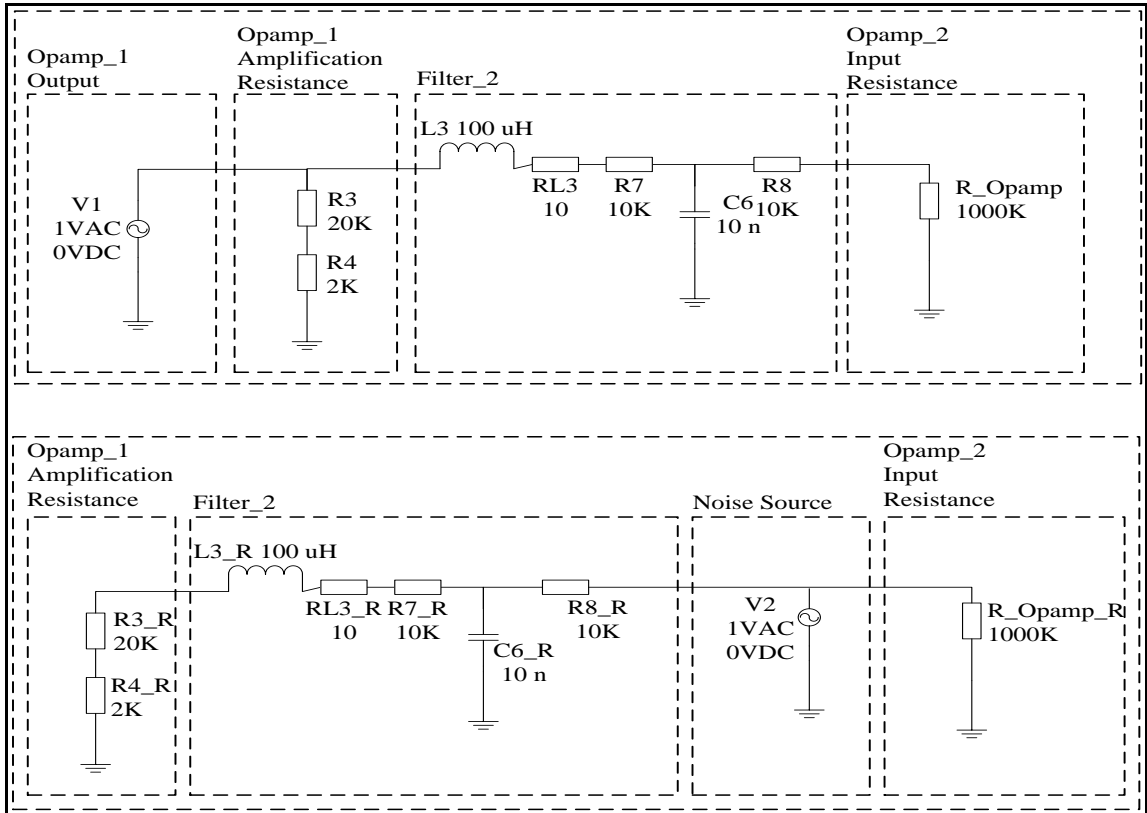


Figure 3.6. Filter-2 simulation circuit

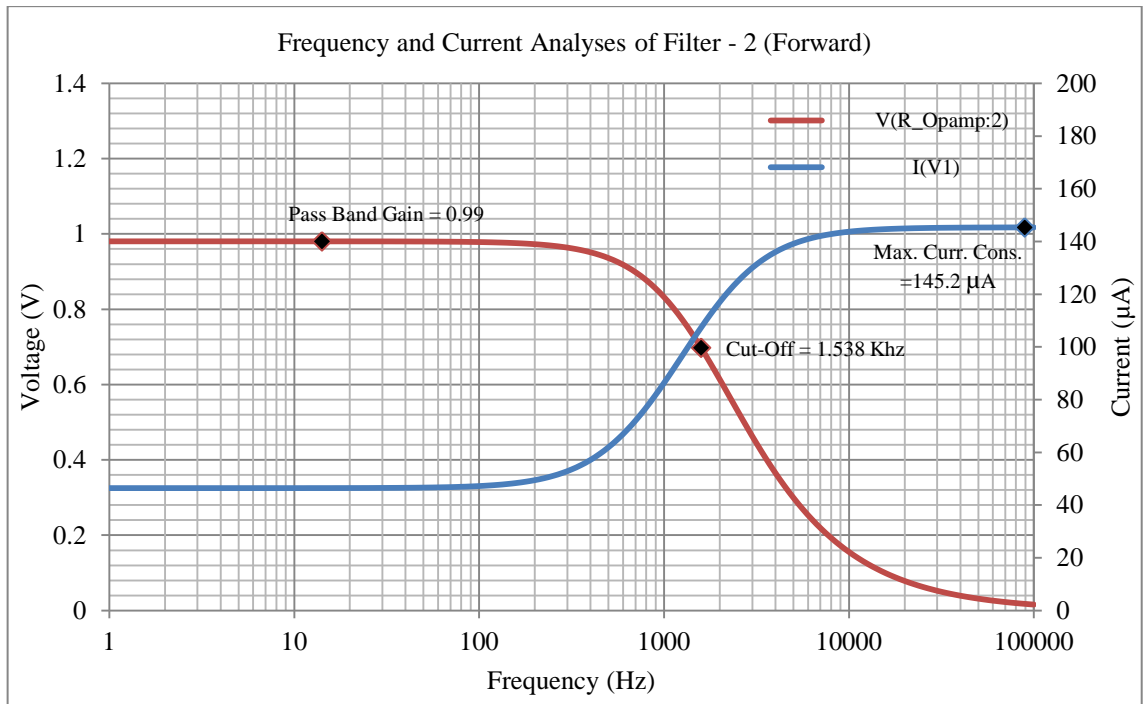


Figure 3.7. Frequency and current analyses of Filter-2 (Forward)

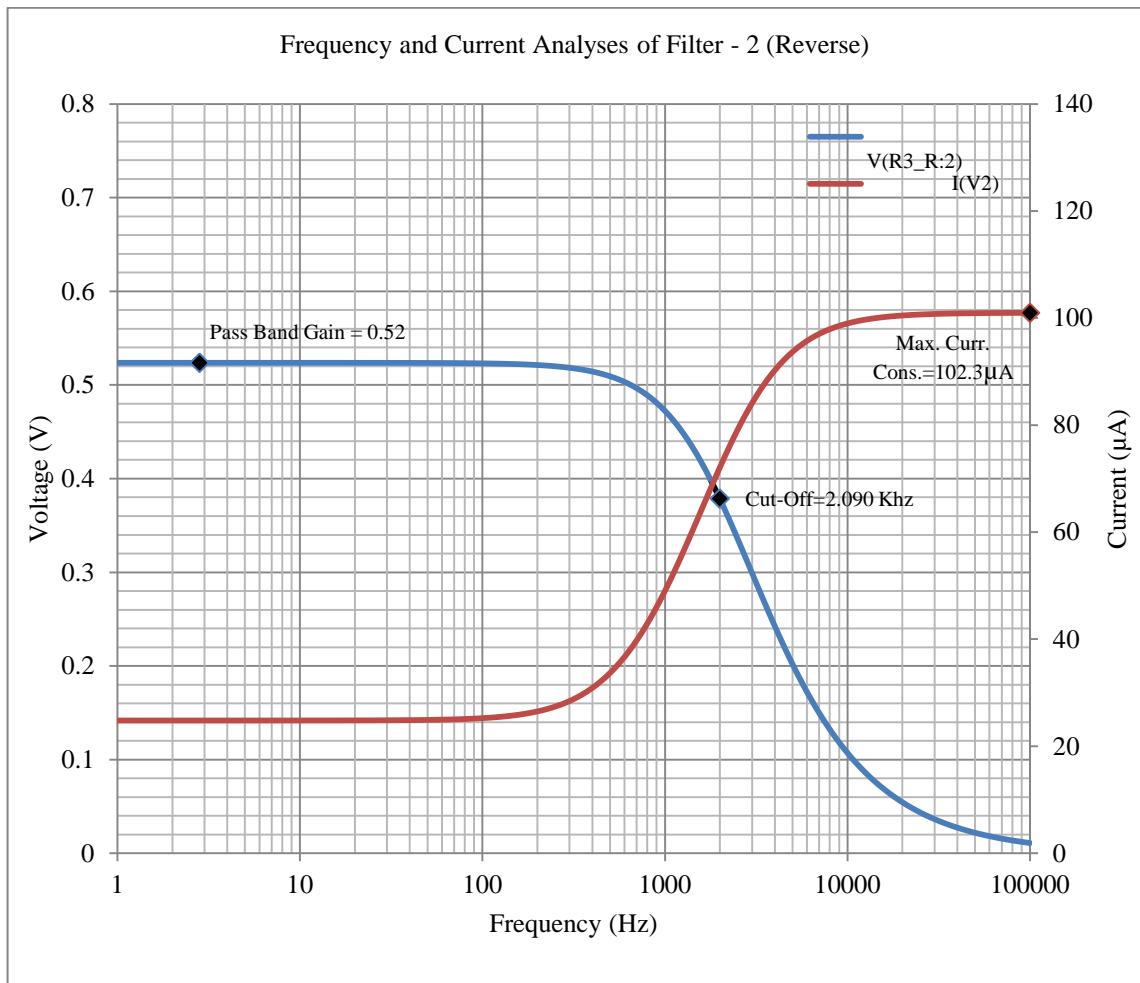


Figure 3.8. Frequency and current analyses of Filter-2 (Reverse)

### 3.2.3. Filter-4 Analysis

Filter-4 is the last filtering stage on the signal line which is placed between the buffer output and the ADC input. Filter-4 is also a T-Type filter to prevent noises in both directions. Same power consumption concerns and cut-off frequency issues are also important in this filter design.

Forward and reverse behavior of the filter are same because, neither at buffer blocks nor at ADC block, any amplification is being done. As seen in Figure 3.10., 3<sup>rd</sup> order low-pass filter provides the necessary cut-off.

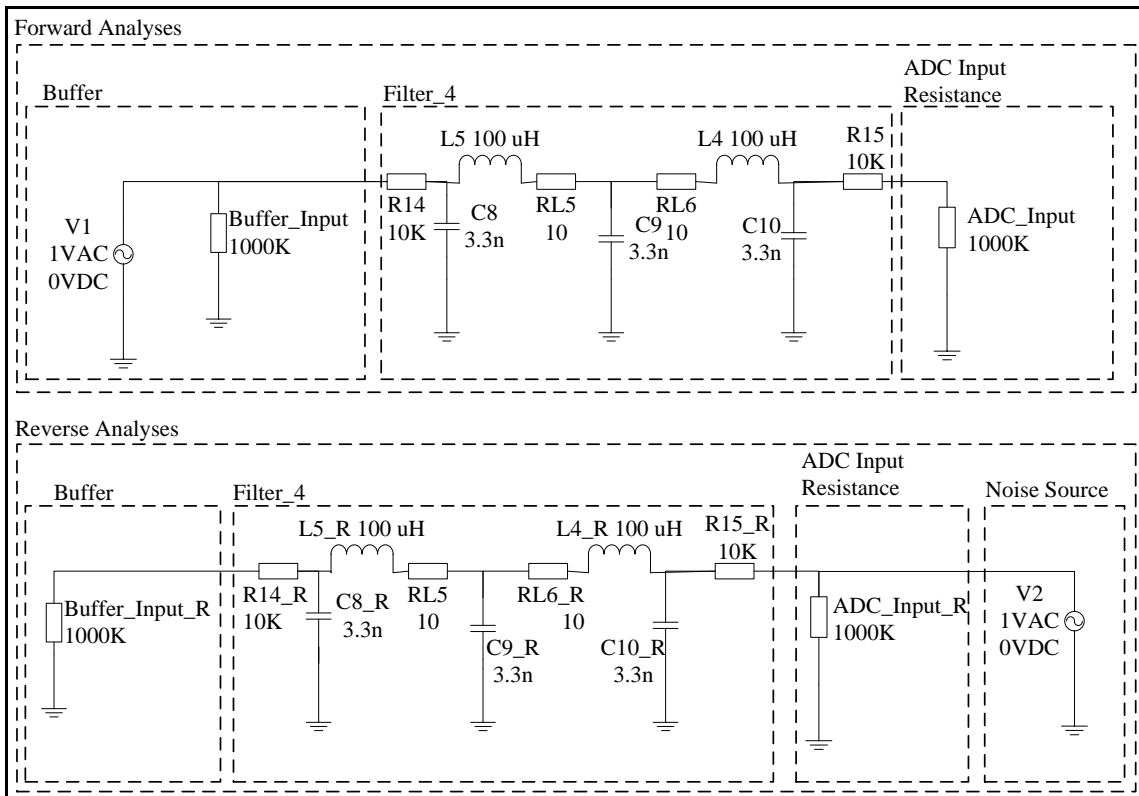


Figure 3.9. Filter-4 simulation circuit

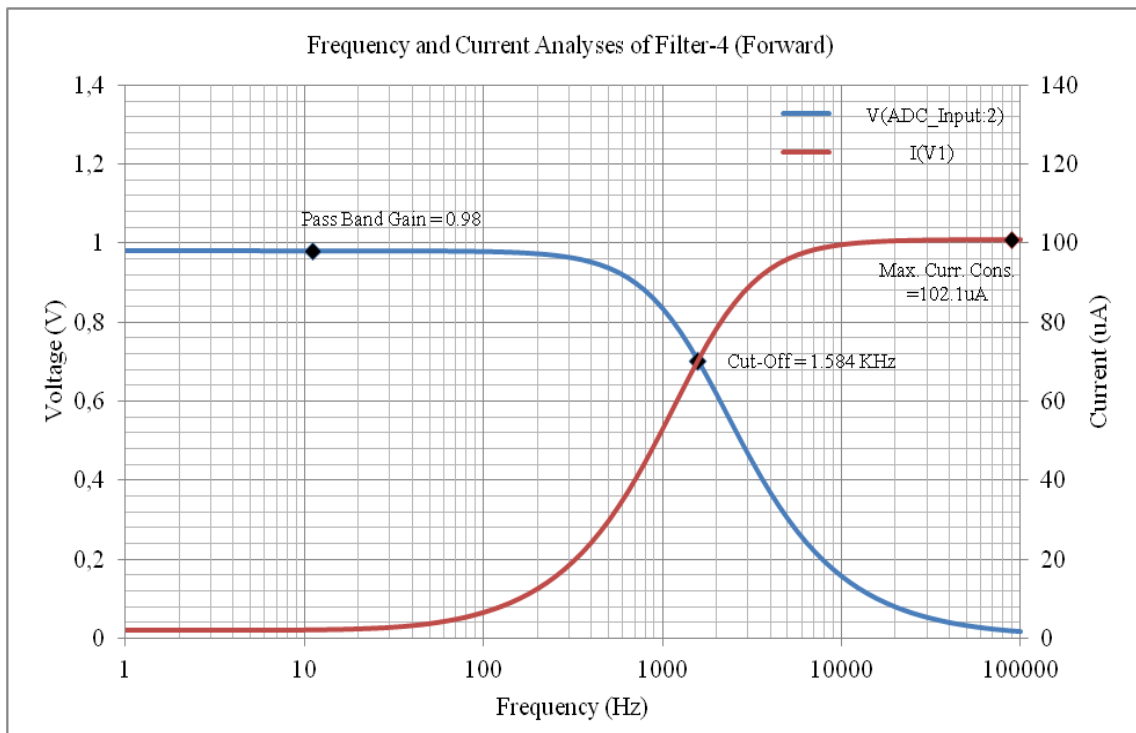


Figure 3.10. Frequency and current analyses of Filter-3 (Forward)

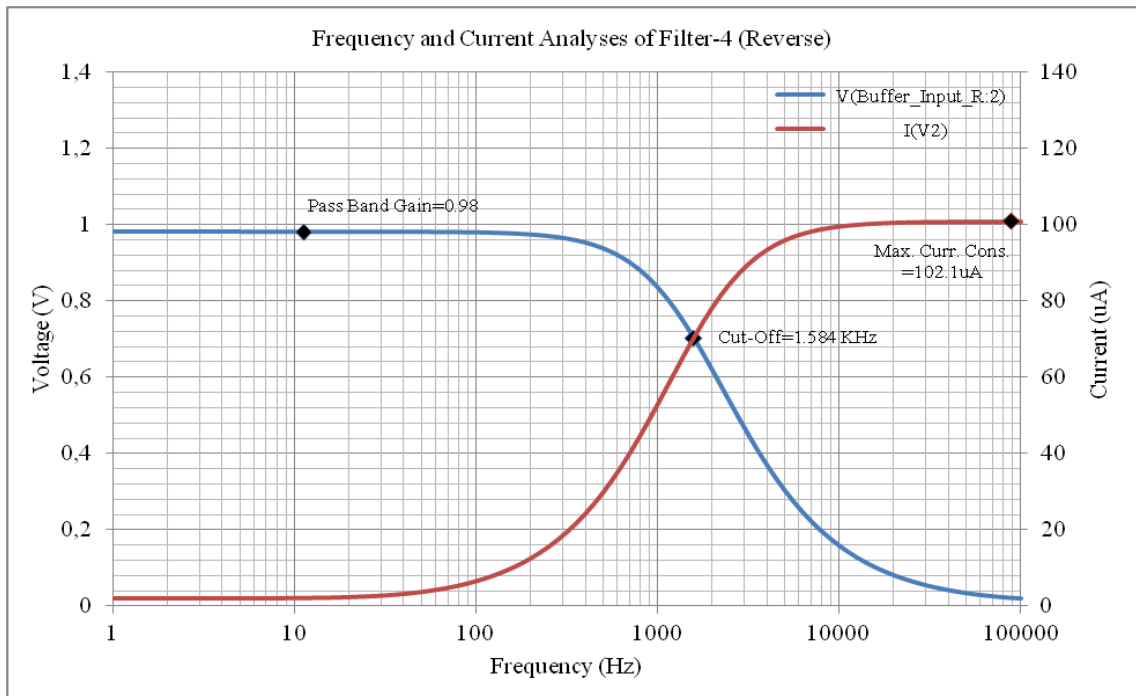


Figure 3.11. Frequency and current analyses of Filter-4 (Reverse)

### 3.2.4. Power Filter Analysis

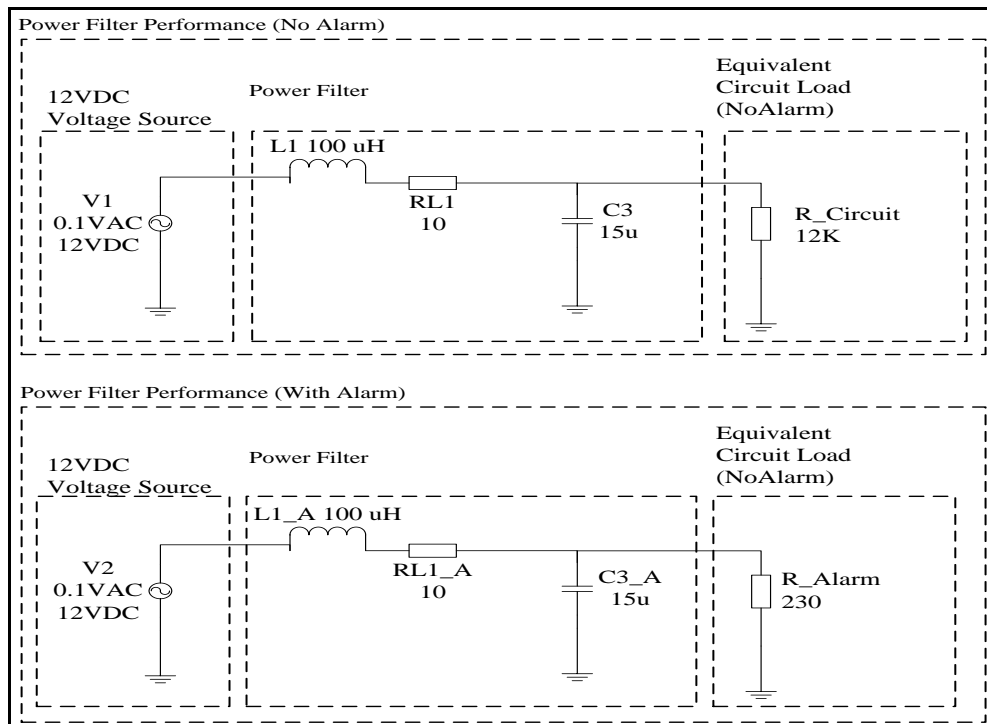


Figure 3.12. Power filter simulation circuit



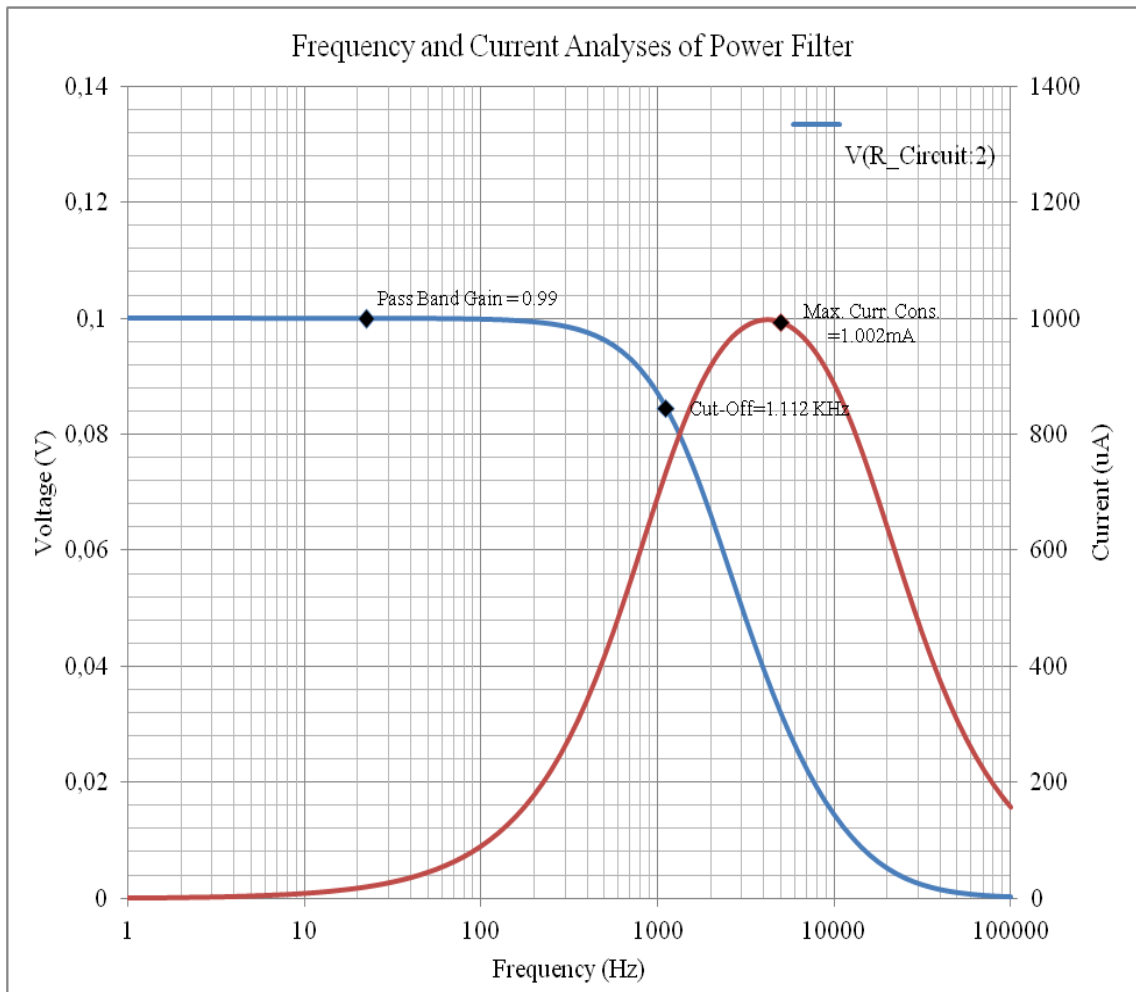


Figure 3.13. Frequency and current analyses of power filter

### 3.2.5. Combined Analysis

The cable of the geophone sensor can act as an antenna at 2.4 GHz. A low pass filter that is from geophone sensor to Op-Amp-1 input will certainly prevent noise due to RFI. There is no need to filter in reverse direction. The filters that are used in between the outputs of Op-Amp-1 and the input of Op-Amp-2 should be bidirectional because the RFI and EMI related noises which may come from both sides can be amplified by the amplifier block. The resistance values in the filter are related to the input and output resistances of Op-Amp. If high resistance values are used in the circuit, the amplified signal will not be transmitted in the ratio of 1 even if in the pass band mode.

The currents that flow through the filters that are used on power line can differ in alarm and non-alarm situations. Available passive circuit elements are used by considering the voltage ratios of them.

One milivolt (AC) input is implemented to Sensor Board input and by looking To\_ADC point, gain analysis is performed. As seen below, the gain value appears in whole sensor board is 0.948 and cut-off frequency is 660.7 Hz.

As seen in the graph below, gain roll at the beginning of the frequency spectrum could be easily seen. After various analyses, source of the problem is the high pass filter behaviour from inverter pin of amplifier-2 to filter 3. If C5 capacitor value is increased, high pass filter cut off frequency would decreased. However, cut-off frequency of that condition does not bother intruder signals frequency spectrum.

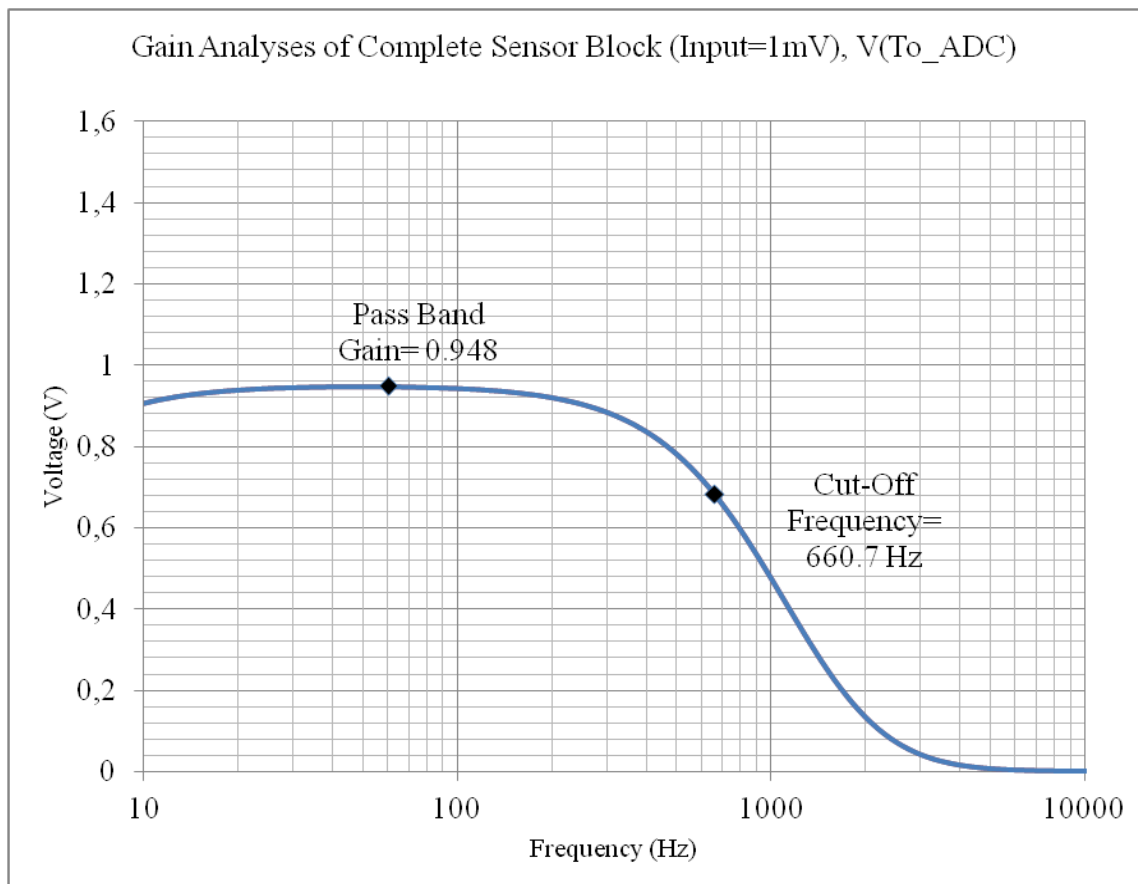


Figure 3.14. Gain analyses of complete sensor board at V (To\_ADC)

### 3.2.6. Total Power Consumption

In order to be able to work SAA system, the total amount of current consumption of sensor board must be lower than 500  $\mu\text{A}$  including the worst-case noise condition.

According to simulation results:

- Maximum current consumption of filter 1 is 90.52  $\mu\text{A}$ ,
- Maximum current consumption of filter 2 is 145.2  $\mu\text{A}$ ,
- Maximum current consumption of filter 3 is 102.1  $\mu\text{A}$ ,
- Maximum current consumption of Power Filter is 1002  $\mu\text{A}$ ,
- Opamp-1 Gain Resistors is 150  $\mu\text{A}$ ,
- Opamp-2 Gain Resistors is 3.2  $\mu\text{A}$ ,
- Opamp-1 Current Consumption is 6  $\mu\text{A}$ ,
- Opamp-2 Current Consumption is 6  $\mu\text{A}$ ,
- Buffer Current Consumption is 6  $\mu\text{A}$ ,

The source of current of Filter-1 will be the geophone sensor, so it does not affect the total current consumption. Increasing the inductance value in low pass filter which is used for decreasing the maximum current consumption of power filter has the same effect with increasing the voltage ratio. Therefore, power filter cable will be considered with the hardware isolated from noises and the related current value will not be counted in the final. The total amount of all units have value 418.5  $\mu\text{A}$ .

### 3.3. DETAILS OF SAA ARCHITECTURE

Because there is a resistance between the sensor nodes the input voltage of each node differs from each other. Therefore, the changes differ from node to node when alarm occurs. The amount of current, the resistance between the nodes, and the power consumed when an alarm does not occur are the most important parameters.

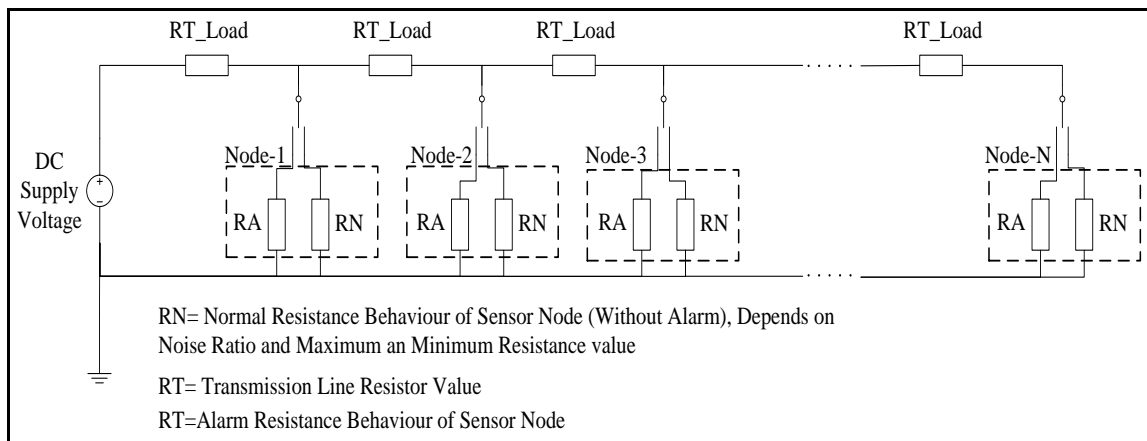


Figure 3.15. Current consumption model of the sensor nodes system

### 3.3.1. Normal Mode Current Consumption

Normal mode current consumption is the amount of charge that flows through the nodes when alarm does not occur. The amount of current decreases with the amount of nodes if the charge amount has large amplitude.

Normal\_Mode\_Current\_Consumption.m file is the power consumption model of sensor nodes when they are not producing any alarm. There are several variables in the code such as; RN\_Min-RN\_Max (Equivalent resistor value of node when there is no alarm), Noise Ratio (Changes the nodes equivalent resistance value between RN\_Min and RN\_Max), Voltage supply, RT\_Load (Resistance value between nodes), Node\_Number\_At\_System and some other variables. Descriptions are detailed in the m-file.

Noise ratio is defined as the oscillation on the common mode current of a node. The RFI and EMI related noises can cause instantaneous current at filters. Noise ratio coefficient determines the location of the noise between RN\_Min and RN\_Max where RN\_Min and RN\_Max represent the minimum and maximum current values of a probe at normal mode. When the noise ratio is minimum, RN\_Min is also minimum so that, the oscillation on nodes is minimized. The most effective parameter in the system is the noise ratio. When noise ratio decreases, the oscillation of a random sensor node decreases. The current in the alarm mode is directly related to input voltage. To obtain true alarm information, the hardware should be designed in a way that the noise ratio is at minimum level.

RT\_Load symbolizes the resistance between the nodes. When the RT\_Load value increases, last node voltage decreases. If the last node voltage decreases exponentially, the maximum node number that can be connected to a sinc unit decreases. When the RT\_Load value decreases, the node voltages come closer and the determination of a node that triggers the alarm becomes more difficult to infer. When number of nodes (Node\_number) increases, last node voltage decreases exponentially.

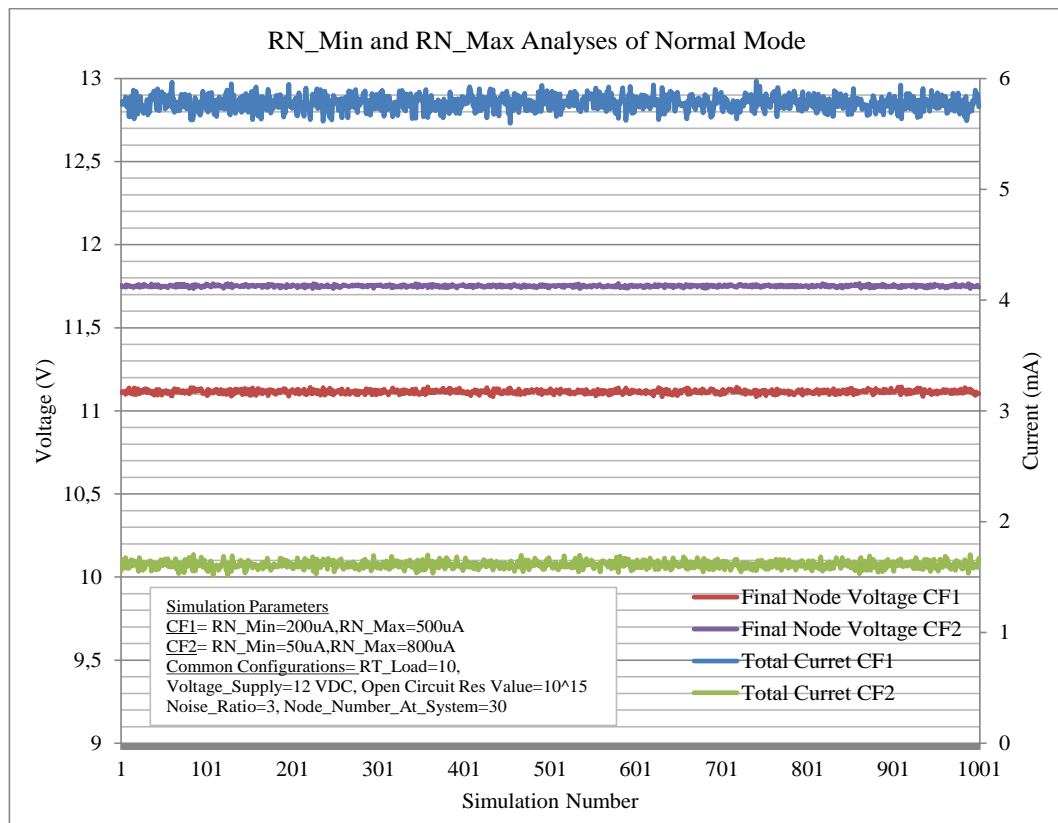


Figure 3.16. RN\_Min and RN\_Max analyses of normal mode

Table 3.3. Results of RN\_Min and RN\_Max analyses at normal mode

Simulation Name	Min Value	Mean Value	Max Value	Difference
Total Current CF1	5.522 mA	5.783 mA	5.968 mA	0.446 mA
Final Node Voltage CF1	11.076 V	11.114 V	11.149 V	0.073 V
Total Current CF2	1.515 mA	1.611 mA	1.716 mA	0.201 mA
Final Node Voltage CF2	11.731 V	11.751 V	11.767 V	0.036 V

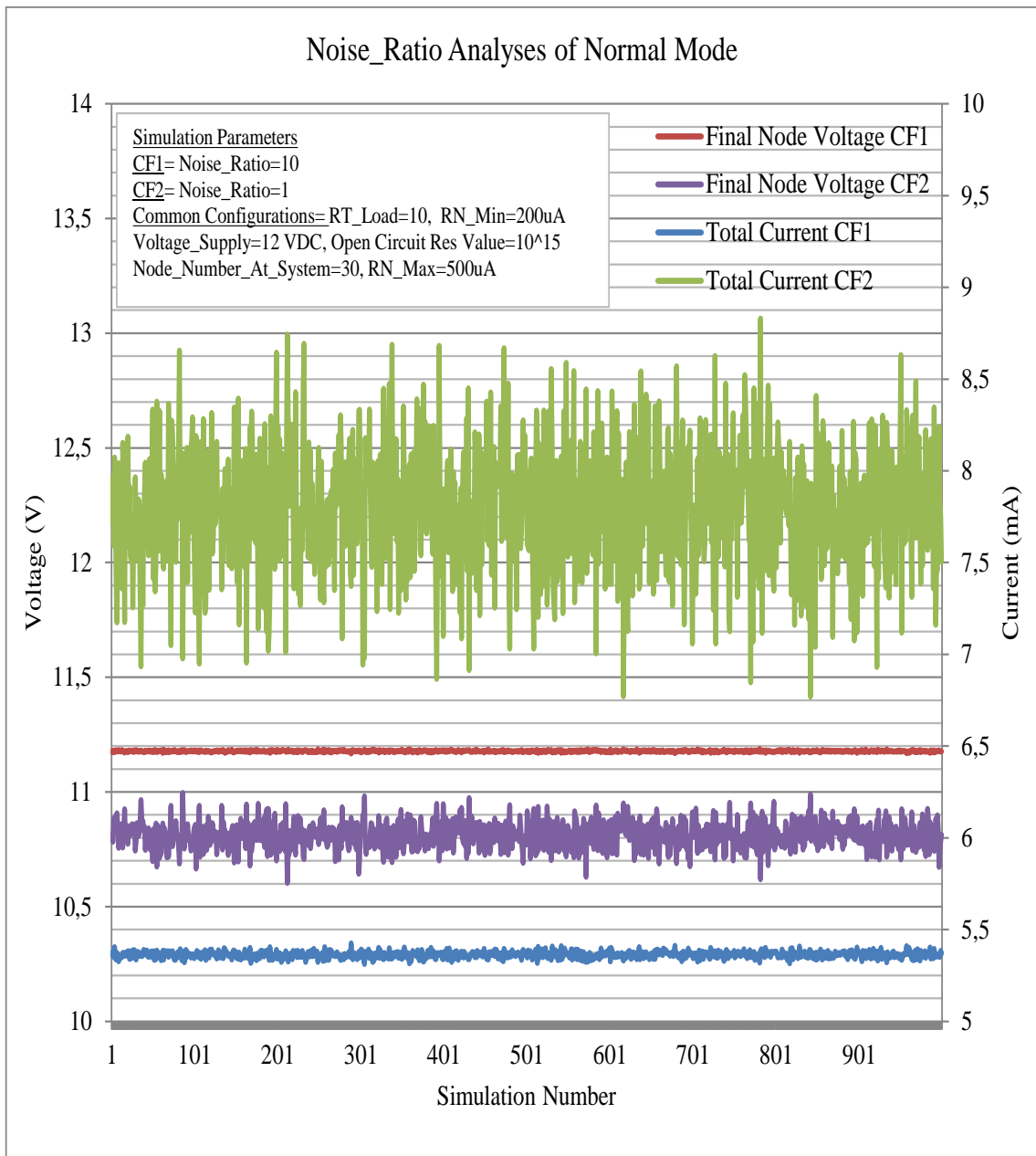


Figure 3.17. Noise\_Ratio analyses of normal mode

Table 3.4. Results of Noise\_Ration analyses at normal mode

Simulation Name	Min Value	Mean Value	Max Value	Difference
Total Current CF1	5.304 mA	5.364 mA	5.417 mA	0.113mA
Final Node Voltage CF1	11.169 V	11.178 V	11.186 V	0.017 V
Total Current CF2	6.657 mA	7.778 mA	8.874 mA	2.217 mA
Final Node Voltage CF2	10.591 V	10.814 V	10.964 V	0.373 V

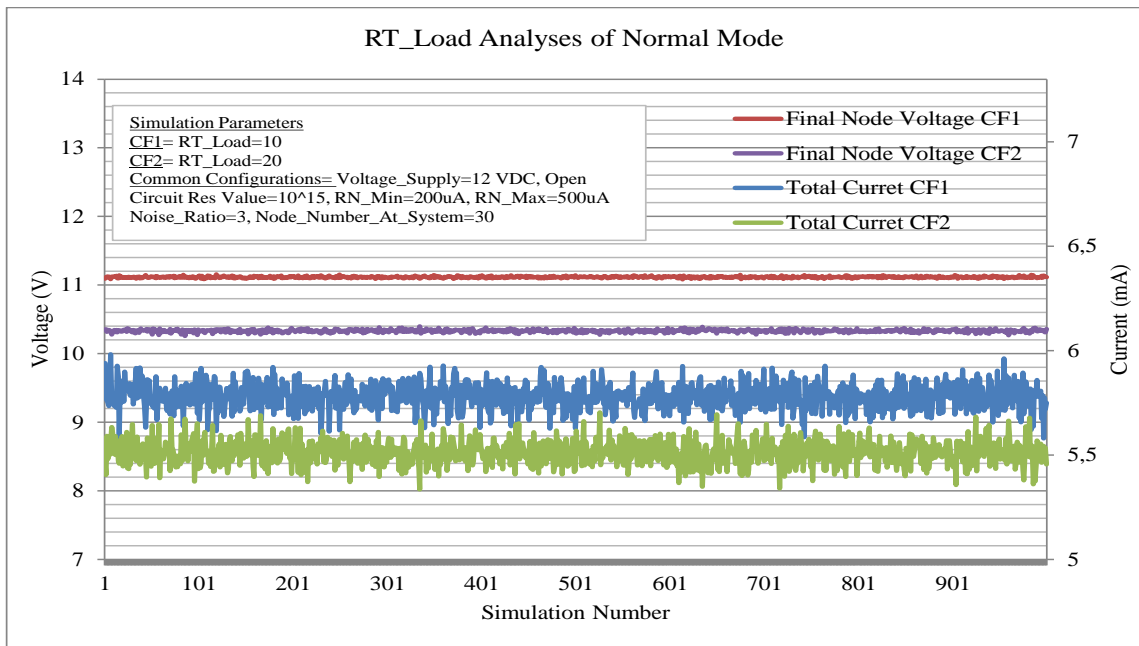


Figure 3.18. RT\_Load analyses of normal mode

Table 3.5. Results of RT\_Load analyses at normal mode

Simulation Name	Min Value	Mean Value	Max Value	Difference
Total Current CF1	5.587 mA	5.785 mA	6.012 mA	0.425 mA
Final Node Voltage CF1	11.082 V	11.115 V	11.151 V	0.428 V
Total Current CF2	5.327 mA	5.509 mA	5.720 mA	0.393 mA
Final Node Voltage CF2	10.273 V	10.334 V	10.388 V	0.115 V

Table 3.6. Results of Node\_Number\_At\_System analyses at normal mode

Node_Number At_System	Total_Current (mA)				Final_Voltage (V)			
	Minimum	Average	Maximum	Differance (Max-Min)	Minimum	Average	Maximum	Differance (Max-Min)
5	0,936	1,013	1,103	0,167	11,967	11,969	11,973	0,006
10	1,879	2,015	2,183	0,304	11,883	11,889	11,896	0,013
15	2,829	2,998	3,159	0,33	11,747	11,761	11,775	0,028
20	3,781	3,962	4,147	0,366	11,567	11,586	11,605	0,038
25	4,7	4,889	5,101	0,401	11,341	11,369	11,399	0,058
30	5,58	5,781	5,999	0,419	11,076	11,115	11,149	0,073
35	6,423	6,626	6,845	0,422	10,785	10,827	10,868	0,083
40	7,221	7,431	7,692	0,471	10,462	10,509	10,554	0,092

### 3.3.2. Single Alarm Mode Current Consumption

Single alarm mode current consumption represents the situation where only one node generates an alarm signal. In other words, only one node generates alarm by flowing current through itself while others continue in the normal mode.

Single\_Alarm\_Mode\_Current\_Consumption.m file is the power consumption model of sensor nodes while only one node is producing alarm. RA\_Load value is defined as the resistance of a node in alarm situation. When the RA\_Load value increases the ratio between RA\_Load and RT\_Load increases and the currents consumed from probes start to come closer to each other as a ratio.

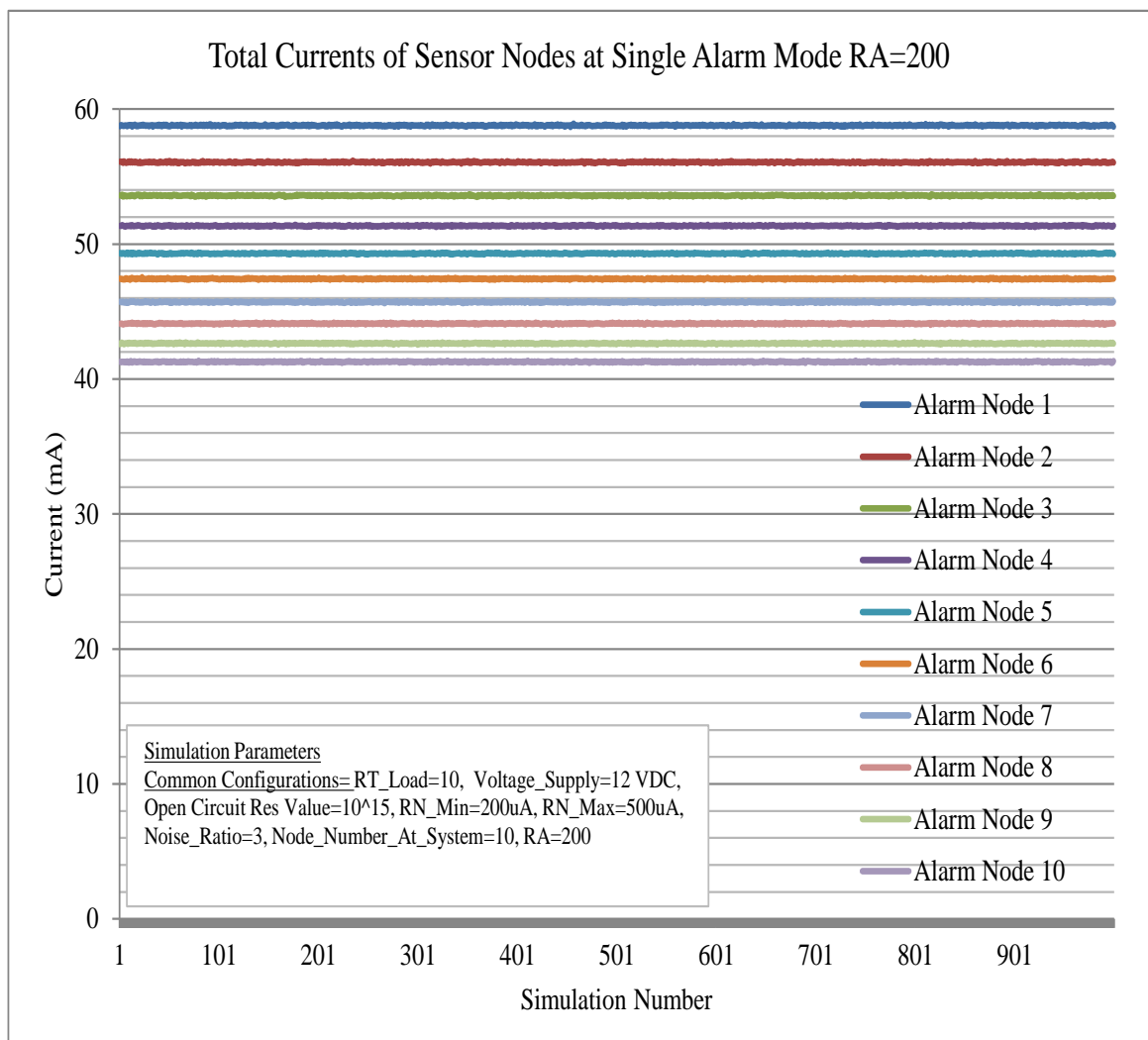


Figure 3.19. Total currents of sensor nodes at single alarm mode RA=200



Table 3.7. Results of total currents of sensor nodes at single alarm mode RA=200

Alarm_Node_Number	Total_Current (mA)			
	Minimum	Average	Maximum	Differance (Max-Min)
1	58.675	58.788	58.898	0.223
2	55.977	56.062	56.169	0.192
3	53.491	53.594	53.696	0.205
4	51.251	51.349	51.425	0.174
5	49.214	49.302	49.394	0.18
6	47.334	47.424	47.534	0.2
7	45.618	45.699	45.795	0.177
8	44.032	44.108	44.189	0.157
9	42.558	42.639	42.727	0.169
10	41.183	41.277	41.35	0.1665

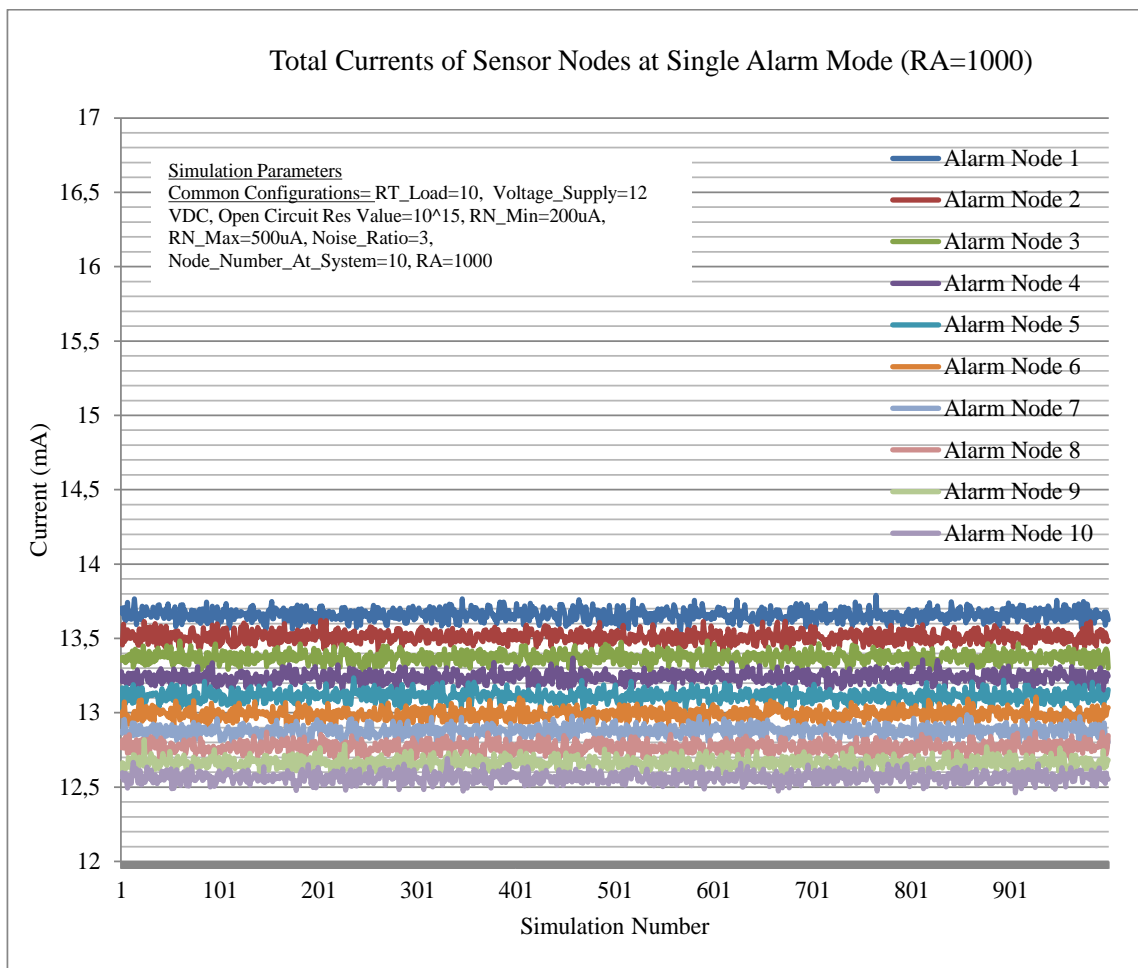


Figure 3.20. Total currents of sensor nodes at single alarm mode (RA=1000)

Table 3.8. Results of total currents of sensor nodes at single alarm mode (RA=1000)

Alarm_Node_Number	Total_Current (mA)			
	Minimum	Average	Maximum	Differance (Max-Min)
1	13.564	13.658	13.753	0.1894
2	13.408	13.511	13.614	0.206
3	13.261	13.371	13.494	0.233
4	13.116	13.243	13.351	0.235
5	13.001	13.114	13.229	0.228
6	12.886	12.993	13.091	0.205
7	12.784	12.877	13.021	0.237
8	12.672	12.766	12.901	0.2283
9	12.545	12.665	12.792	0.247
10	12.458	12.565	12.679	0.2211

As it can be seen in Figure 3.19., the currents of nodes in alarm situation differ from each other together with appropriate RA\_Load values.

Difference between maximum and minimum current consumptions is also an important parameter on defining alarm position. In addition, when the RA\_Load value increases, the alarm charges decrease as it can be seen from Table 3.7. and Table 3.8. RA\_Load parameter is one of the most important parameters that determine the node number which can take place in a system.

### 3.3.3. Double Alarm Mode Current Consumption

Double alarm mode current consumption represents the situation where two nodes generate alarm signal. In other words, only two nodes generate alarm by flowing current through itself while others continue in the normal mode.

Double\_Alarm\_Mode\_Current\_Consumption.m file is the power consumption model of sensor nodes while only two nodes are producing alarm.

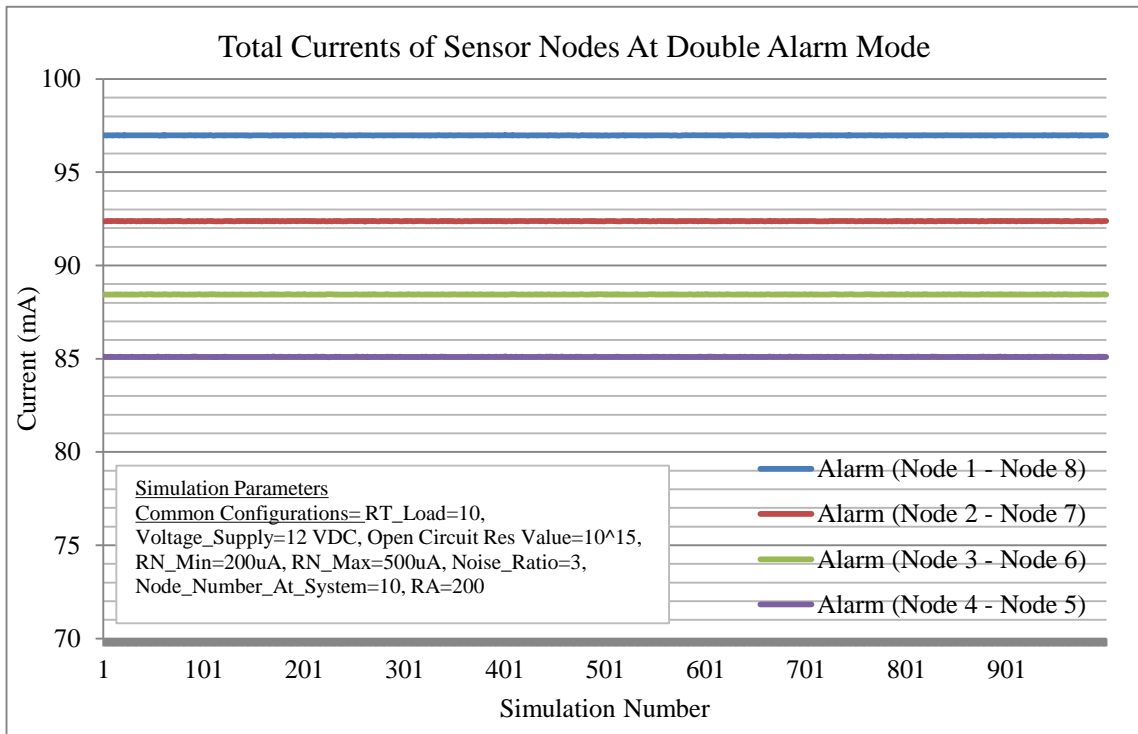


Figure 3.21. Total currents of sensor nodes at double alarm mode

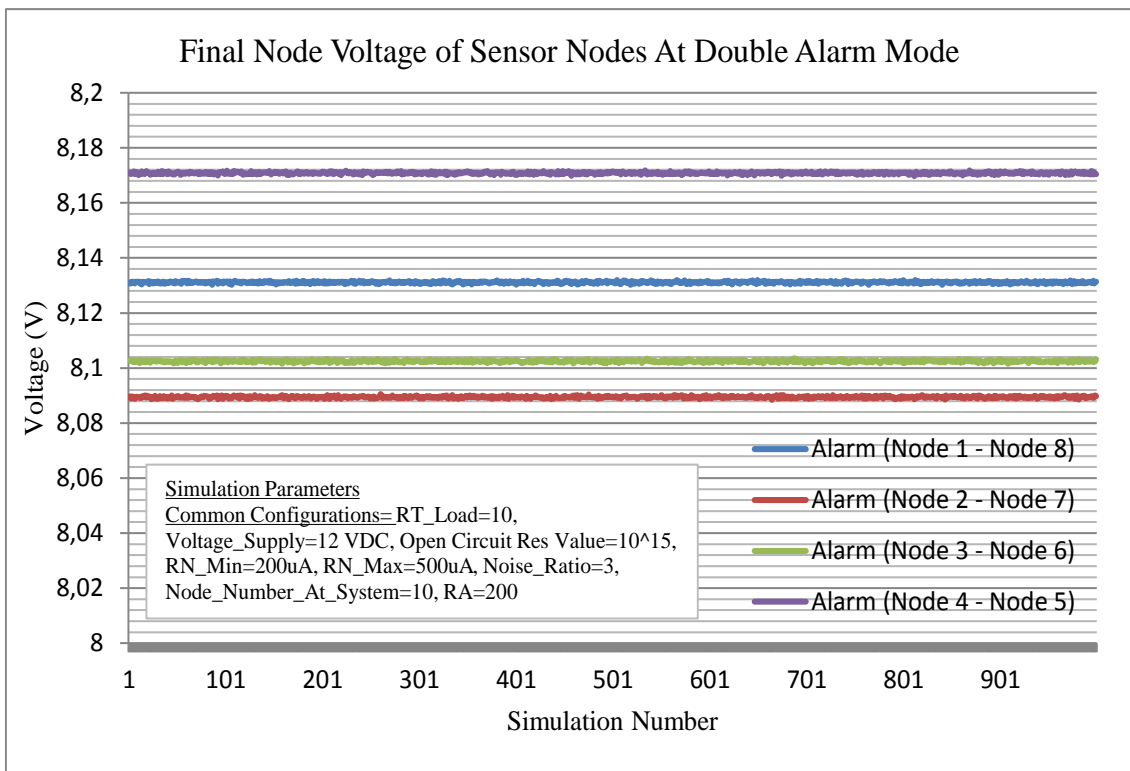


Figure 3.22. Final node voltage of sensor nodes at double alarm mode

As it can see from the figures, the total amount of current consumed differs when different nodes generate current at the same time.

The last node voltage in the line changes together with different node pairs which are triggered at the same time. Total alarm currents of last two node in the system have to be smaller than the first nodes alarm current, to prevent confusion between single and dual alarms.

### 3.4. PROTOTYPES

Prototype circuits and boards are shown in the below figures.

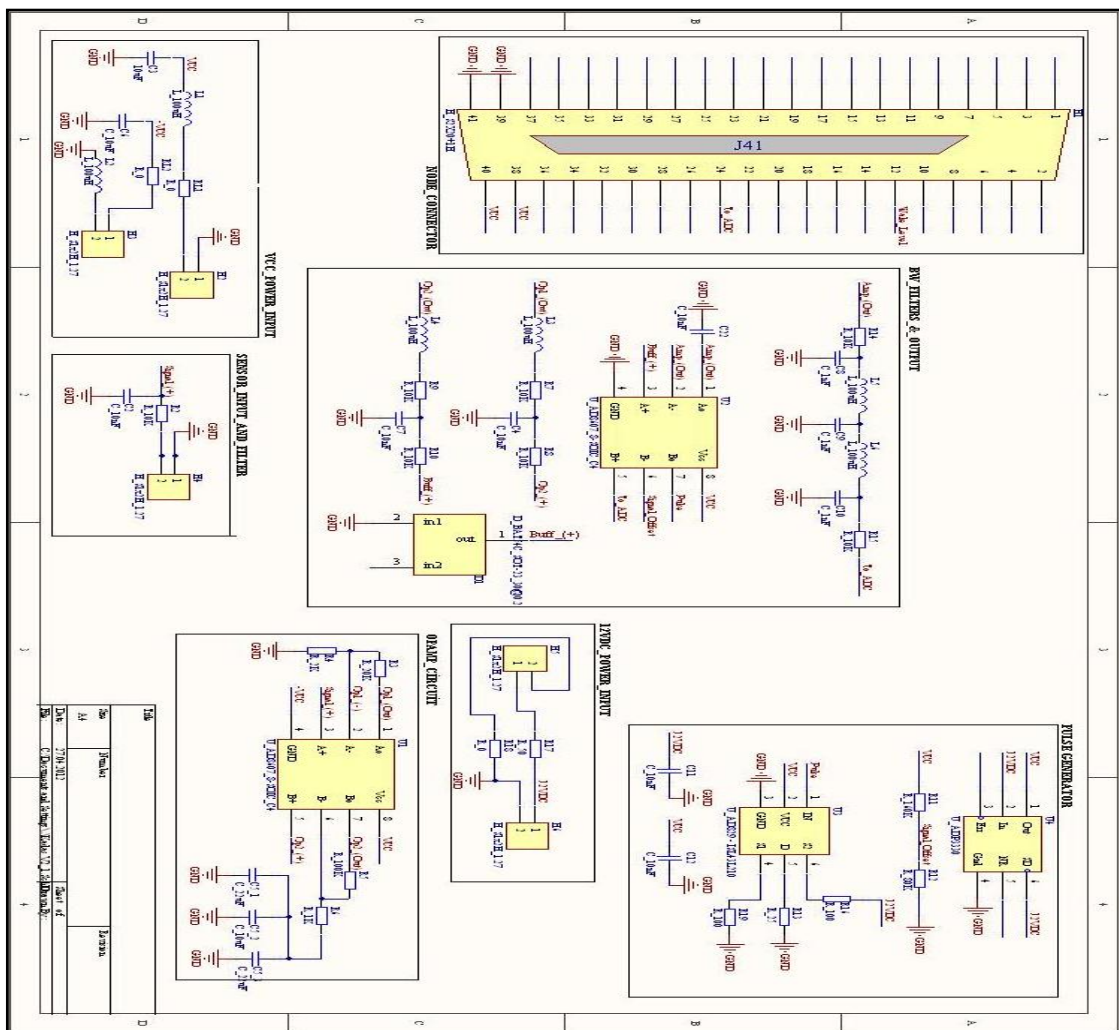


Figure 3.23. Screen capture of sensor board schemantic (Altium)

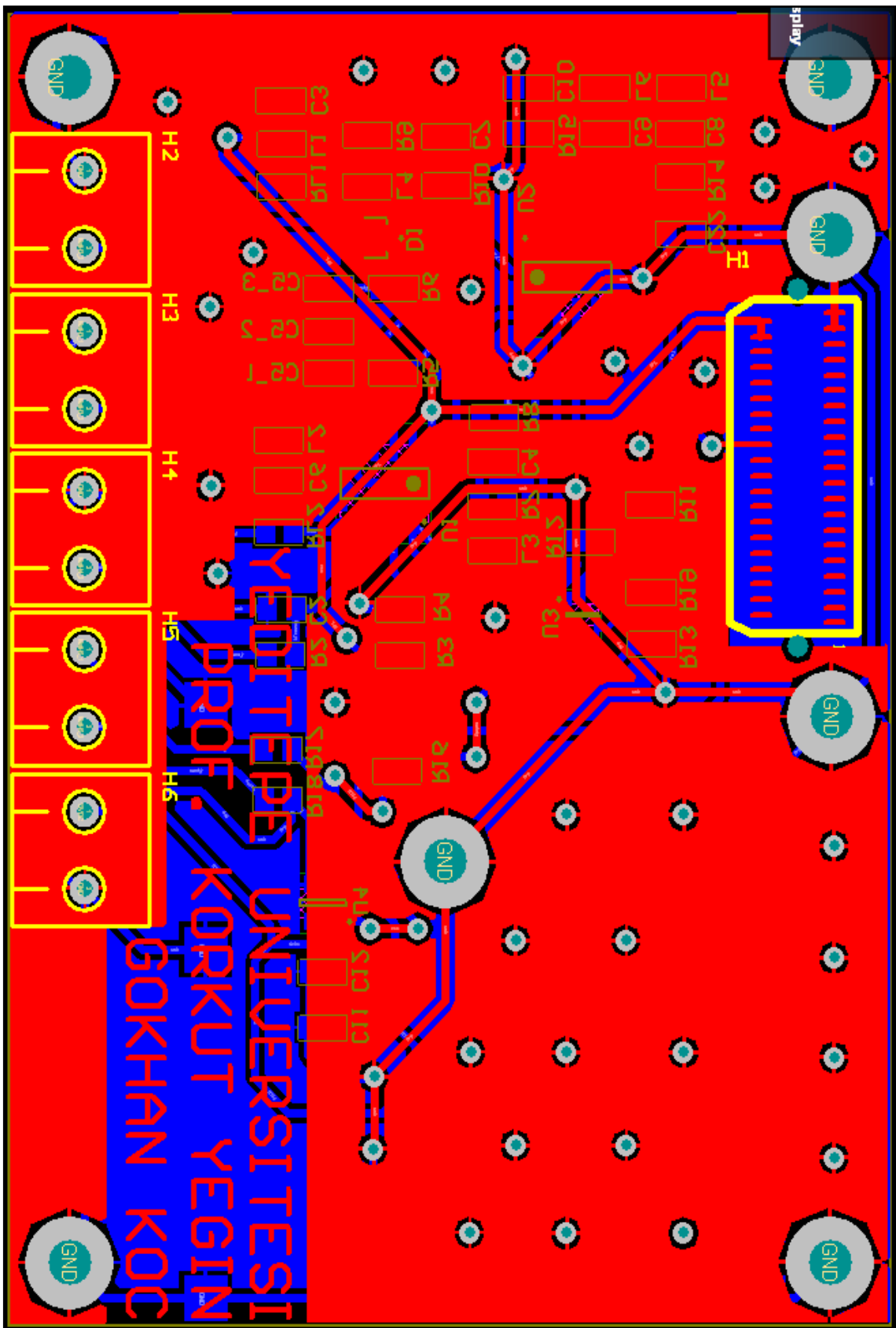


Figure 3.24. Screen capture of top view sensor board pcb (Altium)

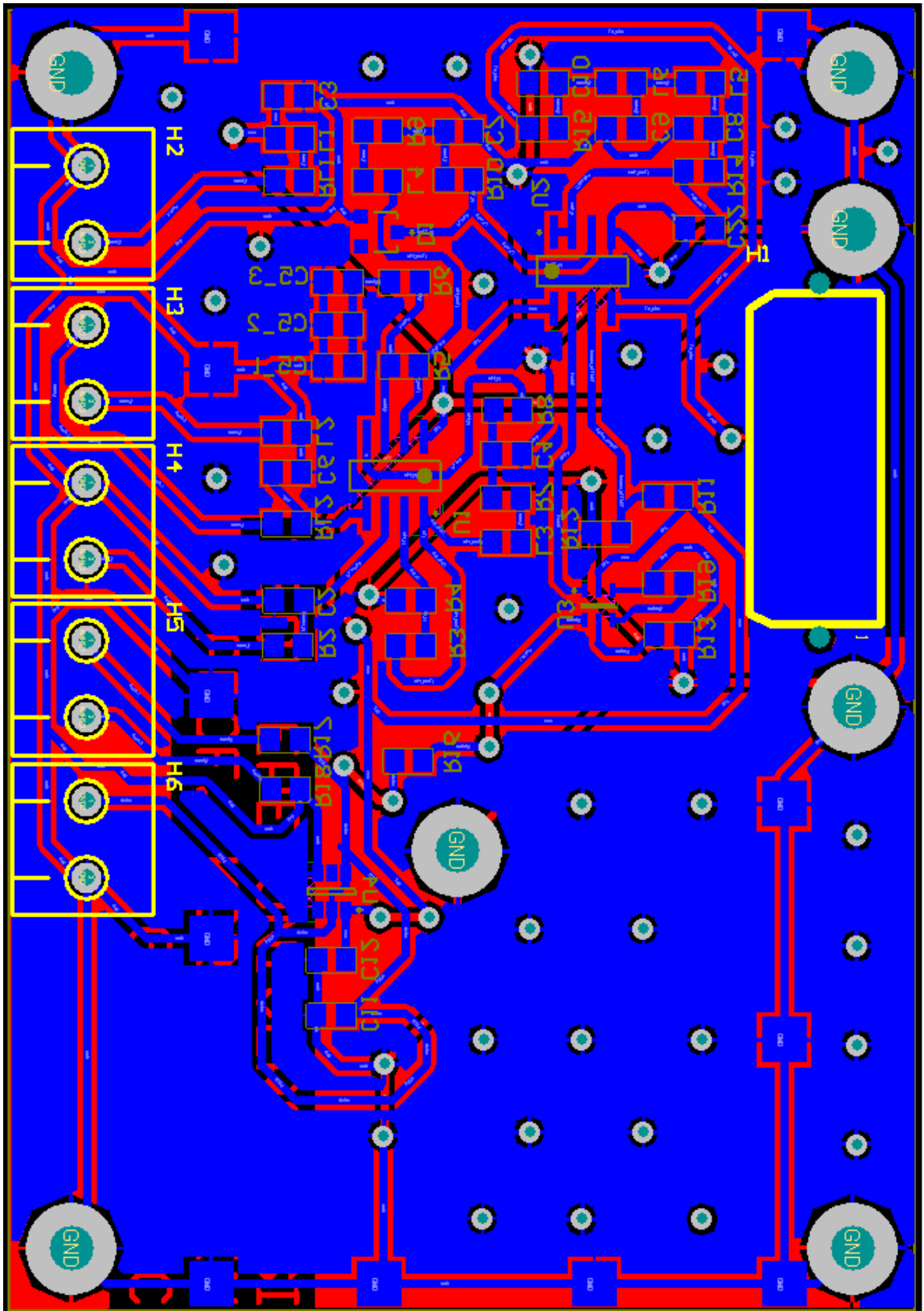


Figure 3.25. Screen capture of bottom view sensor board pcb (Altium)

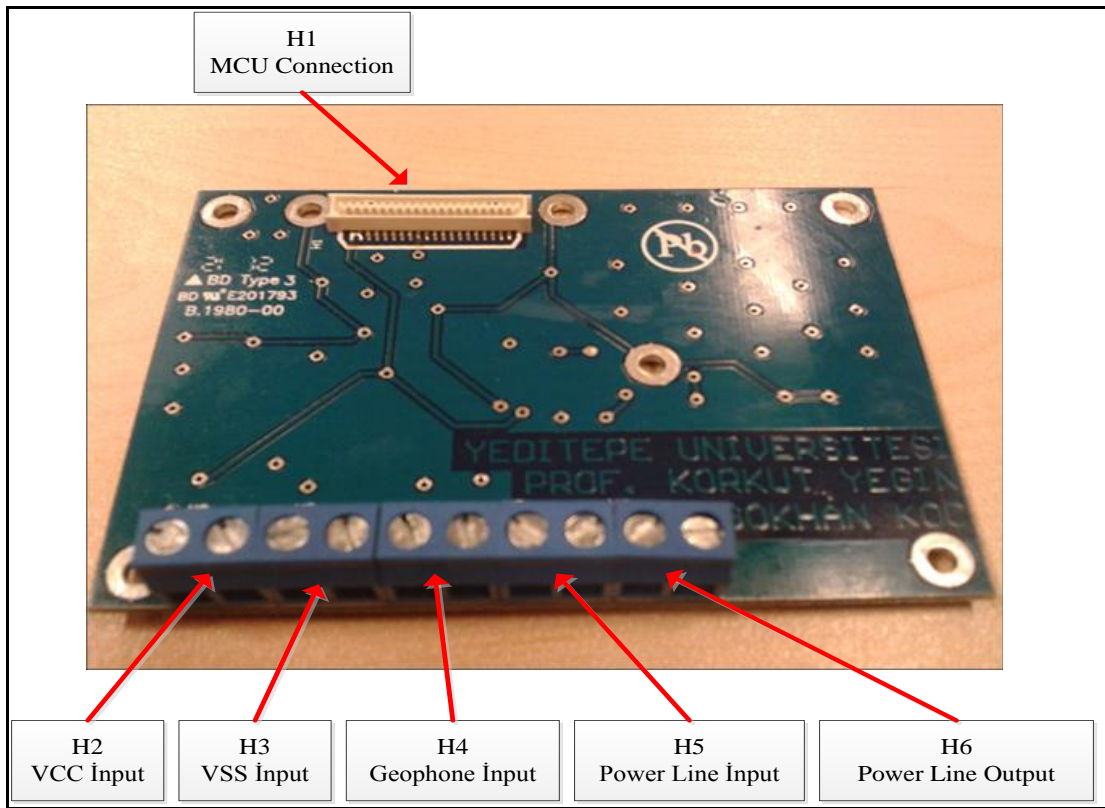


Figure 3.26. Top view of sensor board

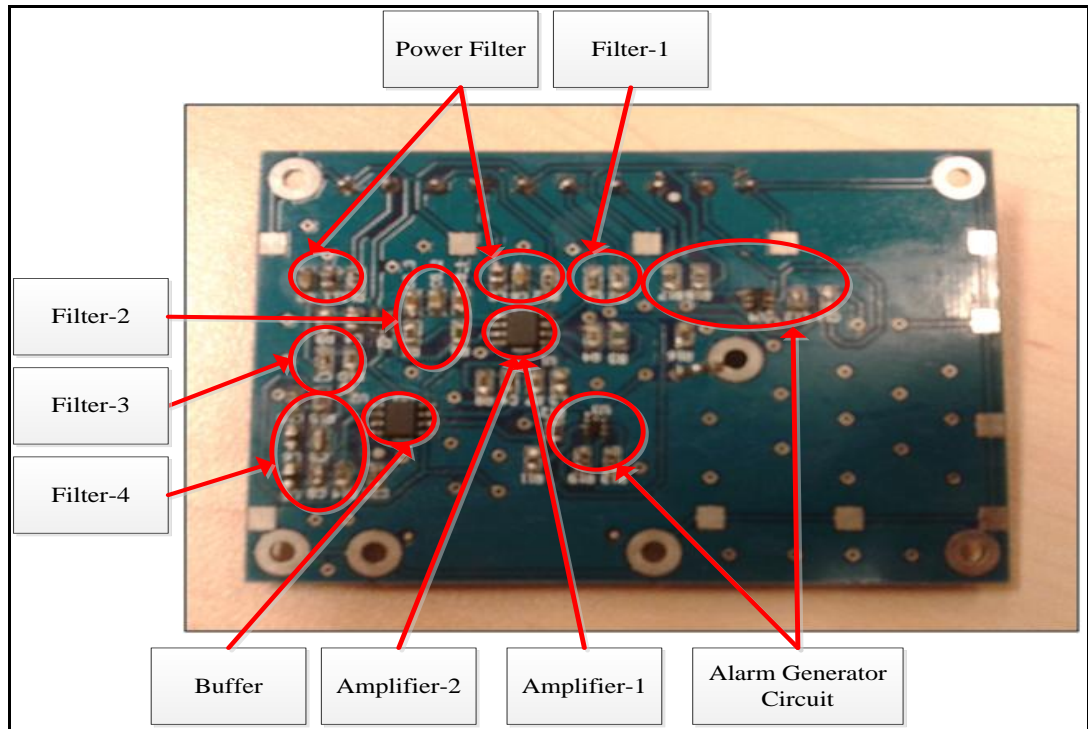


Figure 3.27. Bottom view of sensor board

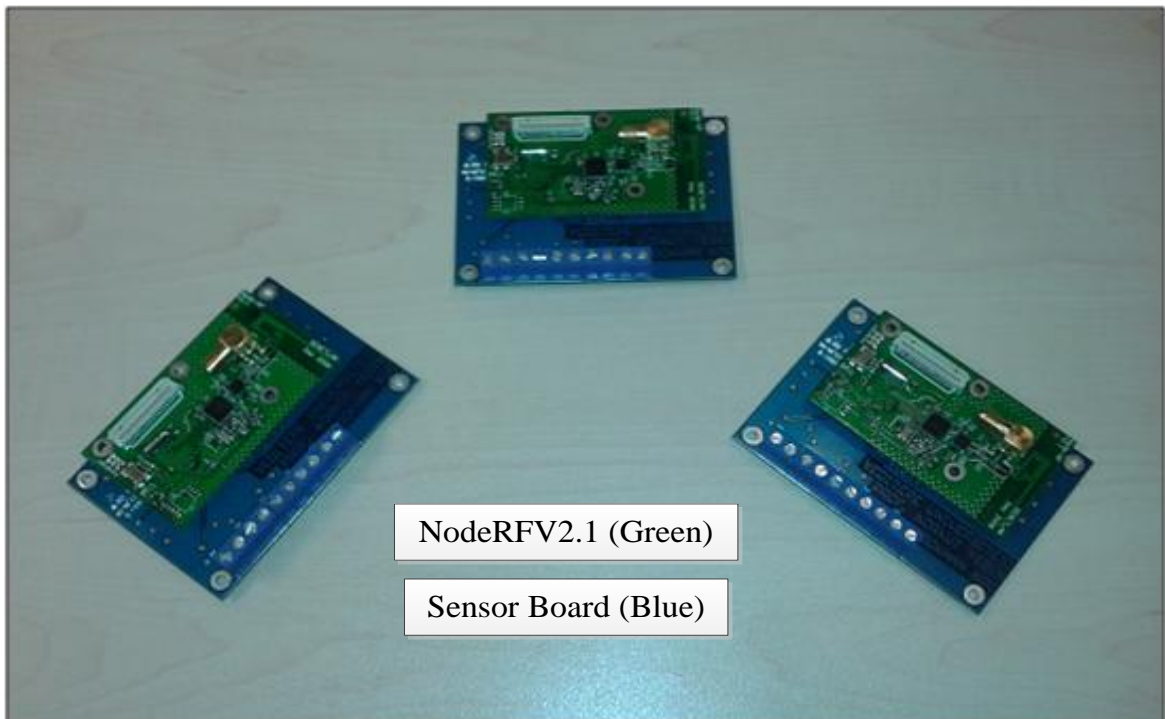


Figure 3.28. Sensor board and NodeRFV2.1 connected

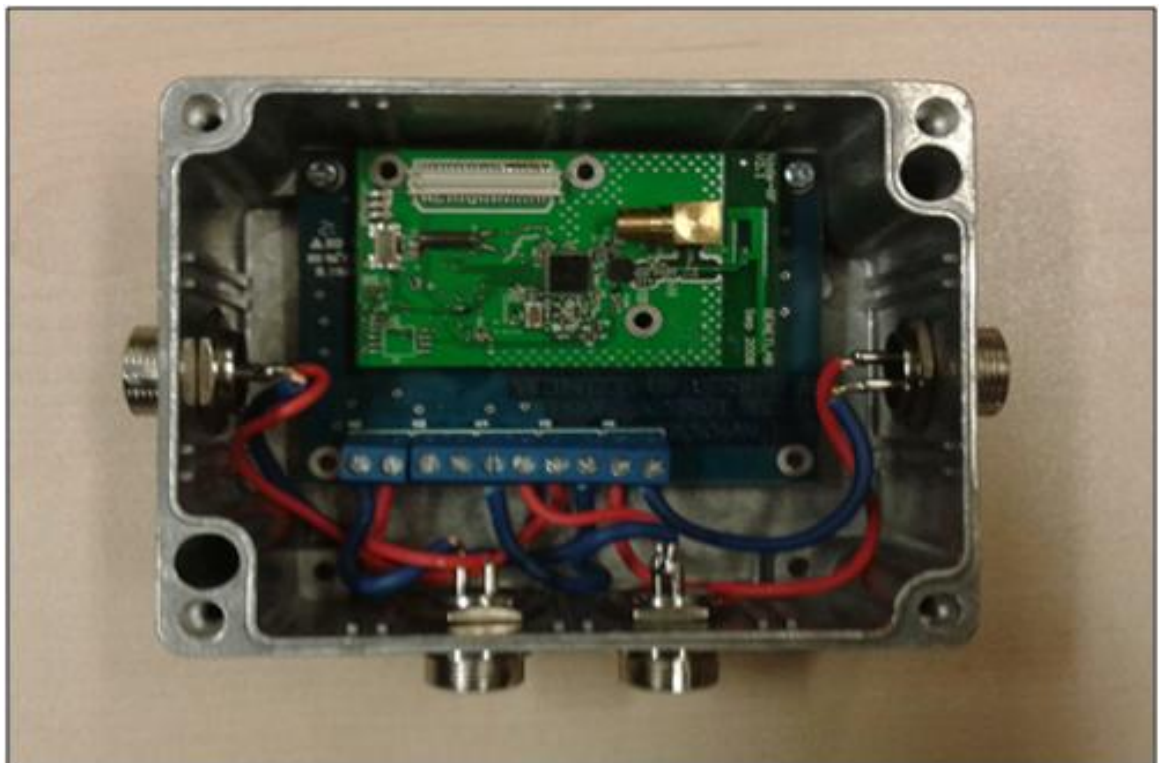




Figure 3.29. Inside view of node box



Figure 3.30. Outside view of node box

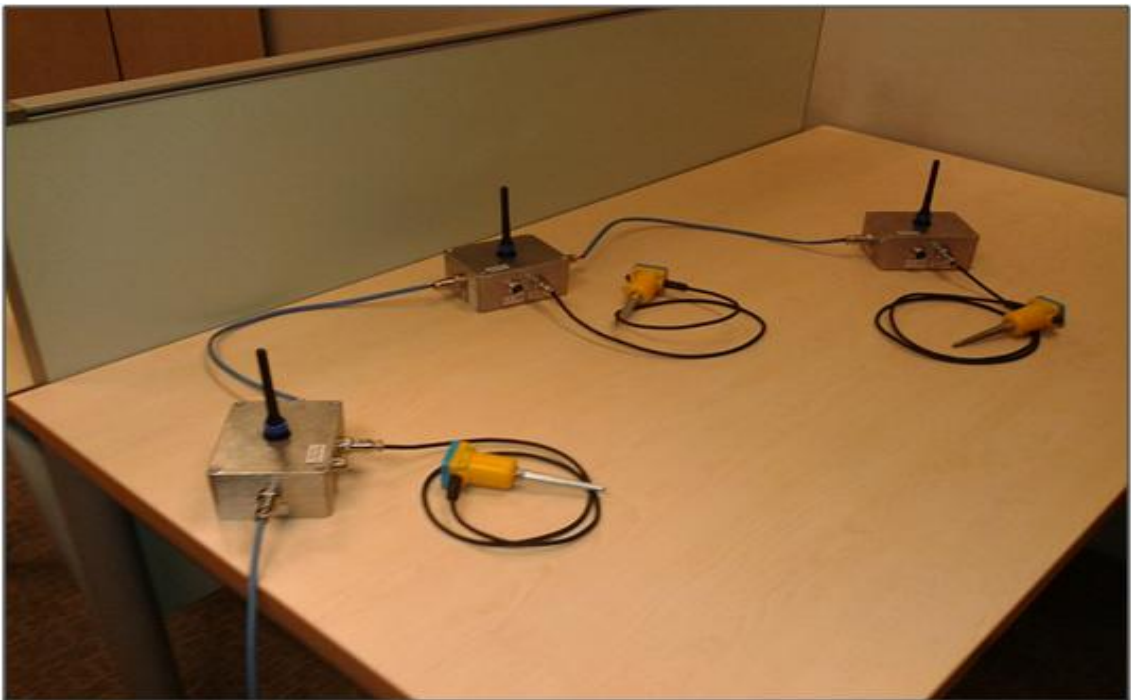


Figure 3.31. SAA connection photo

### 3.5. SENSOR BOARD AMPLIFICATION ANALYSES AFTER PRODUCTION

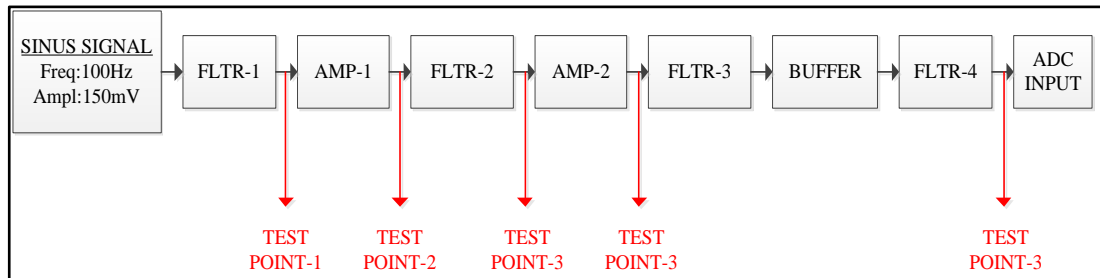


Figure 3.32. Block diagram of amplification line

After the production of sensor board, the amplification performance are measured with 5 different test point. As it can be seen from the above graphic, instead of geophone sensor sinus signal from signal generator is used with 100 Hz frequency and 150mV amplitude. Amplification gains in first stage and second stage are fixed to 10 so the total amplification gain is fixed to 100.

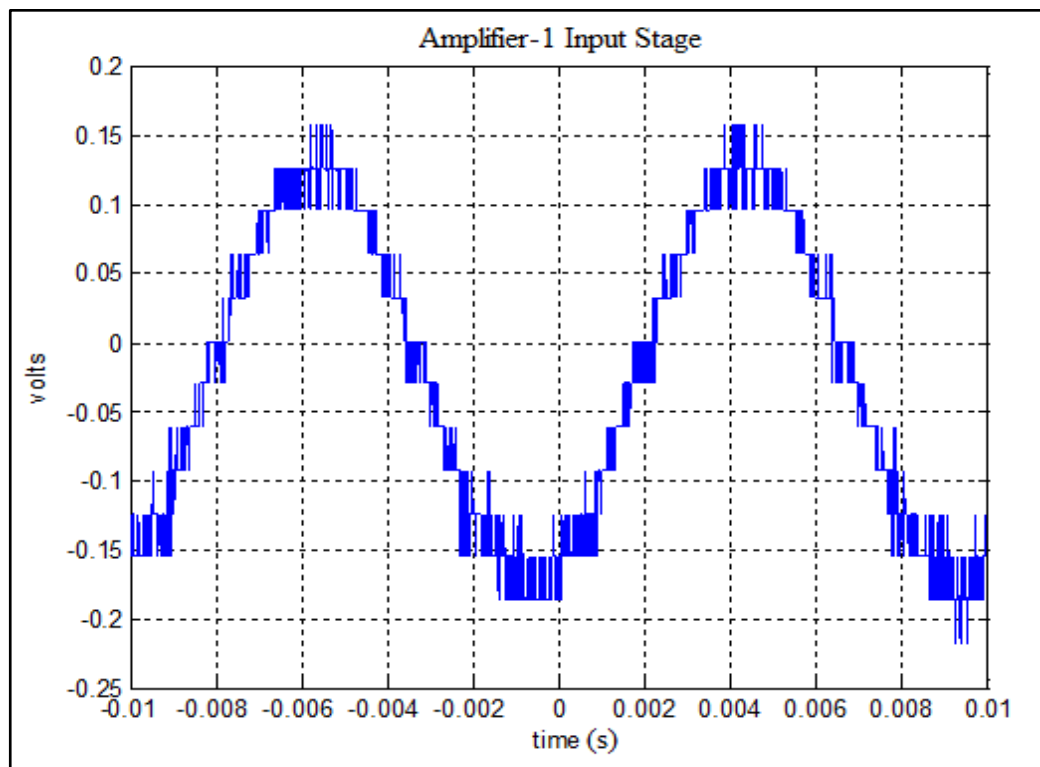


Figure 3.33. Amplifier-1 input stage

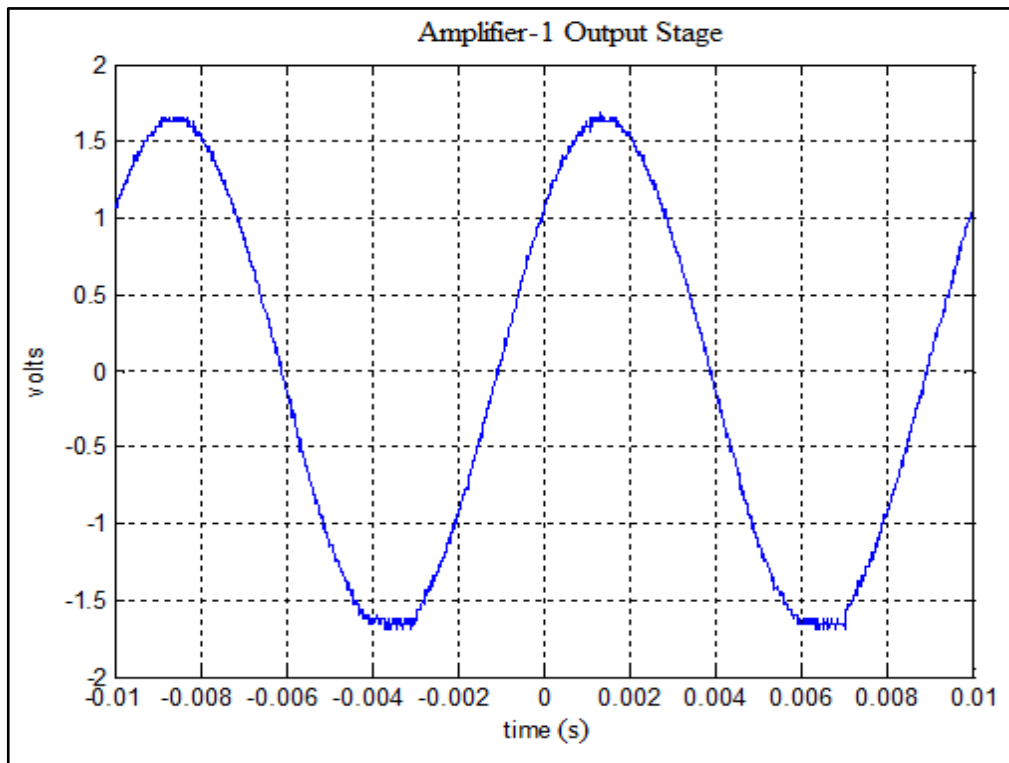


Figure 3.34. Amplifier-1 output stage

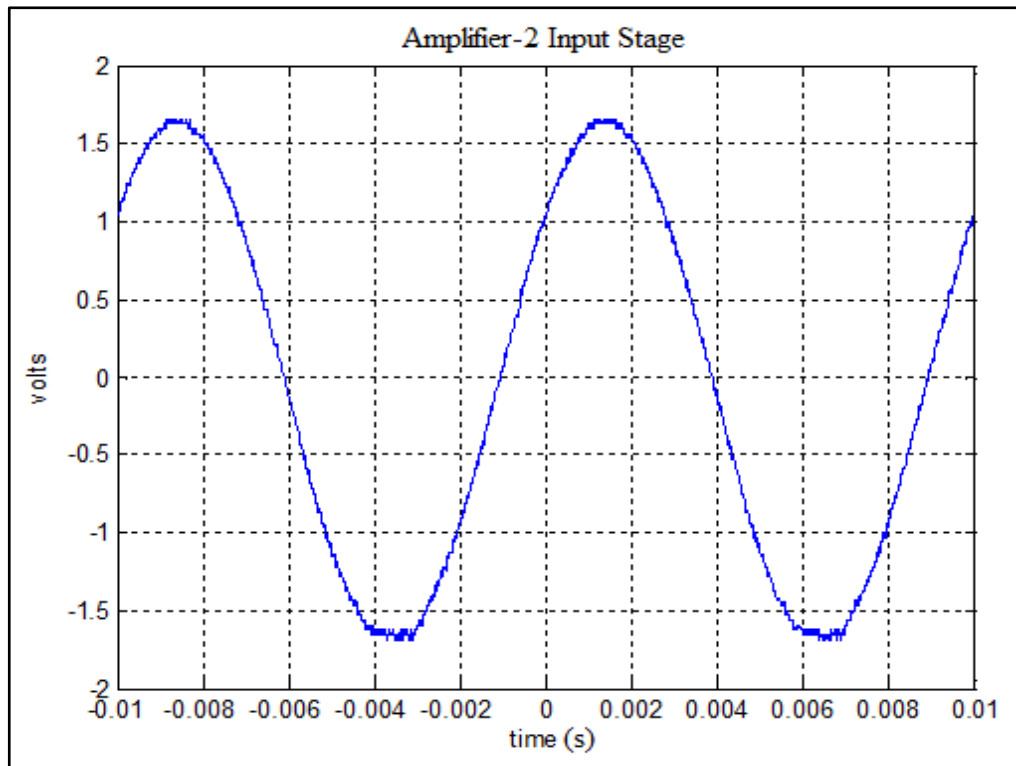


Figure 3.35. Amplifier-2 input stage

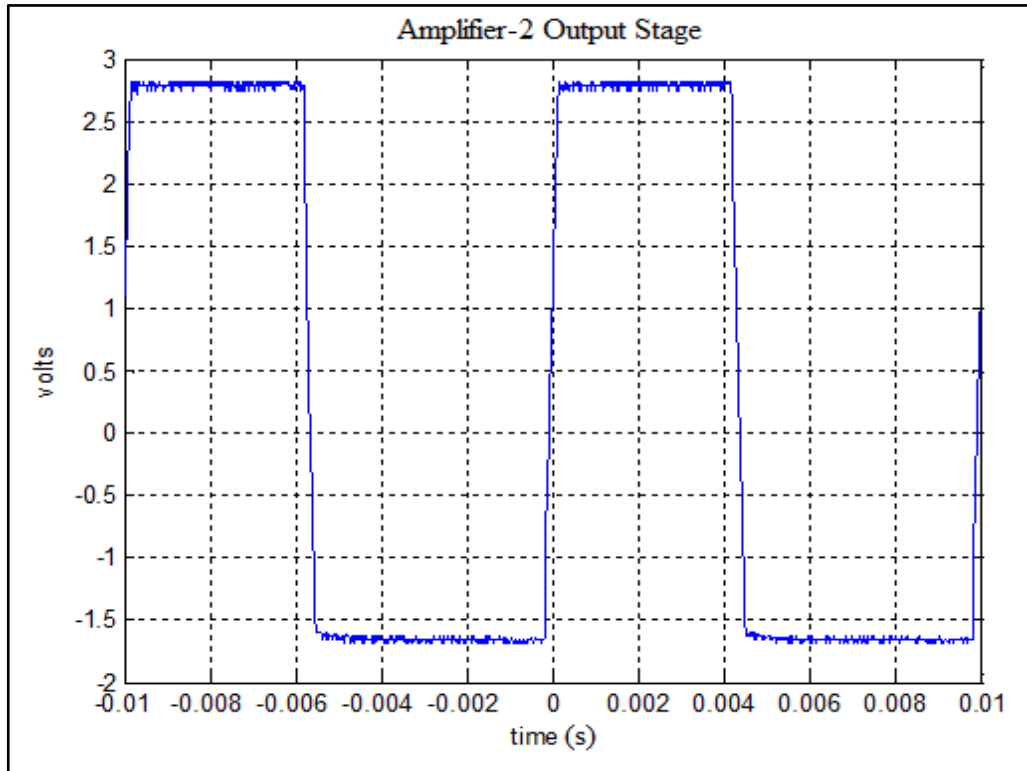


Figure 3.36. Amplifier-2 output stage

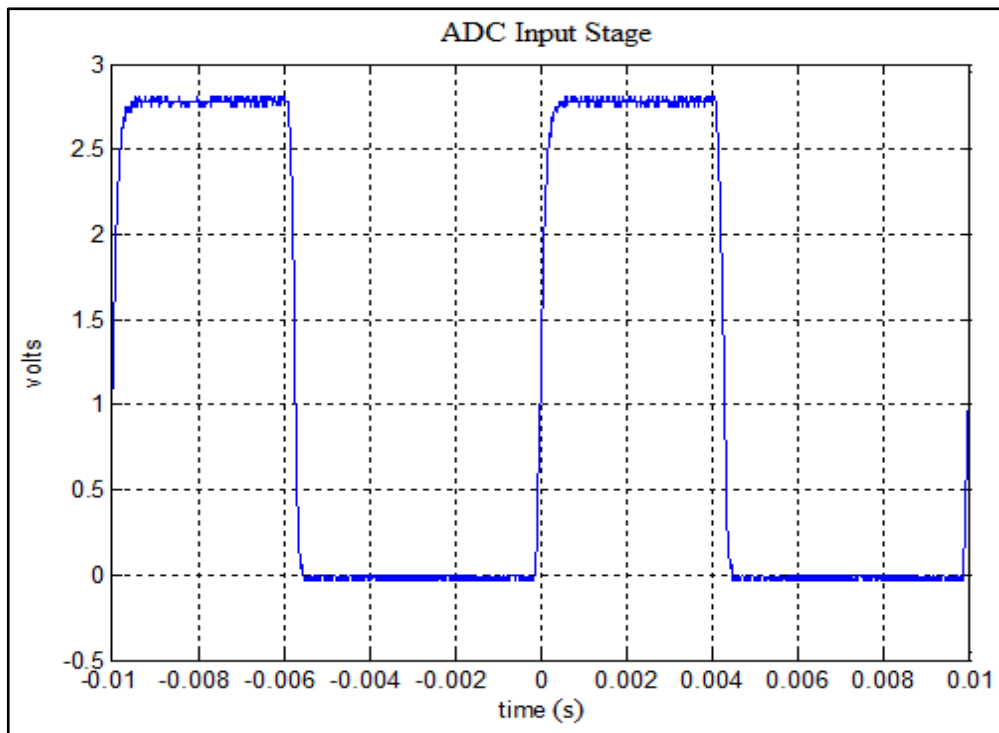


Figure 3.37. ADC input stage

It could be easily seen that first stage amplification gain is close to 10 as fixed before the measurements. In second stage amplification, the signal is cut because of the limited supply voltage.

Difference between figure 3.34 and 3.35 represents the filter-2 performance, however sinus signal which has 100 Hz frequency is in the pass band so the graphics are similar to each other.

Also the difference between figure 3.36 and 3.37 represents the filter-3, filter-4 and buffer performances together. It could be easily seen from figure 3.37 that negative part of the signal is cut by the diode.

### 3.6. GEOPHONE SENSOR EQUIVALENT CIRCUITS

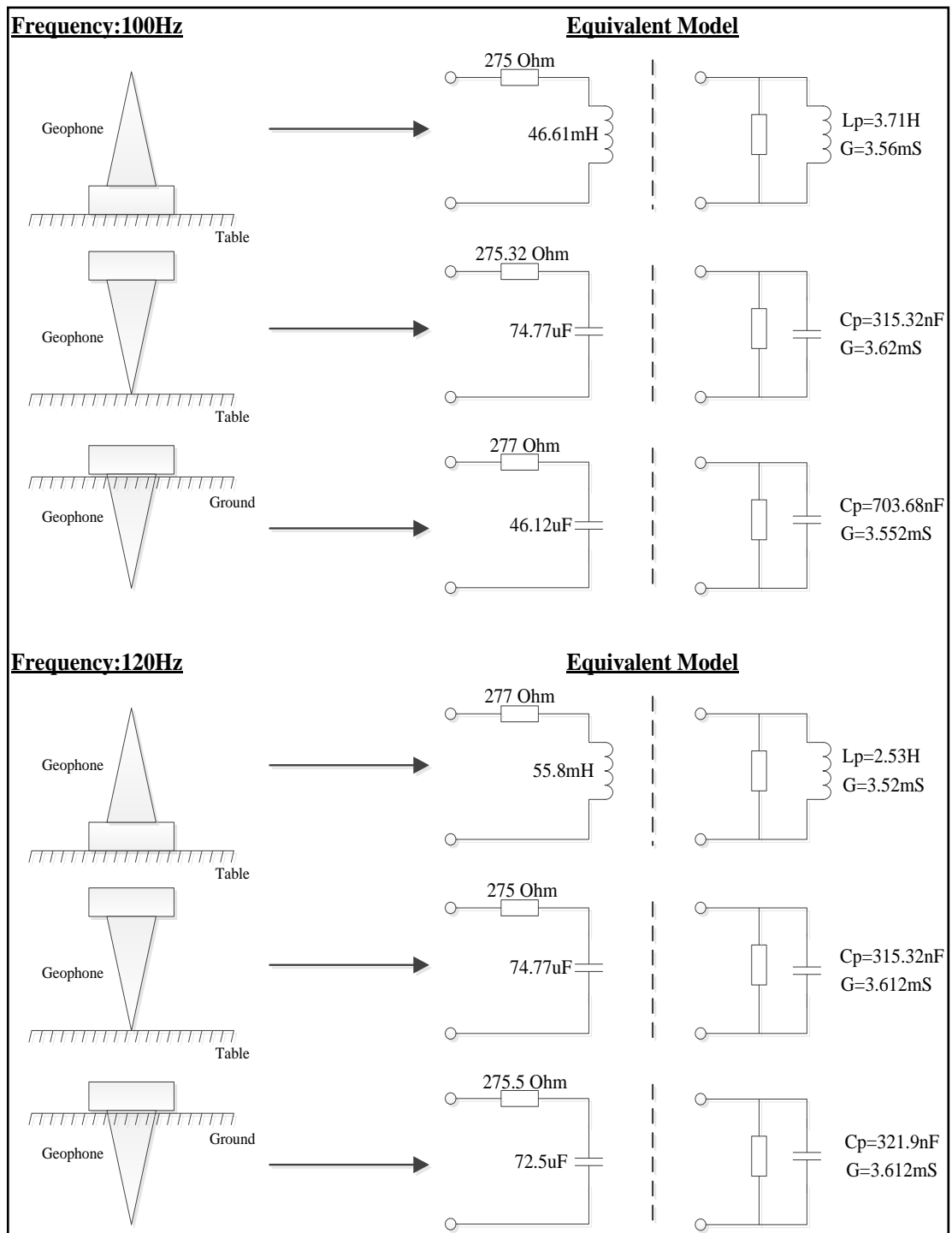


Figure 3.38. Equivalent circuits at low frequencies

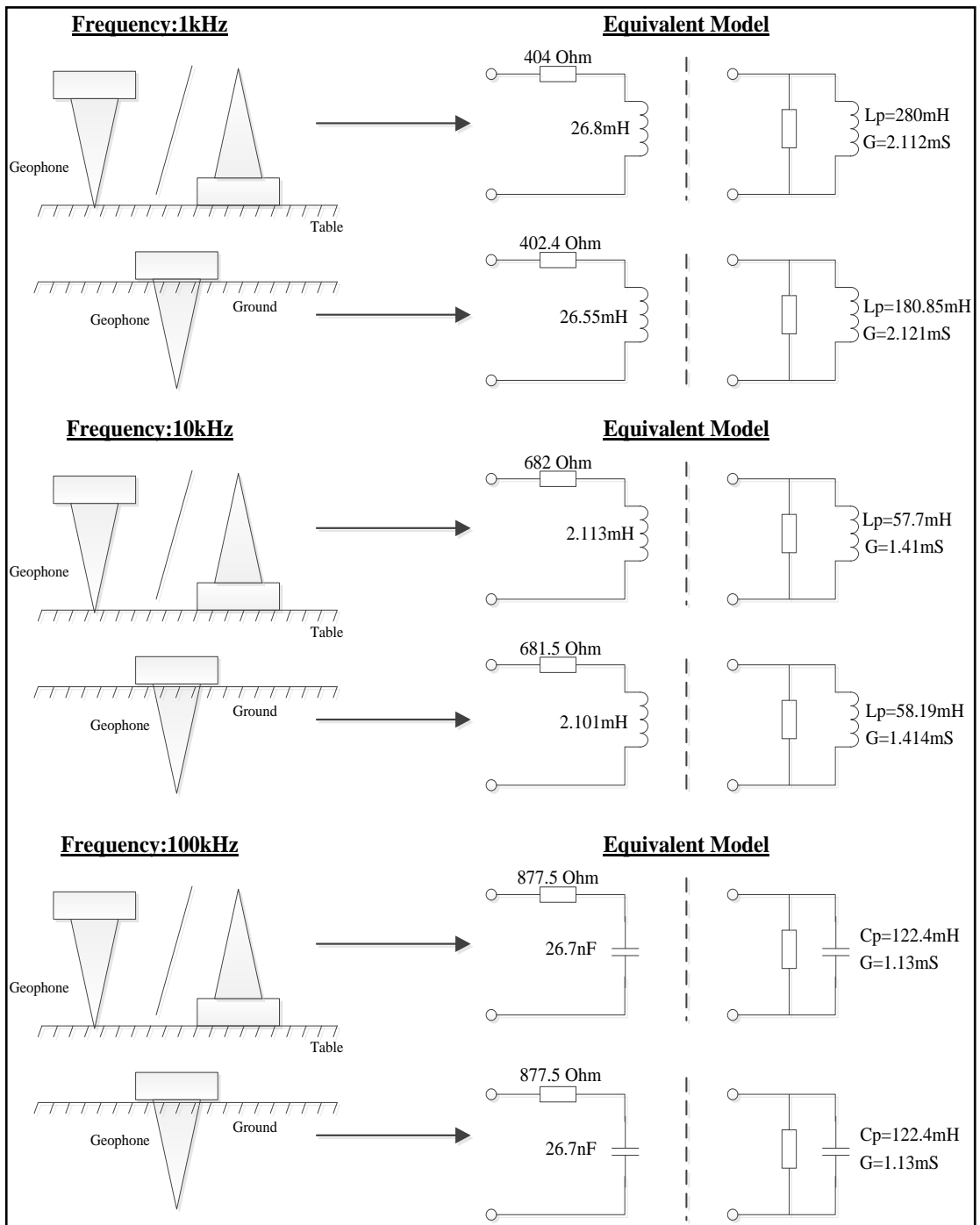


Figure 3.39. Equivalent circuits at high frequencies

## **4. WIRELESS COMMUNICATION UNIT**

In this chapter, details of the wireless communication hardware (NodeRFV2.1) are explained. Communication protocol and the hardware are designed by Genetlab Information Technologies.

### **4.1. DESCRIPTION OF THE COMMUNICATION**

NodeRF V2.1 is a control and communication board on which the sensor board is designed in this thesis. NodeRF V2.1 detects vibrations on the field by the sensors attached to it and pre-processes the detected signal for the assessment such signals. According to the outcome of this assessment, the system decides, pursuant to the previously specified assessment criteria, whether there is any reportable incident, and, if yes, the user is alerted through wireless communication via other nodes. Since the logic of such wireless communication is based on an ad hoc network architecture, the nodes automatically choose the most suitable and reliable way of communication for themselves through intercommunication with adjacent nodes. The nodes at both ends of each segment receive such data and transmit them to user by using conventional communication channels. Any gateway acts at the same time as the substitute of any other, and, as it is the case for the detecting nodes, they substitute each other in their function in case of breakdown so that the probability of shut-down of the system due to any failure in any one of the gateways is minimized. Thus, different than other systems available at the market, any segment continues to work despite any eventual damaging of the system at any point within such segments. This unique feature is an additional measure against any eventual tactical deception attempts.

The working logic of node bases on the two most important features of the wireless sensor networks: ad hoc network architecture and signal processing abilities. Nodes are communicating with each other and with the gateway using 2.4 GHz ISM band. The main properties of this two-way communication protocol are sleeping cycles, communication paths and node-alive query.



If an alarm condition occurs at a node, the node tries to deliver the corresponding alarm data to the gateway through other nodes. To reduce communication traffic and power consumption, relevant alarm data is transmitted over private path which is determined in the node. Also, alternative paths are kept in the node to avoid problems that may arise due to the environment. This hopping technique and keeping backup path also prevent communication breaks against node deaths.

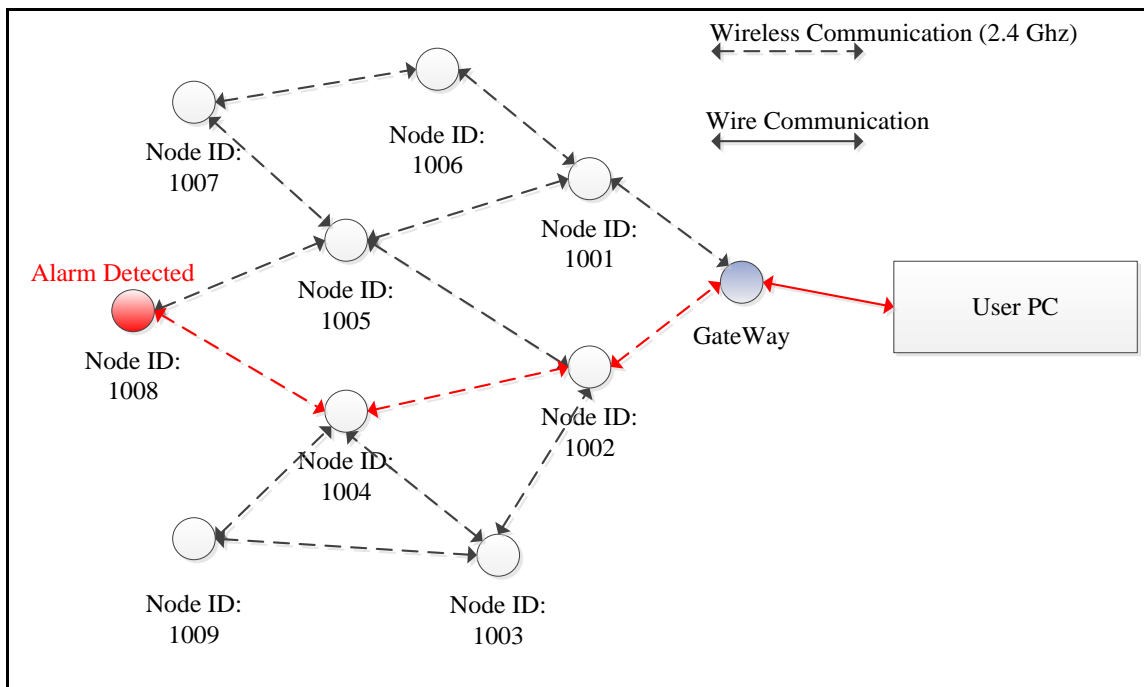


Figure 4.1 Nodes communication paths

To consume less power, sensor nodes are sleeping 17ms in each 20ms cycles unless an alarm situation is occurred or a data is heard from a different node to be transmitted. After a node generates an alarm, attempts to establish communication for 20ms to be heard by other nodes. Once obtaining the handshake between relevant nodes, data transmission begins. *Node alivequery* is an important property of these types of systems. First of all, Gateway sends a specific data periodically to the nodes in the system. Nodes read this data and mark themselves on it, then send it to another node to do the same thing. Finally, the data sent by gateway, returns to gateway with node markings. Gateway checks the markings to notify user about the missing nodes.

## 4.2. HARDWARE

NodeRFV2.1 is the sensor node developed by Genetlab in 2006. It is compatible with the TinyOS and Genos operating systems. To achieve WSN functions, it has several components such as; micro-controller, RF communication device, RF front-end amplifier, connectors and external flash. Sensor board is shown in Fig. 4.2.

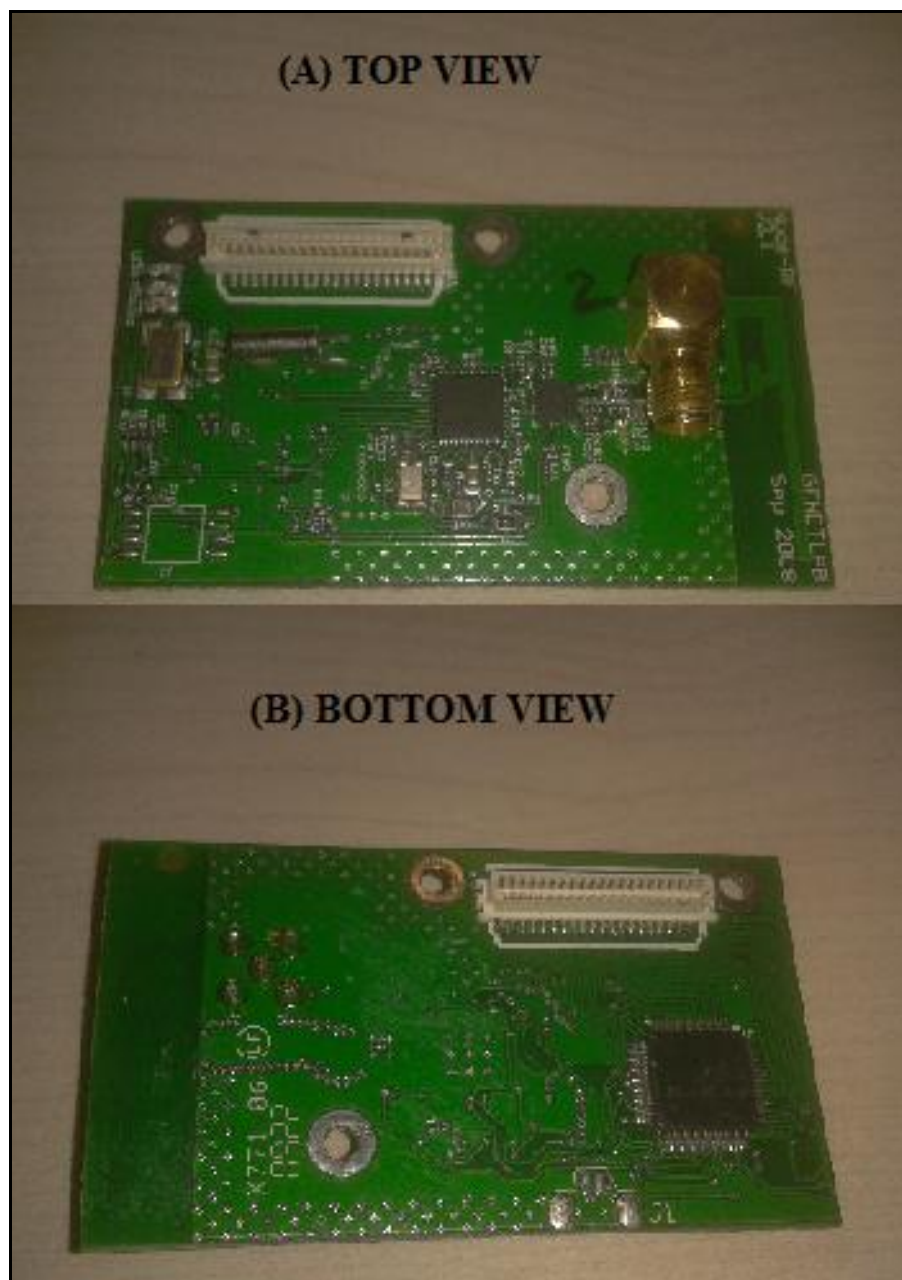


Figure 4.2. NodeRFV2.1 photos, a) Top view, b) Bottom view

Technical details of the node are summarized in Table 4.1.

Table 4.1. NodeRFV2.1 technical specifications

<b>NODE RF V2.1 Technical Specifications</b>	
<b>Communication Properties</b>	<b>Value</b>
RF IC	TI CC2420
RF Amplifier IC	TI CC2591
Central Frequency	2.4GHz
Channel Number	16
Transmission Rate	250kbps
Maximum Output Power	16dBm
Minimum Output Power	- 25dBm
Receive Sensitivity	-98dBm
<b>MCU Properties</b>	<b>Value</b>
MCU	TI MSP430F1611
Operating System	Genos
Programable Flash Memory	48kB
Data RAM	10kB
Serial Ports	2 x USART
Analogue Digital Converter	8-channel 12-bit

Low power operation of NodeRFV2.1 is mainly due to the ultra-low power microcontroller (Texas Instruments MSP430 F1611) with 10kB of RAM, 48kB of flash, and 128B of information storage. This 16-bit RISC processor features extremely low active and sleep current consumption that permits nodes to run for years on a single pair of AA batteries. The MSP430 has an internal digitally controlled oscillator (DCO) that can operate up to 8MHz. NodeRFV2.1 also has a second external crystal (8MHz) for a more stabilized main clock.

The MSP430 has 8 external ADC ports and 8 internal ADC ports. A variety of peripherals are available including SPI, UART, digital I/O ports, watchdog timer, and timers with capture and compare functionality. The F1611 also includes a 2-port 12-bit DAC module, Supply Voltage Supervisor, and 3-port DMA controller. The features of the MSP430F1611 are presented in detail in [37].

Table 4.2. MSP430F1611 technical specifications [37]

<b>MSP430F1611 Tech. Spec.</b>	<b>MIN.</b>	<b>NOM.</b>	<b>MAX.</b>	<b>UNIT</b>
Supply voltage during program execution	1.8		3.6	V
Supply voltage during flash memory programming	2,7		3.6	V
Operating free air temperature	-40		85	°C
Low frequency crystal frequency		32768		kHz
Active current at V <sub>cc</sub> =3V, 1MHz		500	600	μA
Sleep current in LPM3 V <sub>cc</sub> =3V, 32.768kHz active		2.6	3	μA
Wake up from LPM3 (low power mode)			6	μs

NodeRFV2.1 uses the ST M25P80 40MHz serial code flash for external data and code storage. The flash holds 1024kB of data and is decomposed into 16 segments, each 64kB in size. The flash shares SPI communication lines with the CC2420 transceiver. Care must be taken when reading or writing to flash such that it is interleaved with radio communication, typically implemented as a software arbitration protocol for the SPI bus on the microcontroller.

Table 4.3. ST M25P80 technical specifications [38].

<b>ST M25P80 Tech. Spec.</b>	<b>MIN</b>	<b>NOM</b>	<b>MAX</b>	<b>UNIT</b>
Supply voltage during flash memory programming	2.7		3.6	V
Operating free air temperature	-40		85	°C
Erase/Programming cycles			100	cycles
Data Retention			20	Years
Active current (READ)			4	mA
Active current (WRITE/ERASE)			20	mA
Standby current		8	50	μA
Deep Power Down current		1	10	μA

The NodeRFV2.1 can be programmed through JTAG port of the microcontroller. All JTAG compatible programs can be used for programming nodes like “mspgcc”. For TinyOS, typing “make sensenode install jtag” will install the program to module.

NodeRFV2.1 uses Chipcon CC2420 radio for wireless communications [39]. The CC2420 is an IEEE 802.15.4 compliant radio providing the PHY and some MAC functions. With sensitivity exceeding the IEEE 802.15.4 specifications and low power operation, the CC2420 provides reliable wireless communication. The CC2420 is highly configurable for many applications with default radio settings providing IEEE 802.15.4 compliance. The CC2420 is controlled by TI MSP430 microcontroller through SPI port, digital I/O lines and interrupts. The radio may be shut down by the microcontroller for low power duty cycled operation. The CC2420 has programmable output power.

Table 4.4. Output power configuration of CC2420 [39].

PA_LEVEL	TXCTRL register	Output Power (dBm)	Current Consumption (mA)
31	0xA0FF	0	17.4
27	0xA0FB	-1	16.5
23	0xA0F7	-3	15.2
19	0xA0F3	-5	13.9
15	0xA0EF	-7	12.5
11	0xA0EB	-10	11.2
7	0xA0E7	-15	9.9
3	0xA0E3	-25	8.5

Table 4.5. CC2420 technical specifications [39].

CC2420 Tech. Spec.	MIN.	NOM.	MAX.	UNIT.
Supply voltage during radio operation (Vreg on)	2.1		3.6	V
Operating free air temperature	-40		85	°C
RF frequency range	2400		2483.5	MHz
Transmit bit rate	250		250	Kbps
Nominal output power	-3	0		dBm
Programmable output power range		40		dBm
Receiver sensitivity	-90	-94		dBm
Current consumption: Radio transmitting at 0 dBm		17.4		mA
Current consumption: Radio receiving		19.7		mA
Current consumption: Radio on, Oscillator on		365		µA
Current consumption: PowerDown mode, Vreg off			1	µA
Voltage regulator current draw	13	20	29	µA
Radio oscillator startup time		580	860	µs

To improve communication range, front-end amplifier is utilized with CC2420. This front-end amplifier is CC2591 and its technical specifications are given in Table 4.6 [40]. what is max output power?.

Table 4.6. CC2591 technical specifications [40]

CC2591 Tech. Spec.	Test Condition	Min.	Typ.	Max.	Unit
RF Transmit					
Gain			22		dB
Output power, POUT	PIN = 0.5 dBm		20.6		dBm
Maximum output power	PIN = 5 dBm		22		dBm
Power Added Efficiency, PAE	PIN = 0.5 dBm		34%		
Output 1 dB compression			19		dBm
2nd harmonic power			-15		dBm
3rd harmonic power			-30		dBm
Receive Current	High Gain Mode HGM=1		3.4	4	mA
Transmit Current	PIN = 0.5 dBm		112		mA
Transmit Current	No Signal Input		40	50	mA
Power Down Current	EN = PAEN = 0		0.1	0.3	$\mu$ A
High input level (control pins)	EN, PAEN, HGM, RXTX	1.3		VCC	V
Low input level (control pins)	EN, PAEN, HGM, RXTX			0.3	V
Power down - Receive mode switching time			12		$\mu$ S
Power down - Transmit mode switching 1 ms time			1		$\mu$ S
<b>RF Reciever</b>					
Gain, High Gain Mode	HGM = 1		11		dB
Gain, Low Gain Mode	HGM = 0		1		dB
Gain Variation, 2.0 - 3.6 V	HGM = 1		1.3		dB
Gain Variation, 40 °C to 50 °C	HGM = 1		3		dB
Noise figure, High Gain Mode	HGM = 1		4.8		dB
Input 1 dB compression	HGM = 1		-17		dBm
Input IP3	HGM = 1		-2		dBm
Input reflection coefficient, S11	HGM = 1		-11		dB

NodeRFV2.1 can be powered by two AA batteries from two different input ports. While one of these inputs (J1) has direct connection to the system, other input (J2) has voltage matching circuit with stabilized output of 3.3V for an input range 0.6V-3.6VDC. While using the J1 input the module was designed to fit the two AA battery form factor and AA cells may be used in the operating range from 2.1 to 3.6V DC, however the voltage must be at least 2.7V when programming the microcontroller flash or external flash. Both inputs provide power to the module but at no point should the input voltage exceed 3.6V to prevent any damage to the microcontroller, radio, or other parts.

Table 4.7 NodeRFV2.1 power specifications

<b>NodeRFV2.1 Power Spec.</b>	<b>MIN</b>	<b>MAX</b>	<b>UNIT</b>
Supply voltage (J1)	2.1	3.6	V
Supply voltage (J2)	0.6	3.6	V
Supply voltage during flash memory programming (J1)	2.7	3.6	V
Supply voltage during flash memory programming (J2)	0.6	3.6	V
Operating free air temperature	-40	85	°C
Current Consumption: MCU on, Radio RX	21.8	23	mA
Current Consumption: MCU on, Radio TX	100.5	120	mA
Current Consumption: MCU on, Radio off	1800	2400	μA
Current Consumption: MCU idle, Radio off	54.5	1200	μA
Current Consumption: MCU standby	<1		μA

## **5. SIGNAL PROCESSING ALGORITHM**

In the first chapter, the method used for the detection of footsteps and vehicle movements is detailed. In addition, suitability of this method in a WSN is evaluated. The most important factors determining the appropriate signal processing software are limited power, limited memory size, detection range and intruder classification.

Detection methods are usually based on either time or frequency domain. The unsuitability of FFT based methods were mentioned in Chapter 1. In addition, frequency components of vehicle and footsteps can easily overlap due to vibration transmission characteristics of the soil.

High frequency vibrations decay faster than low frequency vibrations so that the frequency components of a signal can be difficult to differentiate depending on measurement distance. In addition, vibration transmission characteristics are dependent on the soil type and weather conditions. WSN compatible, time domain based signal processing method for footstep and vehicle movement detection is designed considering all these points mentioned in this study.

### **5.1. ALGORITHM**

Algorithm is real-time and analyses the durations of signals. Before describing the algorithm, some of the important parameters of footstep and vehicle detection should be determined. As mentioned before, there are several continuous noise sources such as elevators, cranes, high power generators and wind. These types of continuous noise sources generate noise at the same frequency of footsteps and vehicle movements. Rain is not a continuous noise source so it is defined as a classification object.

In the algorithm, there are three main parts: thresholds, duration calculator-filter and classification and alarm decision as shown in Fig. 5.1.



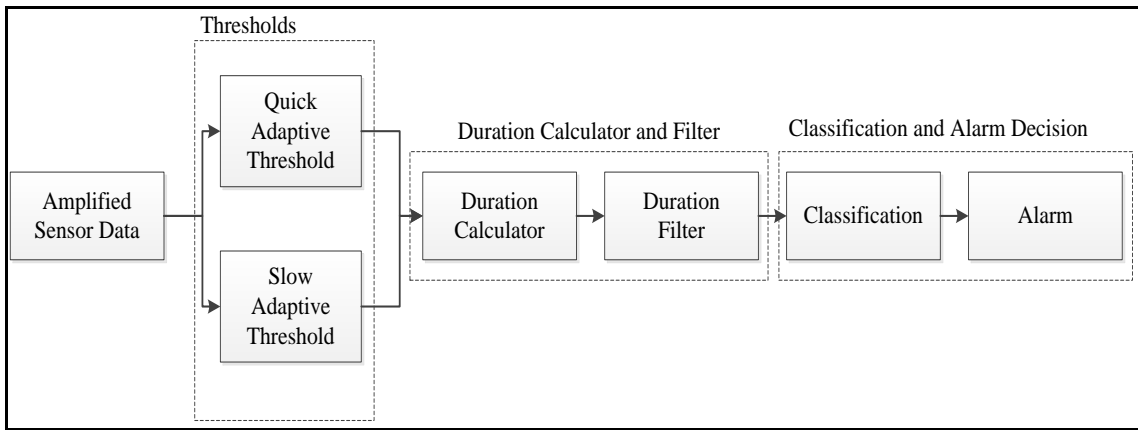


Figure 5.1. Main parts of the signal processing algorithm

Two different thresholds are used to determine the durations of the signals. Slow adaptive threshold (SAT) is following the noise level with a static and dynamic offset. SAT is designed to eliminate continuous noise effects from the classification by taking the average of the last incoming 10 thousand amplified sensor data and adding the offset values. To determine offset values a power factor of average (PFA) is defined. PFA is simply a scalar number. PAF empirically reflects maximum level of ambient noise to average noise. We used a PFA value of 3 in our algorithm to state that maximum noise level is most likely 3 times larger than the average, which is calculated for the last M data points (10K in our algorithm). Another scale factor called dynamic offset scale (DOS) is also defined to account for soil and weather induced noise effects. Static offset is hardware dependent and is based on ambient noise level received by the sensor for the target detection range. The SAT value is stated in (2). It is calculated at every data point.

$$\forall i \in DataSize, \quad i = [1, 2, \dots, DataSize] \quad (5.1)$$

$$SAT(i) = Static\ Offset + Dynamic\ Offset * PF\ of\ Average * \frac{\sum_{k=i-Size\ Mem1}^i Data(k)}{Size\ Mem1} \quad (5.2)$$

In a single intruder vibration signal, it is clearly seen that signal is fluctuating between ground and local maximum. To calculate above-noise durations and filtering noise, quick adaptive threshold (QAT) is defined. QAT is functioning by taking the average of last incoming 30 amplified sensor data and multiplying the result with the predetermined PFA.

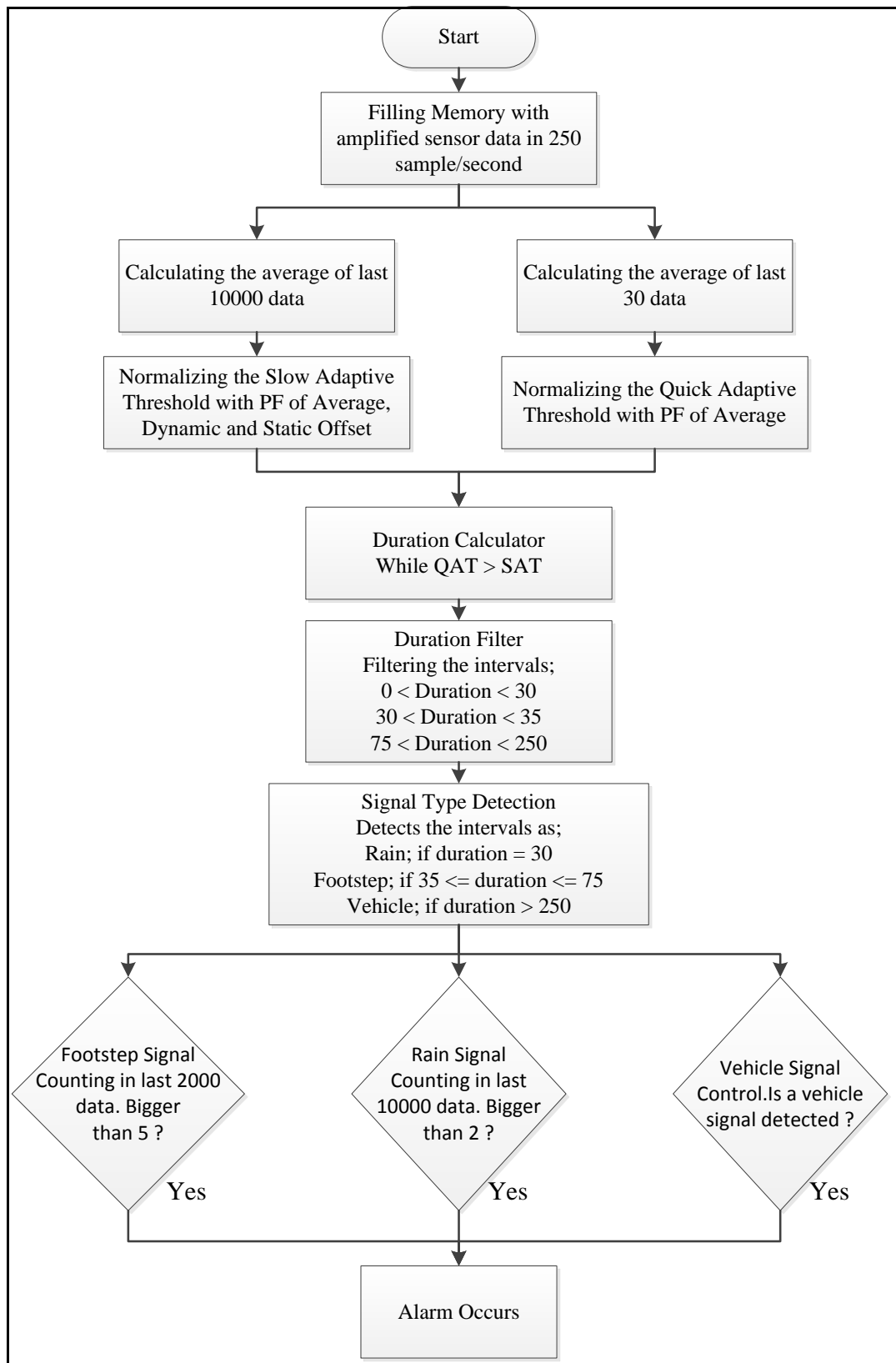


Figure 5.2. Signal processing algorithm flow chart

With QAT, amplified signals get smoother and energy of these signals aids the classification of intrusion, especially presence of rain.

$$QAT(i) = PF \text{ of Average} * \frac{\sum_{k=i-Size\ Mem2}^i Data(k)}{Size\ Mem2} \quad (5.3)$$

Duration calculator function termed as “DR” in (5.4) counts samples if QAT value is higher than the SAT value. With that, duration of the intruder vibration signals are determined and noise signal is cancelled out from calculations.

$$if(x) = \begin{cases} 1, & x \text{ is True} \\ 0, & x \text{ is False} \end{cases} \quad (5.4)$$

$$DR(i) = (DR(i-1) + 1) * if(QAT(i) > SAT(i)) \quad (5.5)$$

After calculating the durations, to minimize false alarm rate, a filtering method is used called “DRF” (Duration Filter). DRF removes durations from the system to improve true alarm rates. In Figure 5.3., relative filtering parameters are defined. DRF function removes durations in the interval A, B, D but does not remove specific duration sizes mentioned in the Figure 5.3..

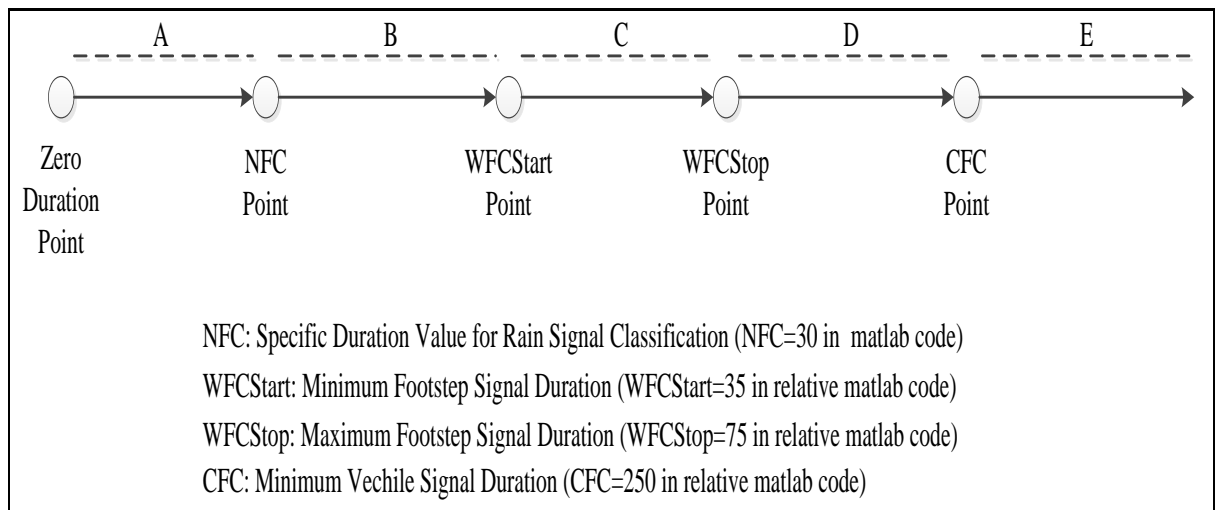


Figure 5.3. Definitions on signal durations

$$\begin{aligned}
DRF(i) = DR(i) * if(DR(i) \geq DR(i + 1)) * (if(DRF(i) = NFC) \\
+ if(WFCStart \leq DRF(i) \leq WFCStop) + if(DRF(i) \geq CFC))
\end{aligned} \tag{5.6}$$

The next step is classifying the intruder from filtered duration sizes. Again, intervals and the duration marks in Figure 5.3 are used to detect the type of the signal. For example, if the filtered duration value is in interval C, then that signal is named as a single footstep. “SA” function (single alarm) given in (5.7) chooses only one signal type which are termed as “RV” (Rain vibration constant), “FV” (Footstep vibration constant), “CV”(Vehicle vibration constant). With this method, type of the signal is being identified. Other parameters are given in Table 5.1.

$$\begin{aligned}
SA(i) = if(DRF(i) * RV + if(WFCStart < DRF(i) < WFCStop) \\
* FV + if(DRF(i) > CFC) * CV
\end{aligned} \tag{5.7}$$

Final stage of the algorithm is classification of signals. To reduce false alarm rates, repetition of similar type signals are examined. To implement this function, virtual memory slots called “RM” (Rain Memory), “FM” (Footstep Memory) and “CM” (Vehicle Memory) are monitoring the “SA” function and collecting correct signals into their memory cells. At the decision stage, “A” (Alarm) function checking these memory slots and count the signal numbers. If the number of signals in the memories exceeds a threshold value, intruder alarm, rain alarm or vehicle alarm is generated.

$$RM(i) = \sum_{k=i-RMS}^i SA(k) * if(DRF(k) = NFC) \tag{5.8}$$

$$FM(i) = \sum_{k=i-FMS}^i SA(k) * if(WFCStart < DRF(k) < WFCStop) \tag{5.9}$$

$$CM(i) = SA(i) * if(DRF(i) > CFC) \tag{5.10}$$

$$\begin{aligned}
A(i) = RM(i) * if(RM(i) > 2) + FM(i) * if(FM(i) > 10) + \\
(CM(i) + 2) * if(CM(i) > 0)
\end{aligned} \tag{5.11}$$

All these functions are implemented in a m-file called “A Footstep and Vehicle Detection Algorithm” also all other details are described in the comment lines of the code.

Table 5.1. Definitions of constants in signal processing algorithm

<b>Constant Name</b>	<b>Value</b>	<b>Definition</b>
Size_Mem1	10000	Memory size of SAT
Size_Mem2	30	Memory size of QAT
Initial_Thr	50	Initial value of memory cells
Static_Offset	200	Static difference between SAT and QAT
Dynamic_Offset	1.3	Proportional difference between SAT and QAT
PF_of_Average	3	The standard ratio between the amplitude of a seismic signal and average.
Noise_Filter_Constant	30	Specific rain vibration duration
Walking_Filter_Constant_Start	35	Minimum duration of a single footstep vibration
Walking_Filter_Constant_Stop	75	Maximum duration of a single footstep vibration
Car_Filter_Constant	250	Minimum duration of a single vehicle vibration
Rain_Memory_Size	10000	Memory, which is used in the classification of rain.
Footstep_Memory_Size	2000	Memory, which is used in the classification of footstep
Rain_Alarm	1	Classified alarm value of rain situation.
Footstep_Alarm	2	Classified alarm value of footstep situation.
Car_Alarm	5	Classified alarm value of vehicle situation.

## 6. SYSTEM EVALUATION

### 6.1. PERFORMANCE OF SIGNAL PROCESSING ALGORITHM

All of the data in this chapter are collected with sensor board that is designed and produced in Chapter 3 and 4, also 250 sample/second sampling frequency is used. However, tests are implemented in different locations and different air conditions. In all tests, intruders are following a line where sensor is placed in the middle. Alarm called “1” is defined as rain, “2” is defined as footstep and “5” is defined as vehicle.

#### 6.1.1. Noise Performance of Signal Processing Algorithm

In noise analysis, long-term noise data were collected without moving or making any vibration on the ground.

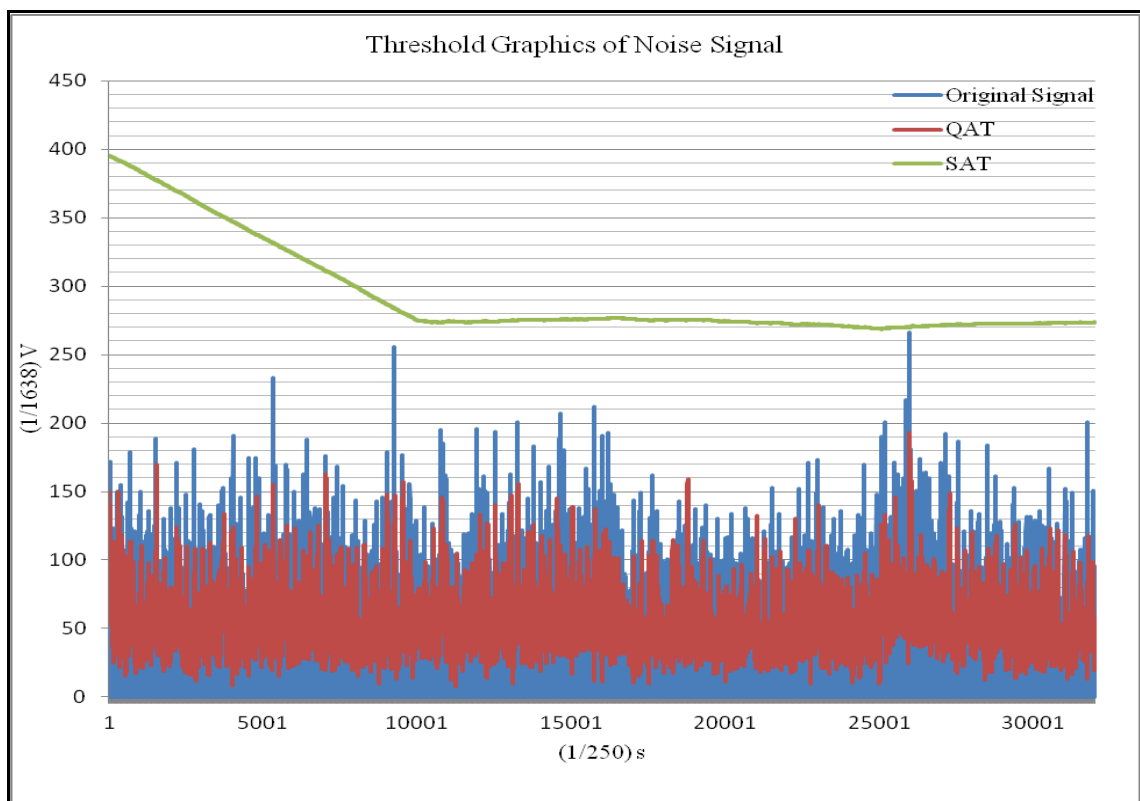


Figure 6.1 Thresholds and original signal for noise only recording.

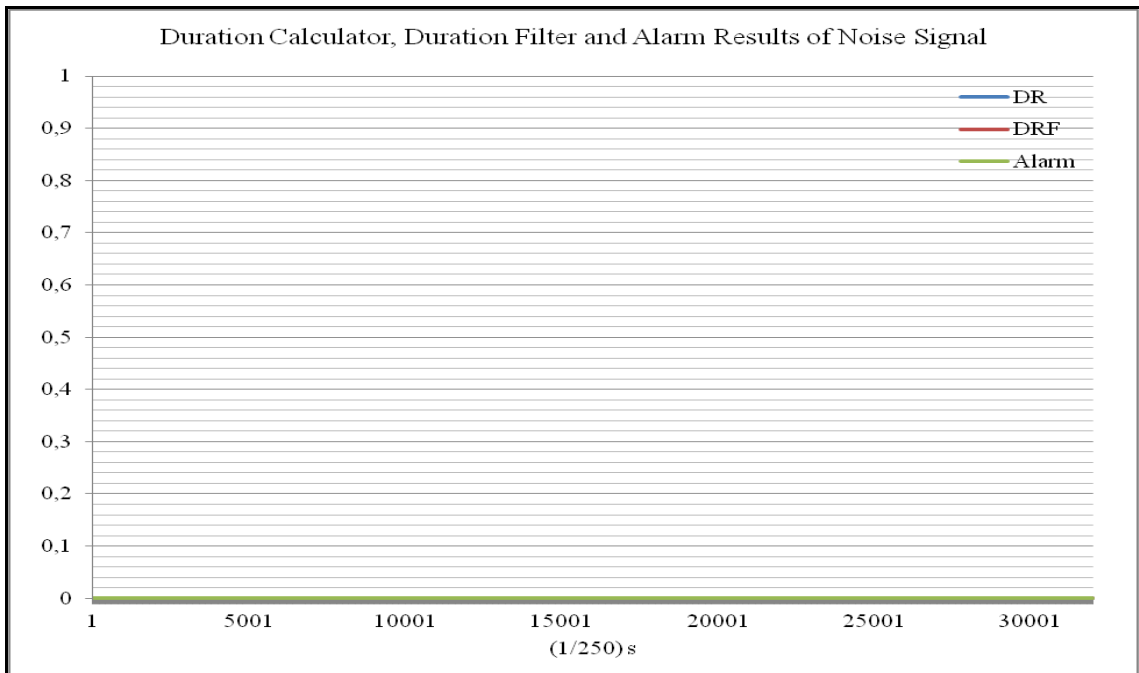


Figure 6.2 Duration, filtered duration and alarm results due to noise

As it is seen from Figure 6.2., an alarm is not being produced by the algorithm. Also QAT did not pass SAT any point of the original signal. This result is the expected behavior of the algorithm for noise listening conditions.

### 6.1.2. Footstep Detection Performance of Signal Processing Algorithm

Two type of footstep detection tests were executed in two different test locations and with two different amplification gains. In Test-1, amplification gain is chosen as 3K and in test-2 5K. In footstep tests, 30-meter path walked down and 40 footsteps were generated.

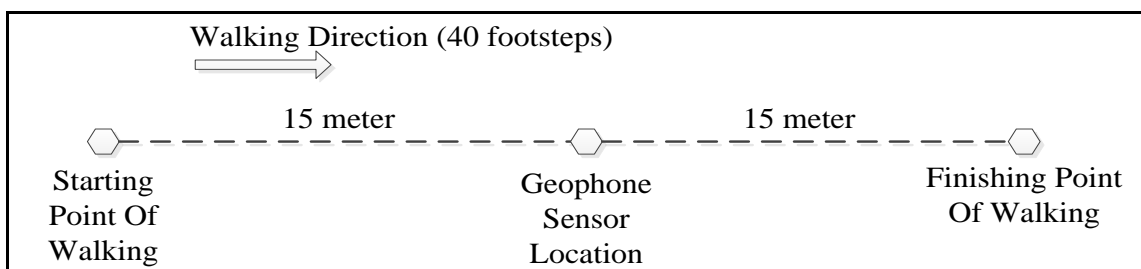


Figure 6.3. Physical test details

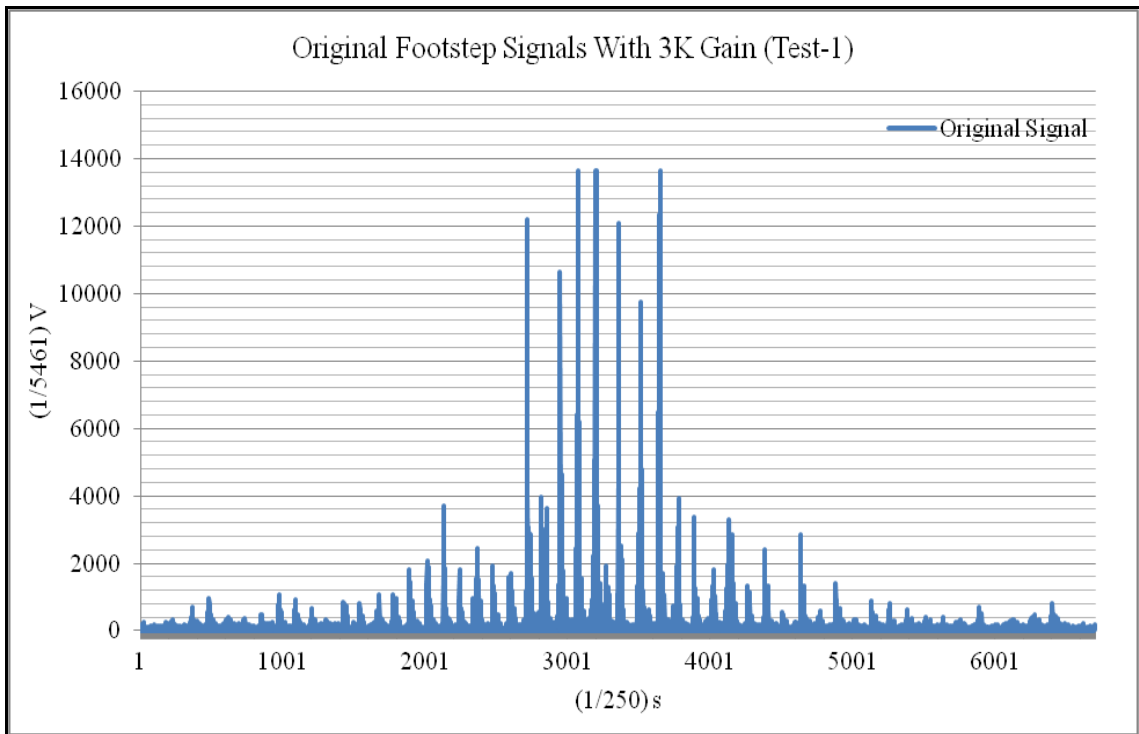


Figure 6.4. Original footstep signals with 3K gain (Test-1)

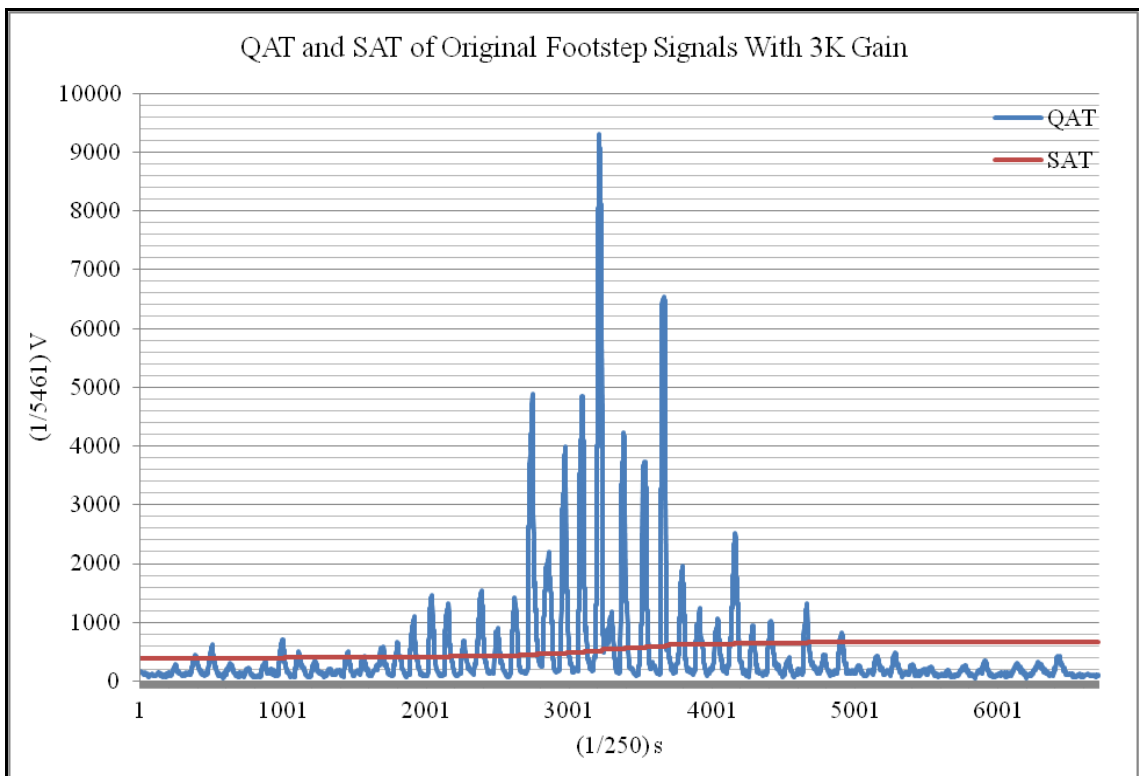


Figure 6.5. QAT and SAT of original footstep signals with 3K gain (Test-1)



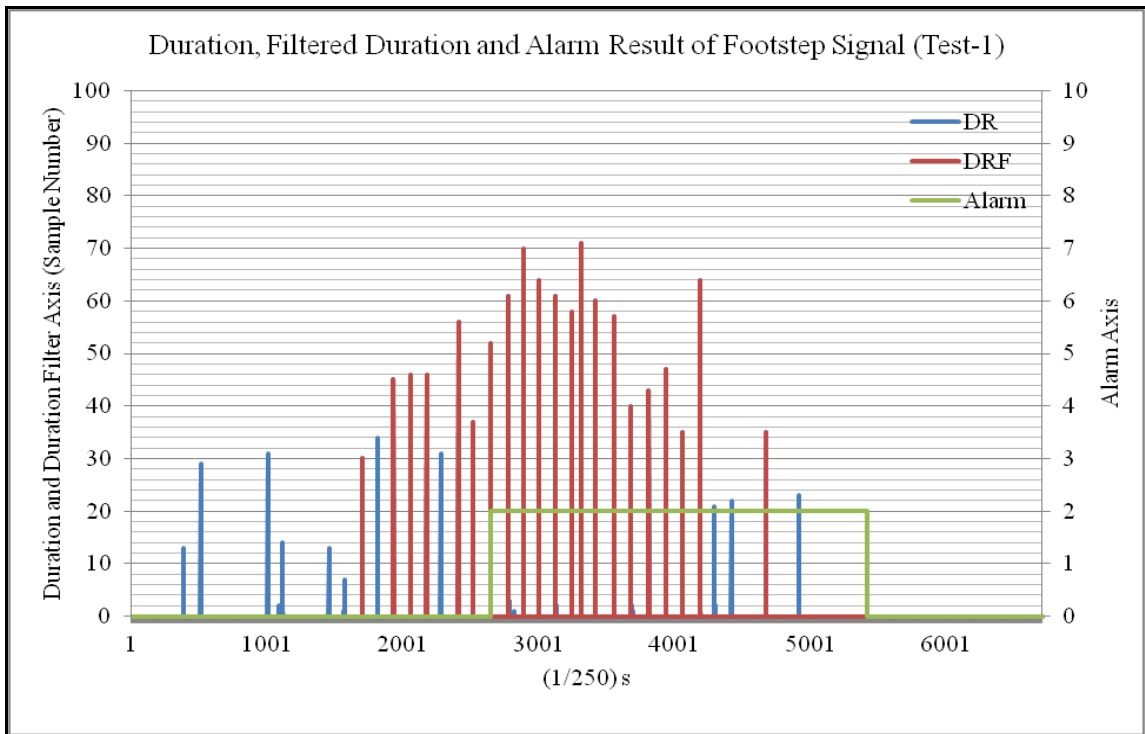


Figure 6.6. Duration, filtered duration and alarm result of footstep signal (Test-1)

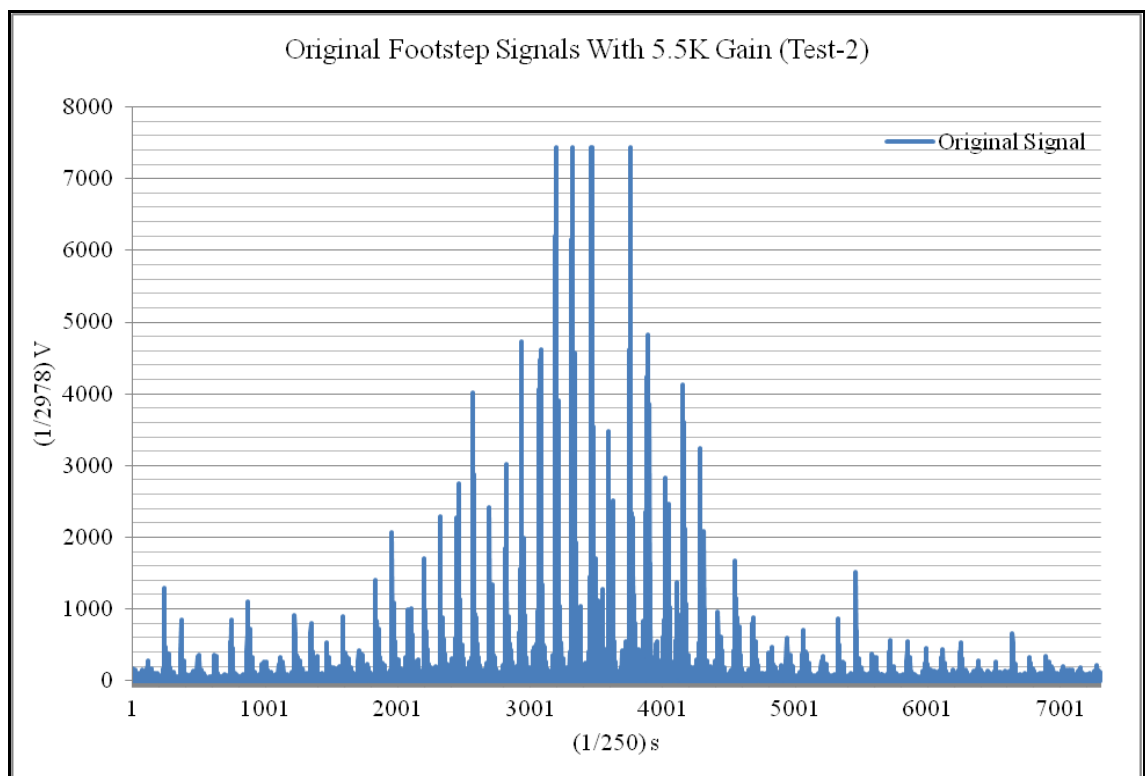


Figure 6.7. Original footstep signals with 5.5K gain (Test-2)

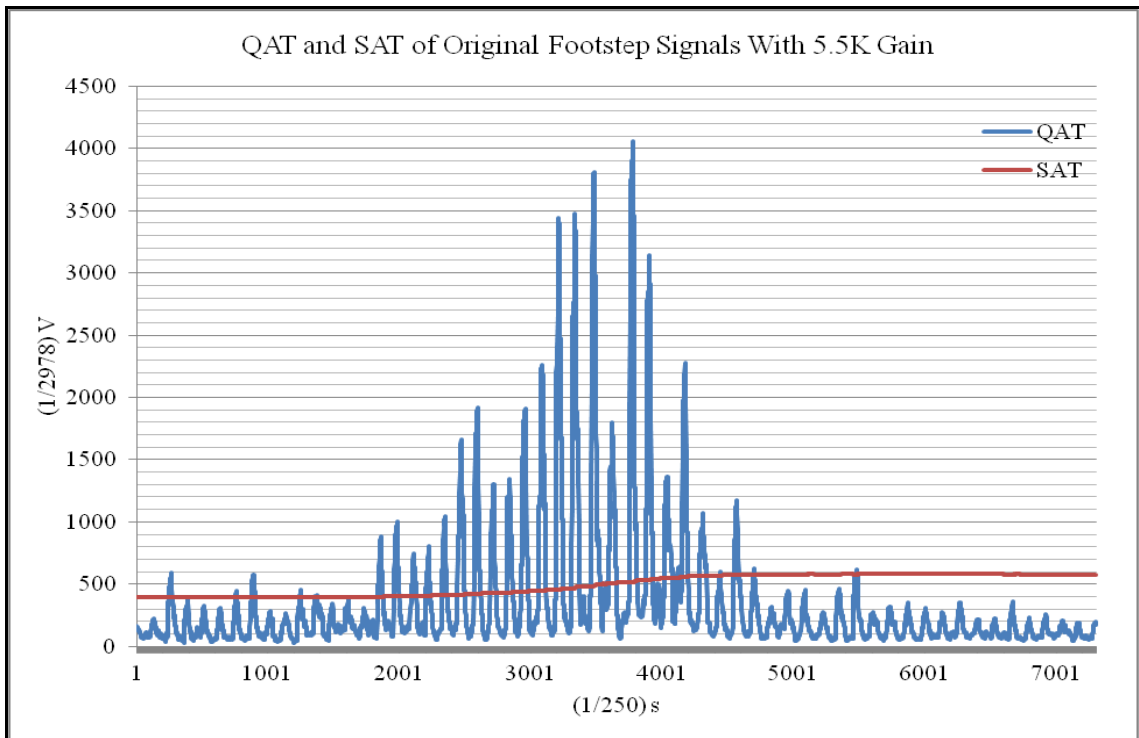


Figure 6.8. QAT and SAT of original footstep signals with 5.5K gain (Test-2)

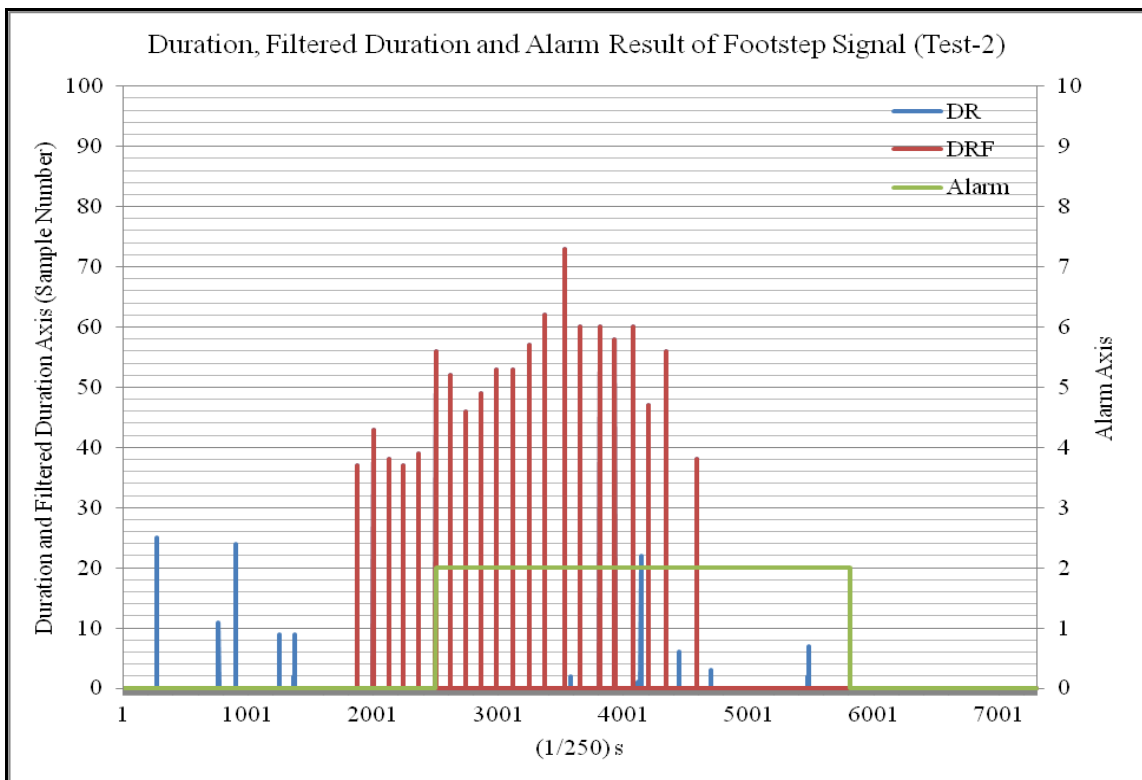


Figure 6.9. Duration, filtered duration and alarm result of footstep signal (Test-2)

Table 6.1. Footstep detection tests performance

Detected Signals	Test-1 (Figure 6.6.)	Test-2 (Figure 6.9.)
Detected as Noise	11	10
Detected as Footstep	20	21
Detected as Rain	1	0
Detected as Vehicle	0	0
Total	32	32

In both tests, 40 walking steps have been taken and only 20 of them have been detected as footsteps. With this, footstep detection range was observed to be close to 5-6 meter. 32 of 40 footsteps have been detected and 11 of them were classified as a noise.

The algorithm produced one false alarm only. Classification resulted in success.

### 6.1.3. Vehicle Detection Performance of The Signal Processing Algorithm

Two type of vehicle detection tests were executed in two different test locations and with two different vehicle speeds. In Test-1, vehicle speed is 10 Km/h and in test-2 it is 30 Km/h.

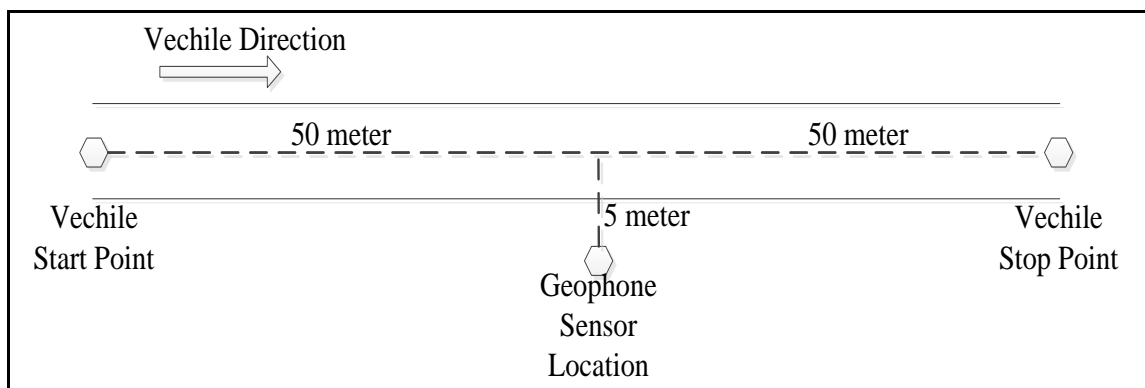


Figure 6.10 Physical test details

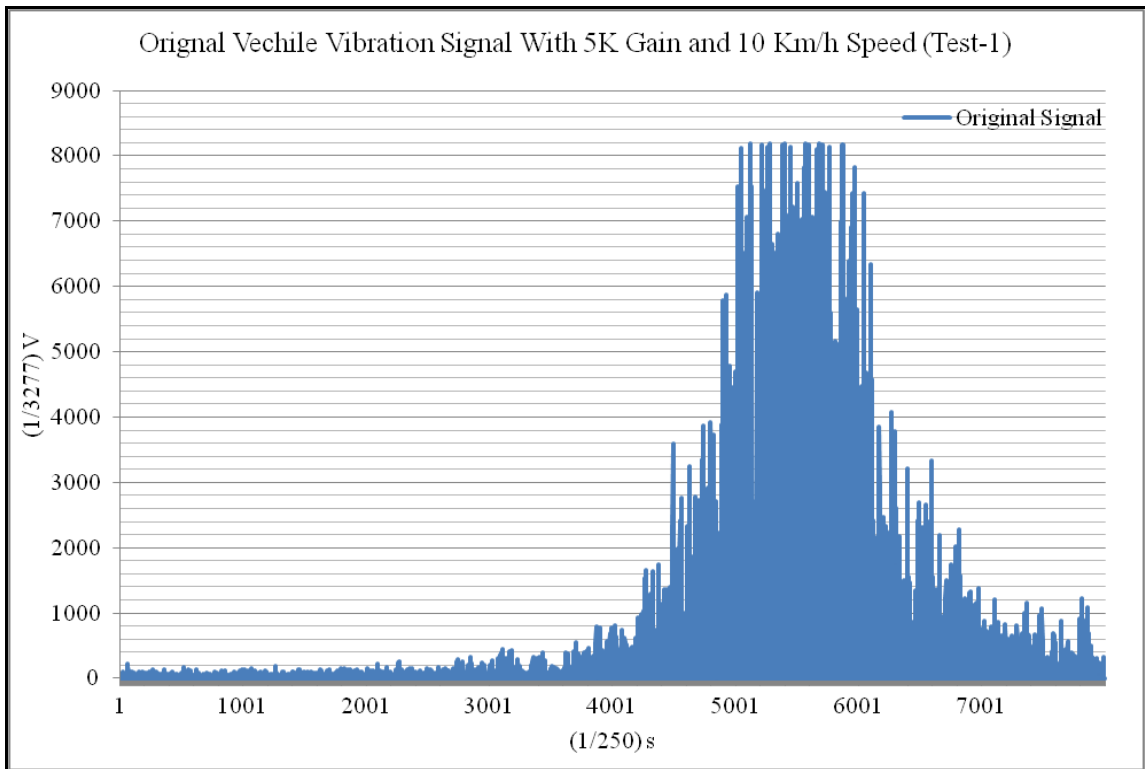


Figure 6.11. Original vehicle vibration signal with 5K gain and 10 Km/h speed (Test-1)

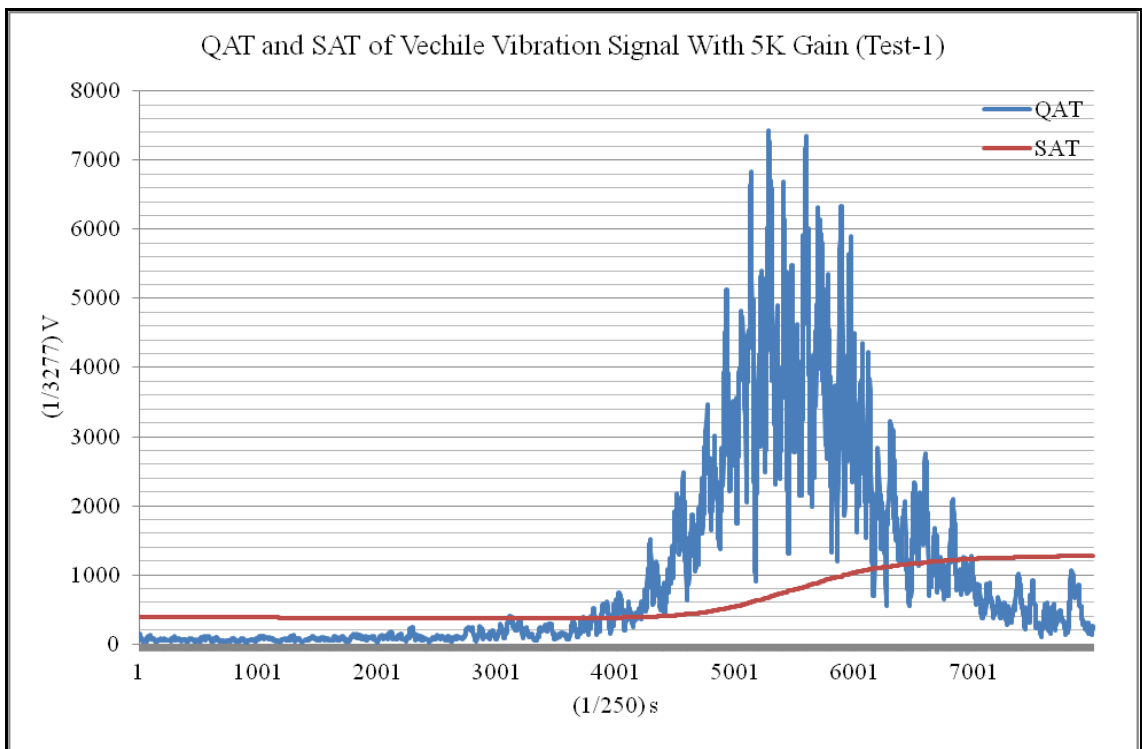


Figure 6.12. QAT and SAT of original vehicle signals with 5K gain (Test-1)

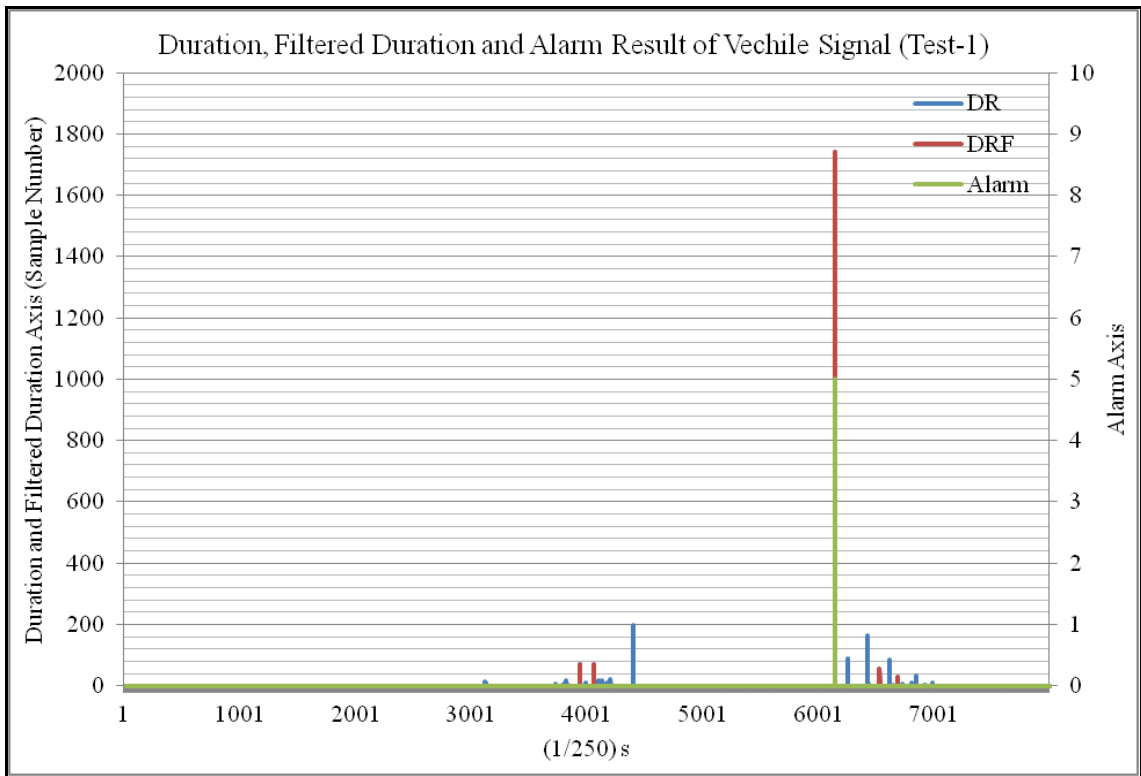


Figure 6.13. Duration, filtered duration and alarm result of vehicle signal (Test-1)

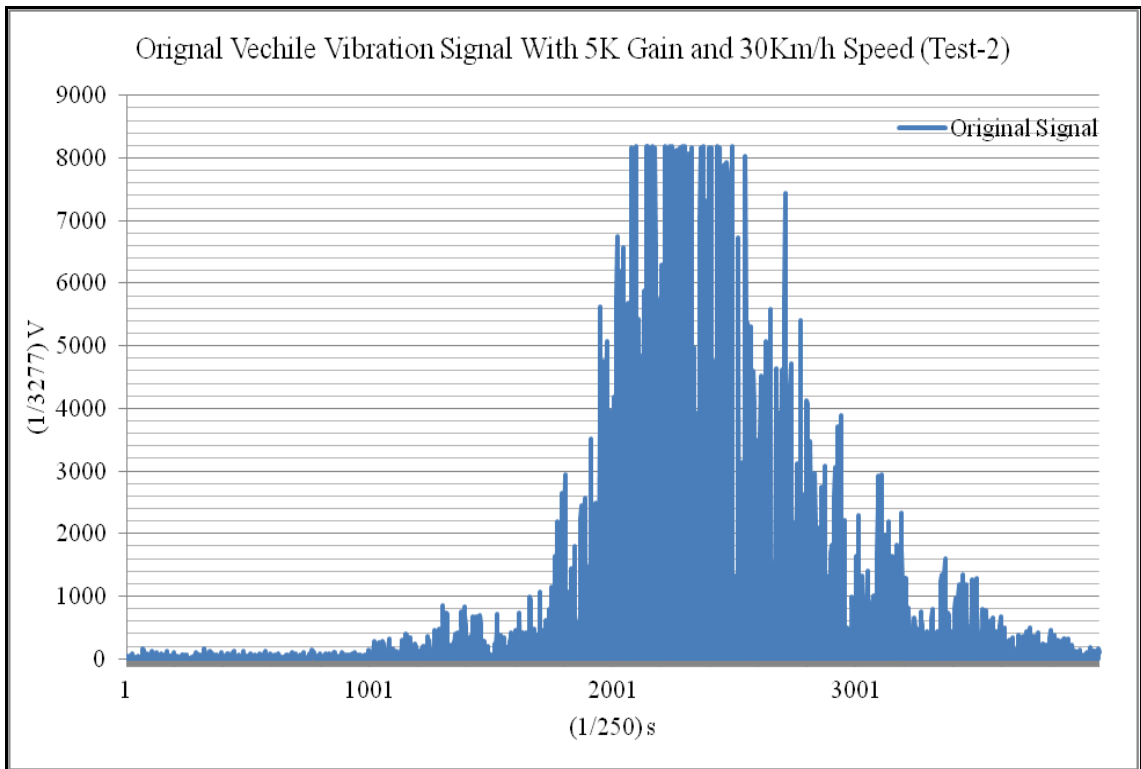


Figure 6.14. Original vehicle vibration signal with 5K gain and 30 Km/h speed (Test-2)

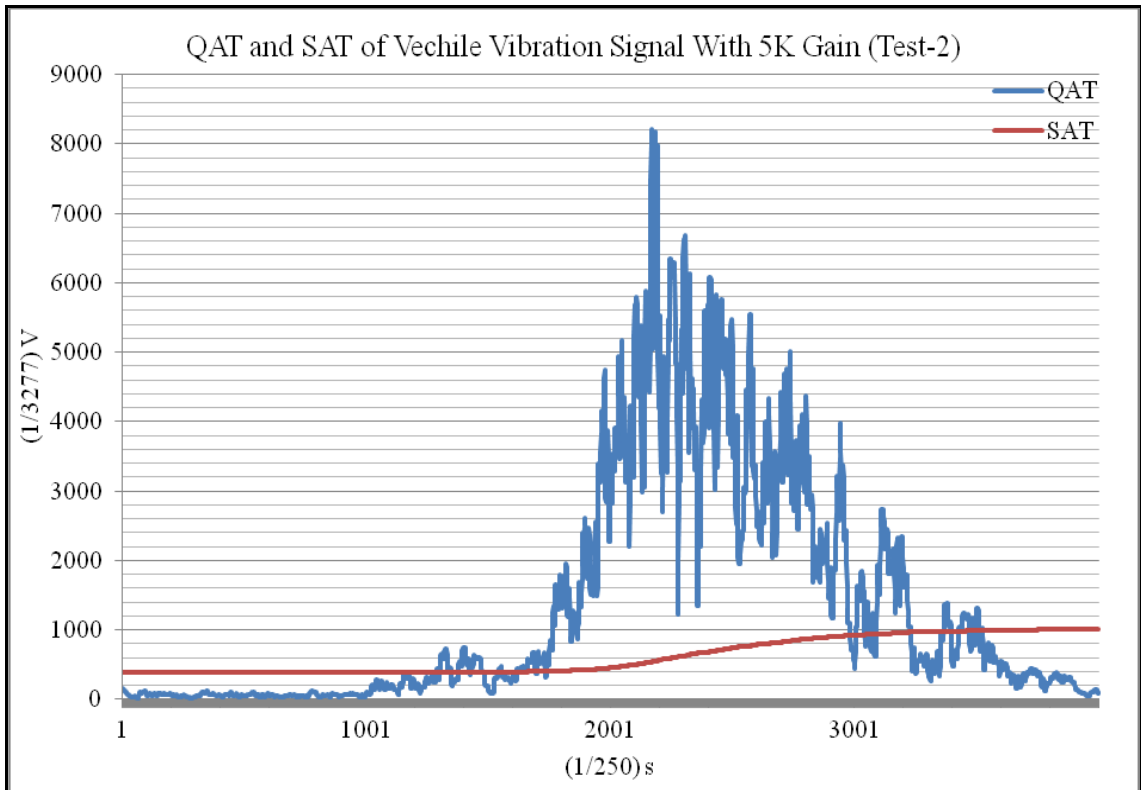


Figure 6.15. QAT and SAT of original vehicle signals with 5K gain (Test-2)

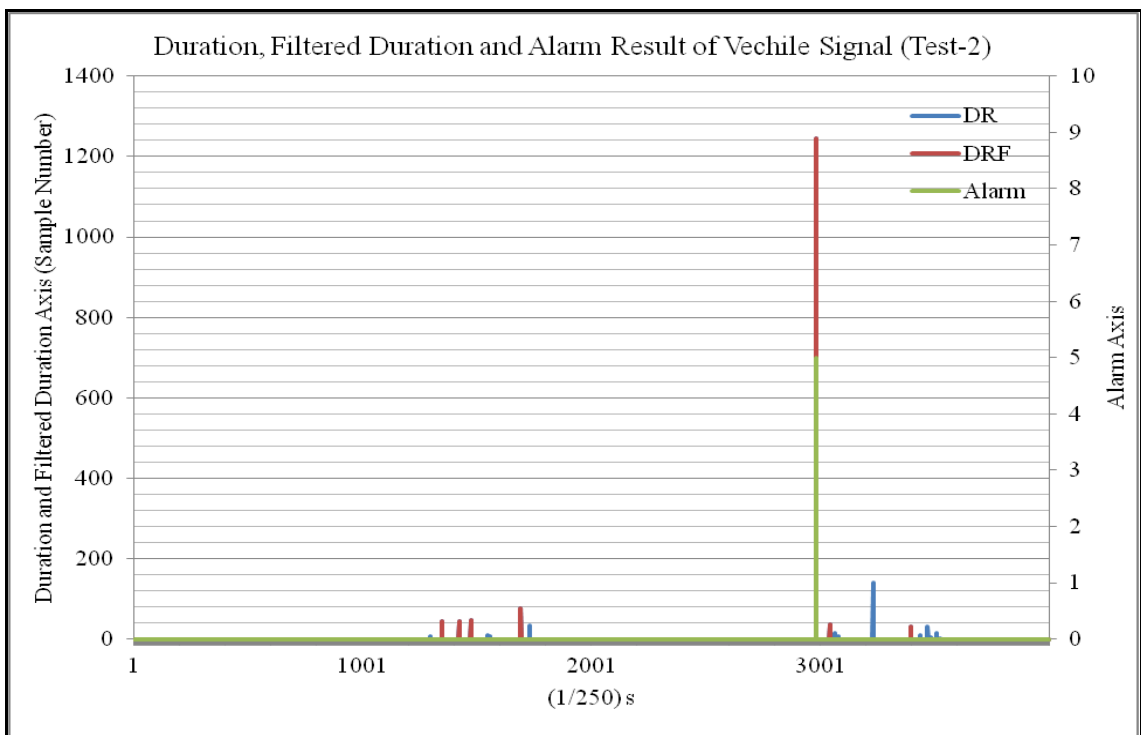


Figure 6.16. Duration, filtered duration and alarm result of vehicle signal (Test-2)

Table 6.2. Vehicle detection tests performance

Detected Signals	Test-1 (Figure 6.12.)	Test-2 (Figure 6.15.)
Detected as A Noise	17	11
Detected as a Footstep	3	5
Detected as a Rain	1	1
Detected as a Vehicle	1	1
Total	22	18

In both testes, there were unwanted signals detections, however these did not produce any false alarms.

#### 6.1.4. Rain Detection Performance of Signal Processing Algorithm

Two types of rain detection tests were executed at two different test locations.

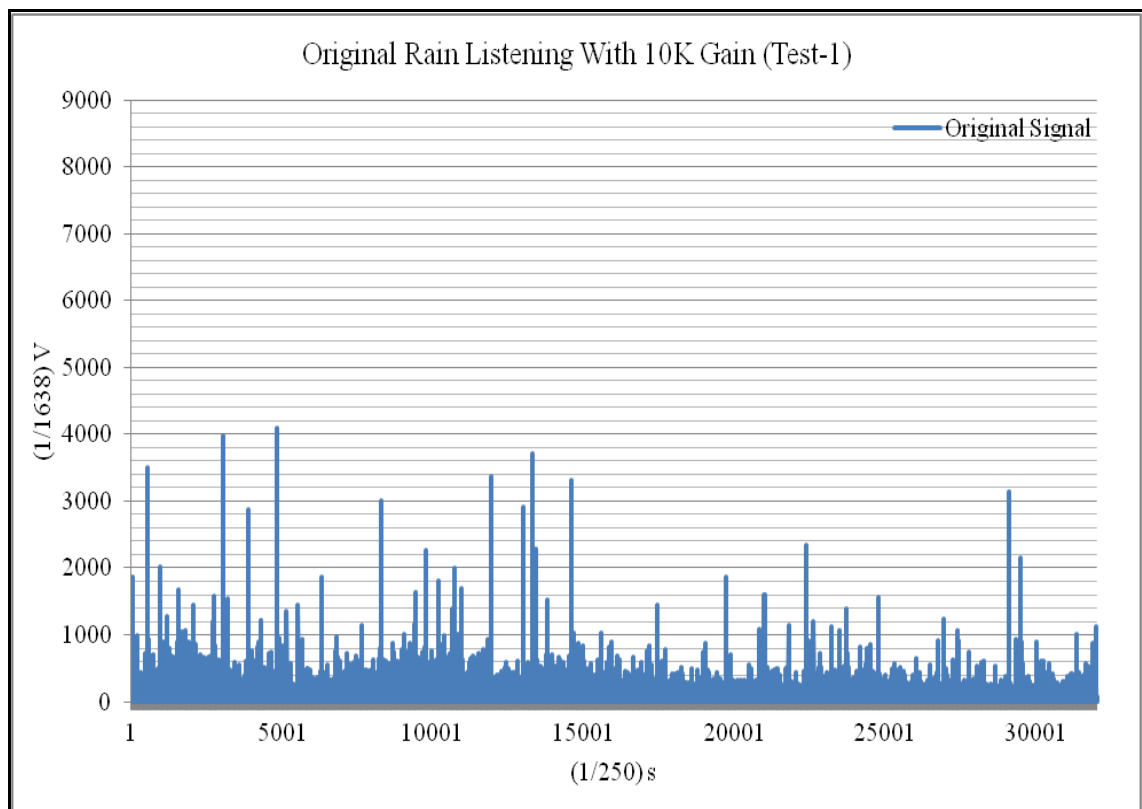


Figure 6.17. Original rain listening signal with 10K gain (Test-1)

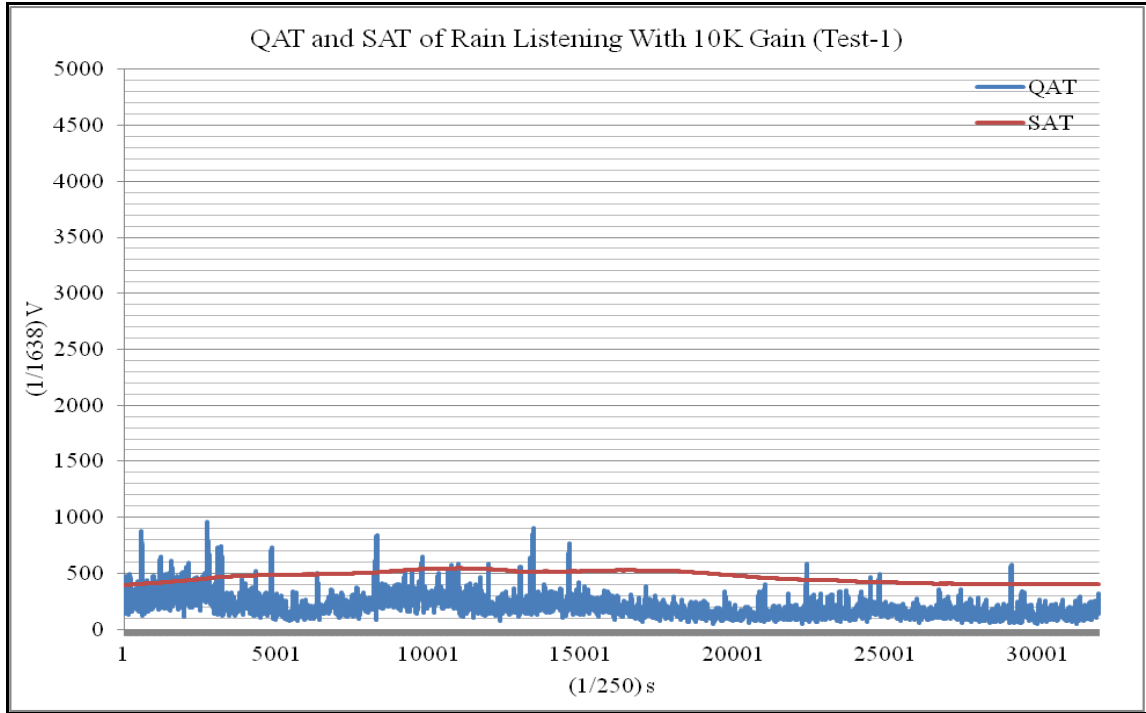


Figure 6.18. QAT and SAT of rain listening signal with 10K gain (Test-1)

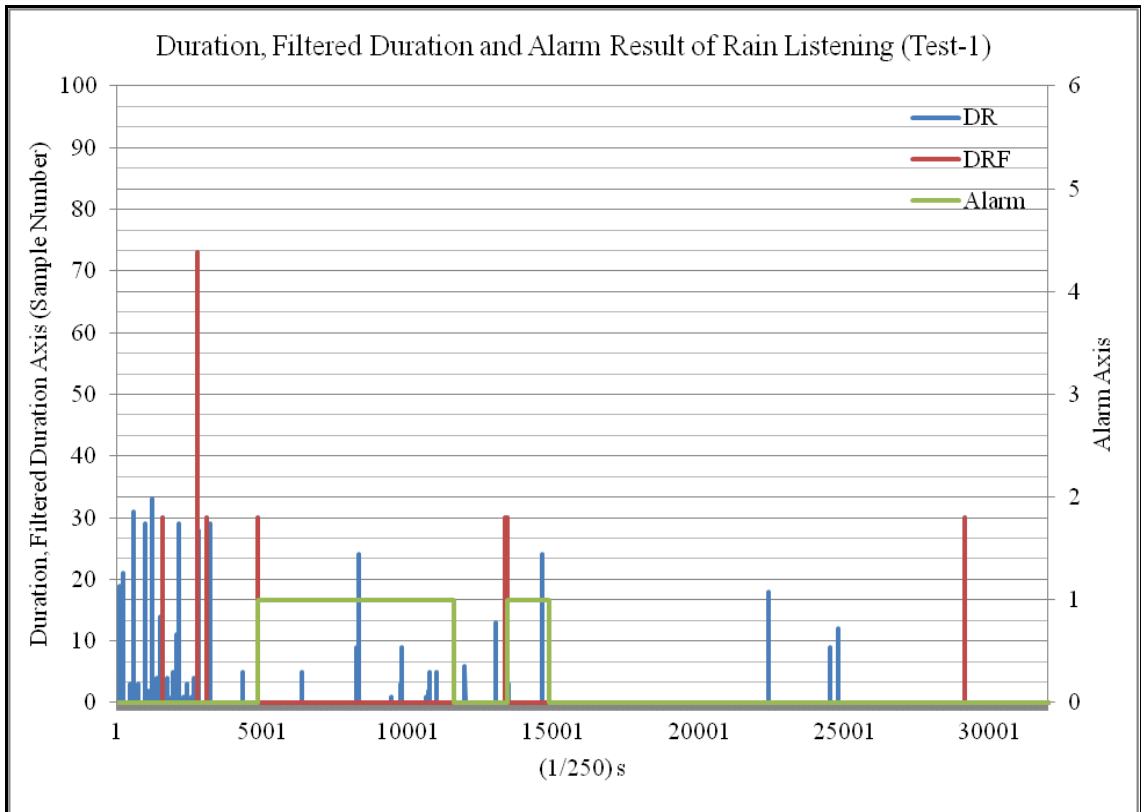




Figure 6.19. Duration, filtered duration and alarm result of rain listening signal (Test-1)

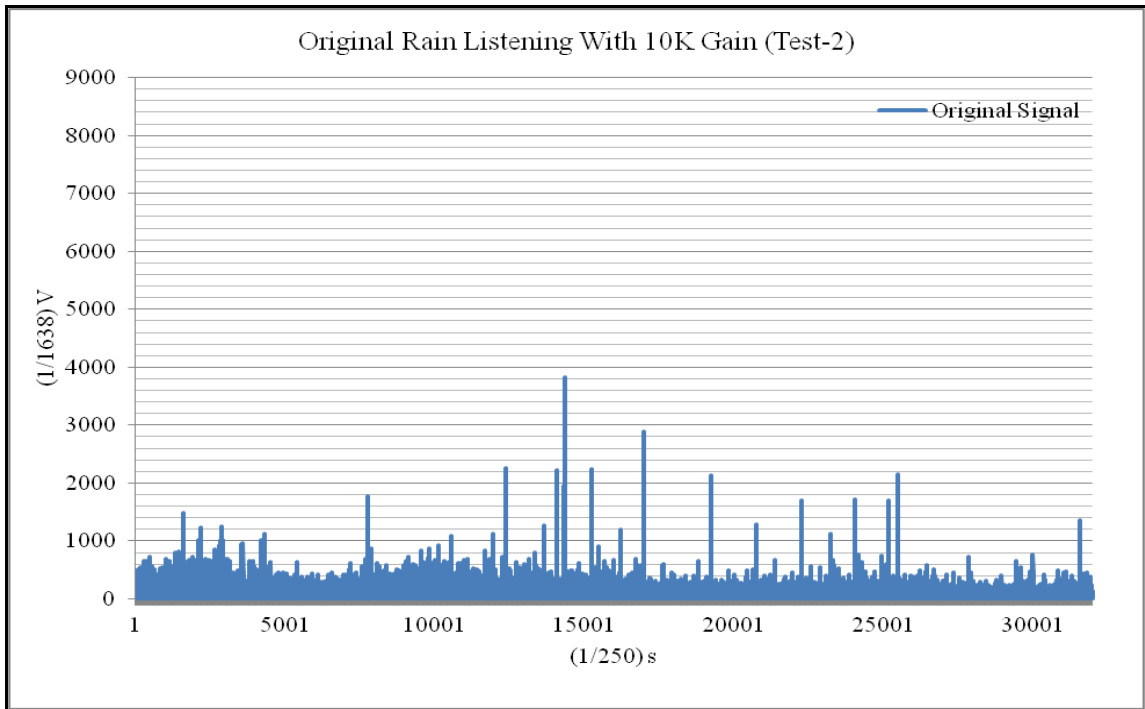


Figure 6.20. Original rain listening signal with 10K Gain (Test-2)

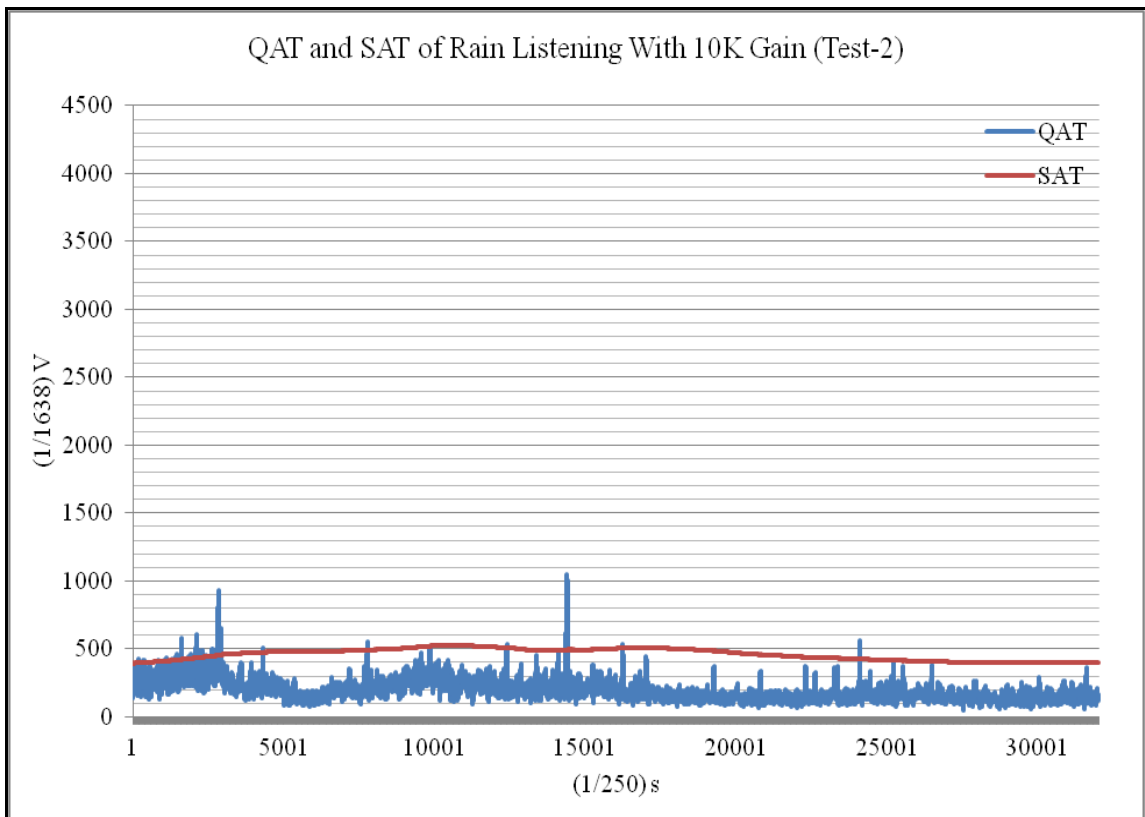


Figure 6.21. QAT and SAT of rain listening signal with 10K gain (Test-2)

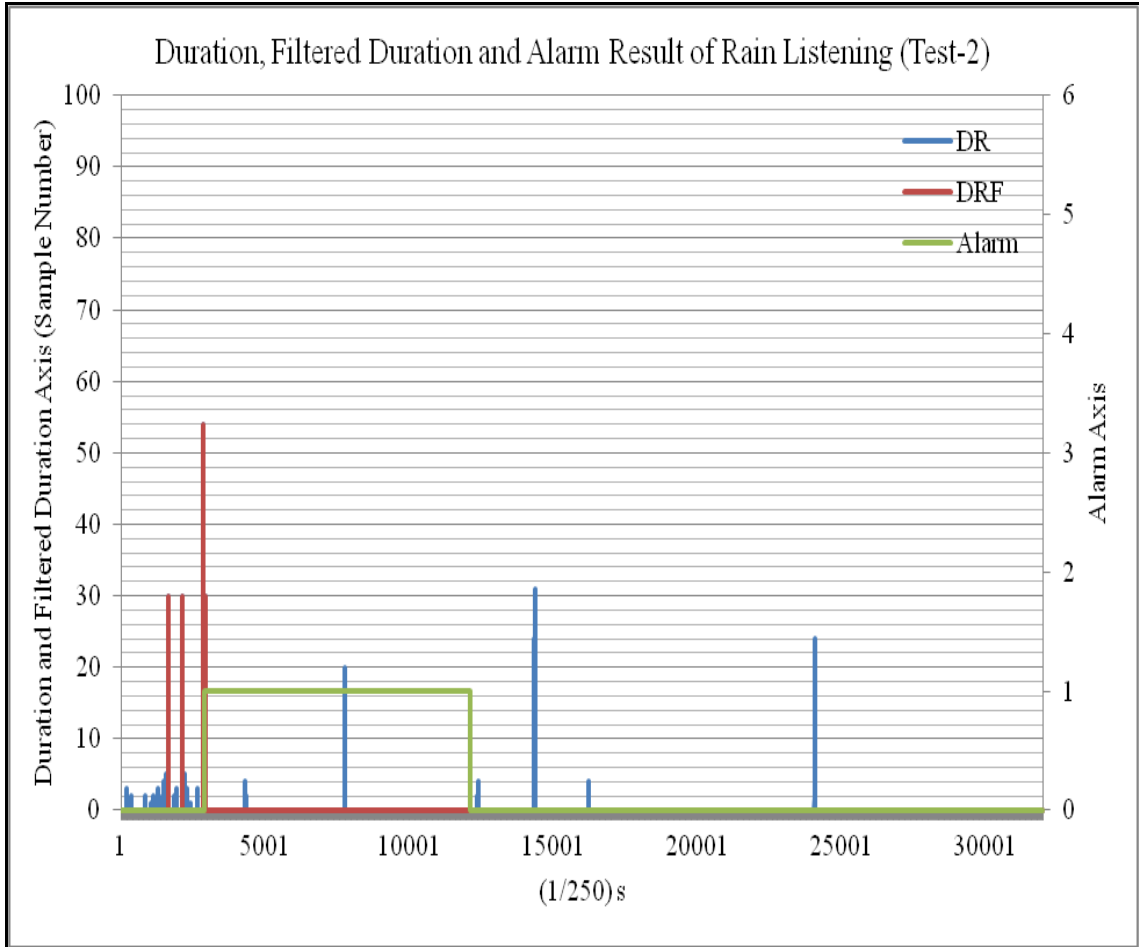


Figure 6.22. Duration, filtered duration and alarm result of rain listening signal (Test-2)

Table 6.3. Rain listening test performance

Detected Signals	Test-1 (Figure 6.19.)	Test-2 (Figure 6.22.)
Detected as A Noise	32	22
Detected as a Footstep	1	1
Detected as a Rain	6	3
Detected as a Vehicle	0	0
Total	39	26

In both testes, there were unwanted signals detected, however they did not produce any false alarms.

### 6.1.5. Combined Detection Performance of Signal Processing Algorithm

The combined detection performance test was performed to measure signal processing algorithm performance in 35-minute time (510.000 samples) with different types of signals. In test explanation, short cuts like “TS-ARPAS20-TF-GO” used to define test blocks. As it is seen in Table 6.4, intruders using different speeds, different directions and different locations are investigated.

Table 6.4 Combined signals test definitions

Definitions	Explanations
TS	Test start signal, hitting ground 3 times quickly
TF	Test stop signal, hitting ground 2 times quickly
Y1	Quick walking
Y2	Normal walking
Y3	Slow walking
DX	Distance between signal source and sensor
DIN	Walking to sensor (starting point is 30 meter far from sensor)
DOUT	Opposite of DIN
GO	Walking very slowly from one test point to other test point
ARPASX	Vehicle is passing tangential to sensor point with X km/h speed

Test i:; -TS-Y1D5--TF-GO-TS-Y1D10--TF-GO-TS-Y1D15--TF-GO-TS-Y1D20--TF-GO-TS-Y1D25--TF-GO-TS-Y1D30--TF-GO-TS-Y1DIN--TF-GO-TS-Y1DOU-T--TF-GO-TS-Y1DIN--TF-GO-TS-Y11DOU-T--TF-GO-TS-Y11DIN--TF-GO-TS-Y1DOU-T--TF-GO-TS-Y2D30--TF-GO-TS-Y2D25--TF-GO-TS-Y2D20--TF-GO-TS-Y2D15--TF-GO-TS-Y2D10--TF-GO-TS-Y2D5--TF-GO-TS-Y2DOU-T--TF-GO-TS-Y2DIN--TF-GO-TS-Y2DOU-T--TF-GO-TS-Y2DIN--TF-GO-TS-Y22DOU-T--TF-GO-TS-Y22DIN--TF-GO-TS-Y3D5--TF-GO-TS-Y3D10--TF-GO-TS-Y3D15--TF-GO-TS-Y3D20--TF-GO-TS-Y3D25--TF-GO-TS-Y3D30--TF-GO-TS-Y3DIN--TF-GO-TS-Y33DOU-T--TF-GO-TS-Y33DIN--TF-GO-TS-Y33DOU-T--TF-GO-TS-K30--TF-GO-TS-K20--TF-GO-TS-ARPAS10--TF-GO-TS-ARPAS20--TF-GO-TS-ARPAS30--TF-GO-TS-ARPAS10Y2DOU-T --TF-GO-TS- ARPAS10Y2DIN --TF-GO-TS-ARPAS10--TF-GO-

TS-ARPAS20--TF-GO-TS-ARPAS30--TF-GO-TS- ARPAS10Y2DOU-T --TF-GO -TS-  
 ARPAS10Y2DIN --TF-GO

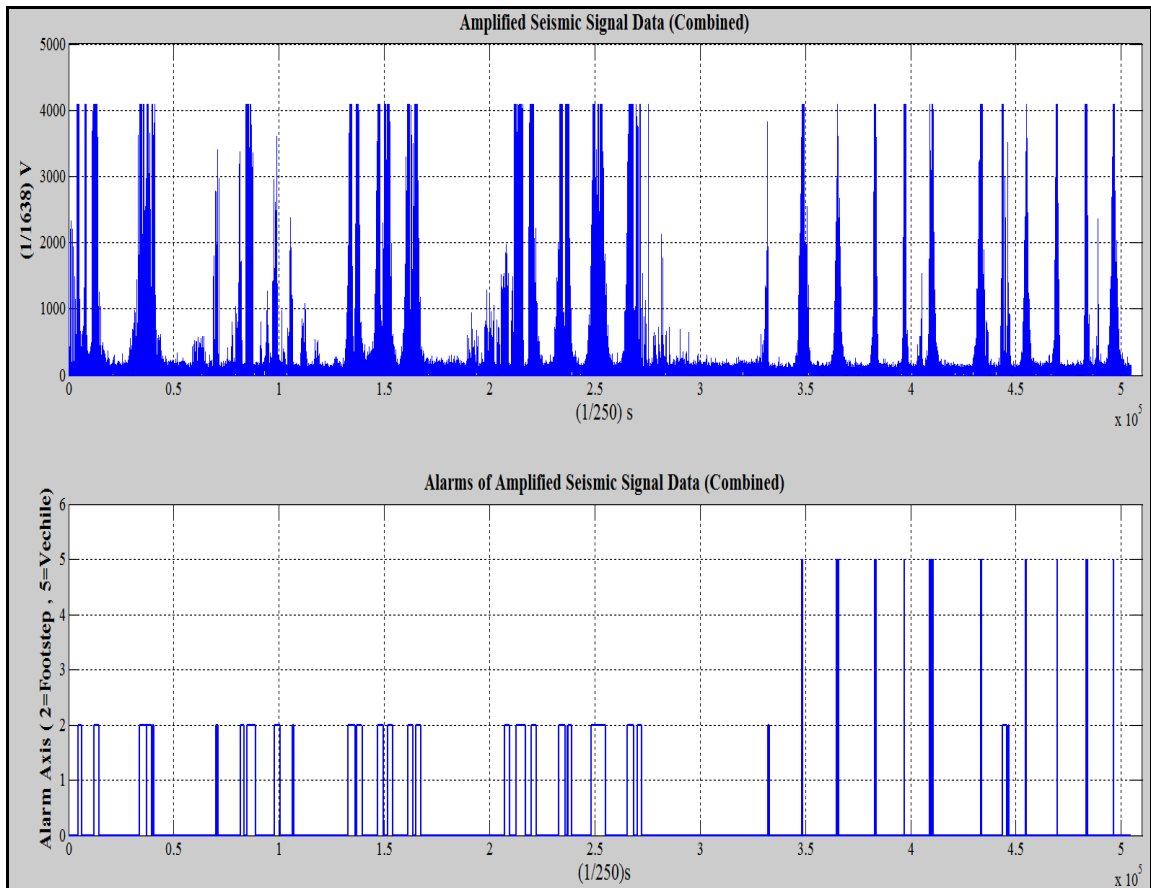


Figure 6.23. Classification results of combined test

As shown in the chart above; not any rain signature seen also there is not any rain situation occurred in test environment.

At the beginning of the test, there is only walking vibrations are occurred and results are same with this. Judging by the last part of the test, vehicle alarms could be seen easily.

A total of 10 vehicle tests performed and all of them were classified correctly. In some tests, human and vehicle are both intruder at the same time, however only vehicle vibrations are classified. Thus, it can be easily said that classification is successful.

## 6.2. PERFORMANCE OF STAND ALONE APPLICATION

Because of not considering the digital switch's operating voltage, we had a problem during the application. Between the switching pins of ISL43L210 and supply inputs, there are diodes. These diodes cause an extra current when a voltage greater than 3.6 VDC is present to switched pins. Therefore, the respective current circuit should be modified. The small modification can be seen in Figure 6.24. RA\_New resistance is connected to R\_Switch as parallel. Thus, when the R\_Switch is off the voltage level in pin could be decreased to 3.6 VDC. However, in order to minimize Normal Mode Current Consumption, supply voltage is decreased to 4 VDC. Normal mode current consumption is measured below 500  $\mu$ A before the RA\_New resistance.

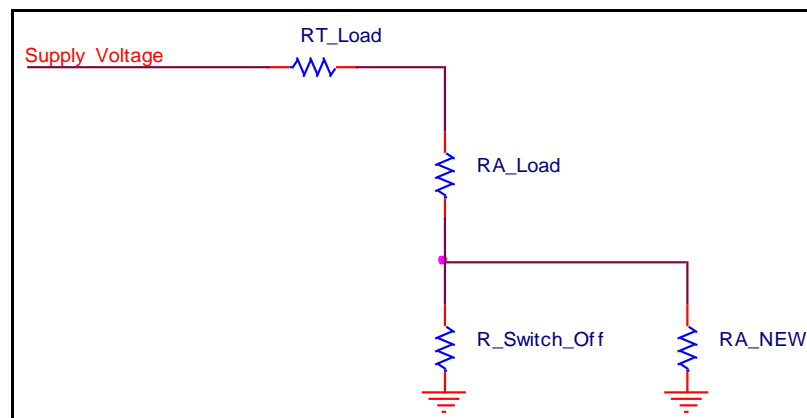


Figure 6.24. Additional parallel resistor to R-Switch

The changes of resistances in the circuit are as in the following:

- RT\_Load is 33 Ohm,
- RA\_Load is 33 Ohm,
- RA\_New is 540 Ohm,

The combined alarm test's current consumptions can be seen in Figure 6.25. Three sensor nodes are connected to each other in order and alarm signal is given three of them so, differences of currents that they consumed are observed and this is shown in Figure 6.25.

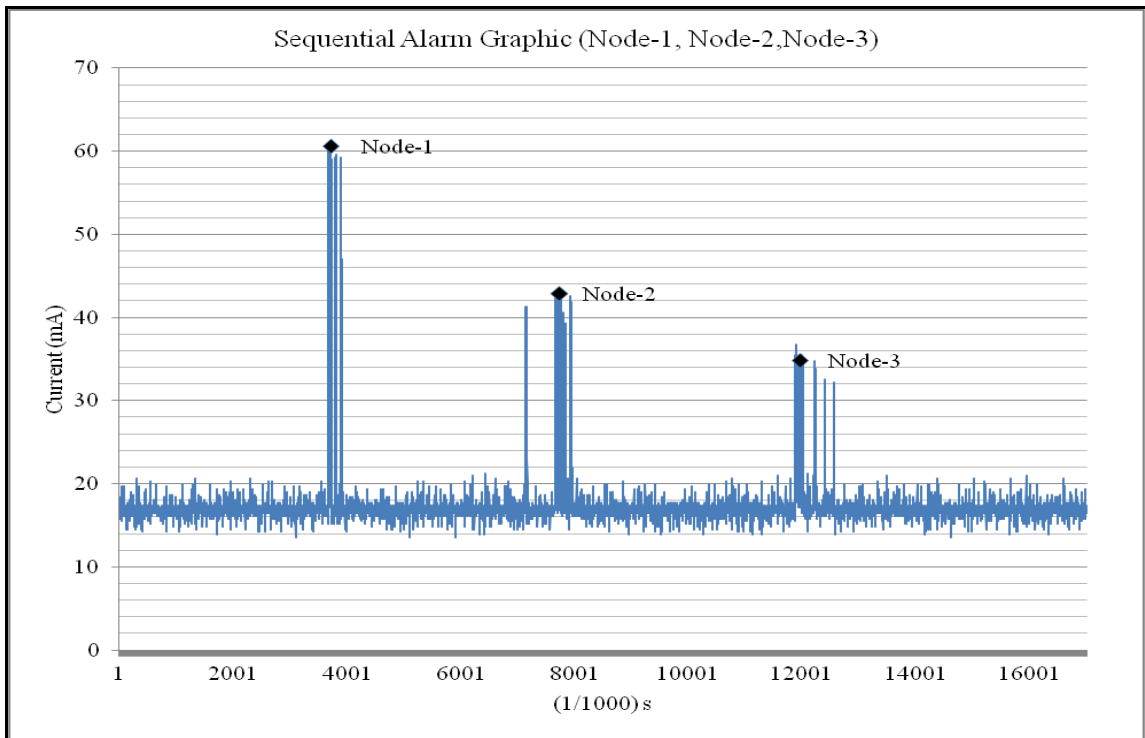


Figure 6.25. Combined alarm test current graphic

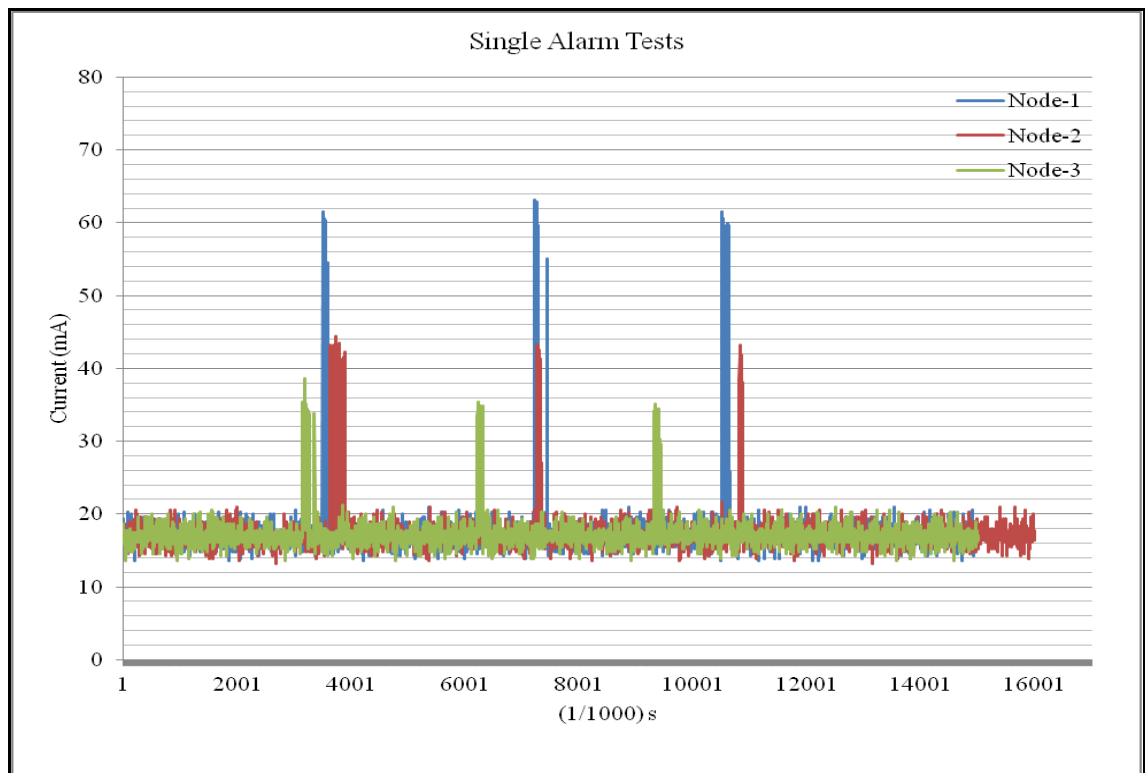


Figure 6.26. Single alarm test.

As it is shown in the Figure 6.26, the current draw of nodes are different. Additionally, the duration information of seismic signal can be inferred from current consumption by using a fast switch.

Average currents of nodes (in alarm situation) are as in the following:

- Node1 is 55.7 mA,
- Node2 is 38.24mA,
- Node3 is 32.88mA,

Total power consumption is seen in figure 6.25 is different than the simulation results, because of the problem which is about digital switch operating voltages. However, a fixed current consumption value is achieved in the figure 6.25.

### 6.3. MEASURES OF KURTOSIS EQUATION

In probability theory and statistics, kurtosis is measuring the "peakedness" of the real random variable that is collected from the environment. There are various versions of kurtosis equation are exist but in this thesis project; analysis are done with the common version used in intruder detection systems (Eq 6.1). It could be easily seen from the equation that kurtosis is more sensitive to sudden changes in the data. Therefore, before the analyses, it could be easily predicted that kurtosis will perform best results for rain detection and worst for vehicle movements.

$$Kurtosis = \frac{\frac{\sum_i^N (X_i - \mu)^4}{N - 1}}{\left(\frac{\sum_i^N (X_i - \mu)^2}{N - 1}\right)^2} \quad (6.1)$$

Kurtosis values are calculated by dividing the data to extracted intervals. The sample number in these intervals are called "N" in the equation and "μ" is the mean of this interval.

In this section, analyzes are executed on the previously used single signals. First, kurtosis equation will be executed on noise data with different interval size. At this stage, kurtosis values are expected to be close to each other with relatively small amplitude. In the next step, the equation will be applied on footsteps with different interval size. Kurtosis values of footsteps should be bigger than the previous stage (noise values) in order to obtain detection probability. Then, similar operations will be repeated on vehicle movements. Because of the equation architecture, good results are not expected at this stage. Finally, the similar operations will be applied on rain data. The tests will be repeated for different interval sizes to determine the most appropriate one.

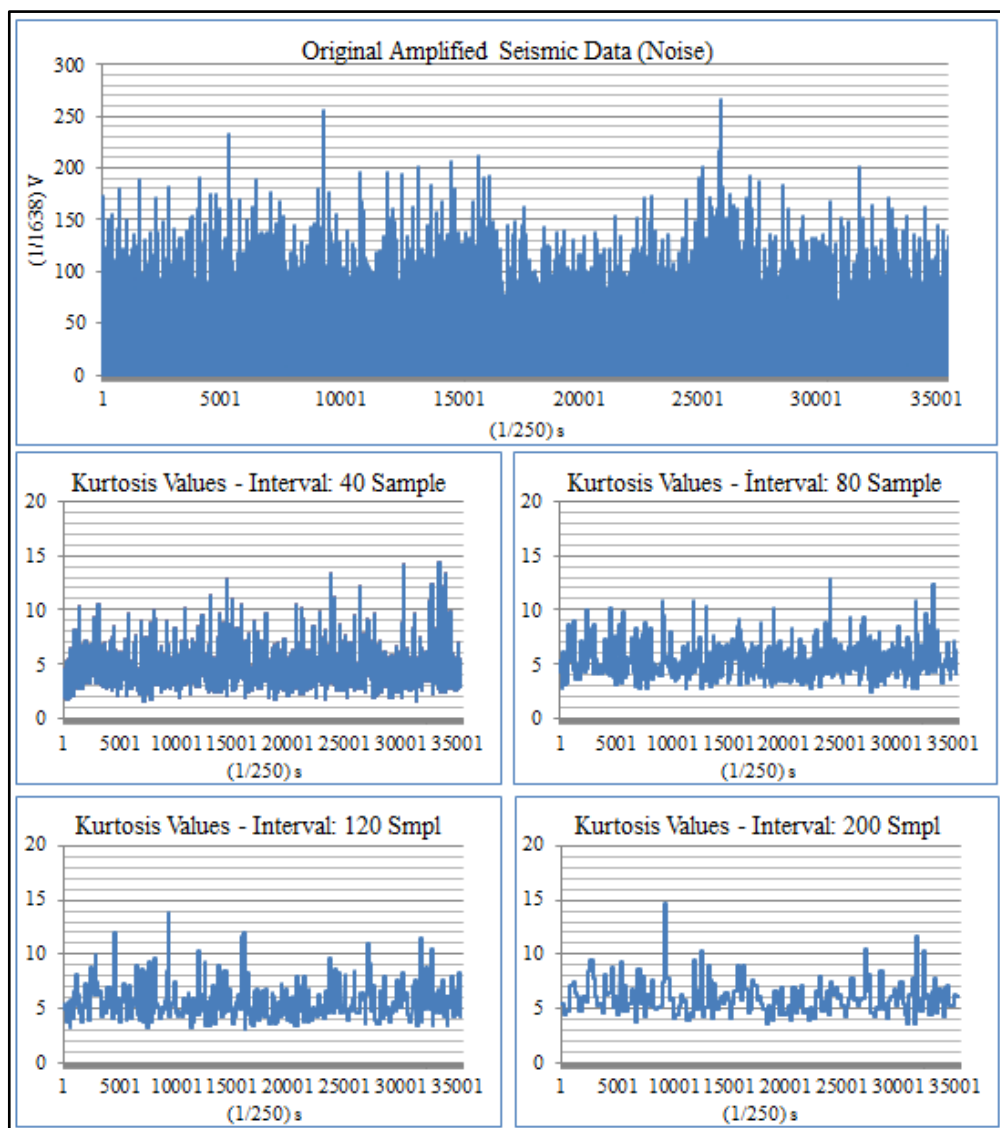


Figure 6.27. Kurtosis values of noise data with different interval sizes.



As shown in graphics, kurtosis values are oscillating between 4 and 15. Size of the oscillation will be compared with other kurtosis values which will be obtained on footstep, vehicle and rain data. However, it could be easily seen that oscillation is getting smaller with higher interval size.

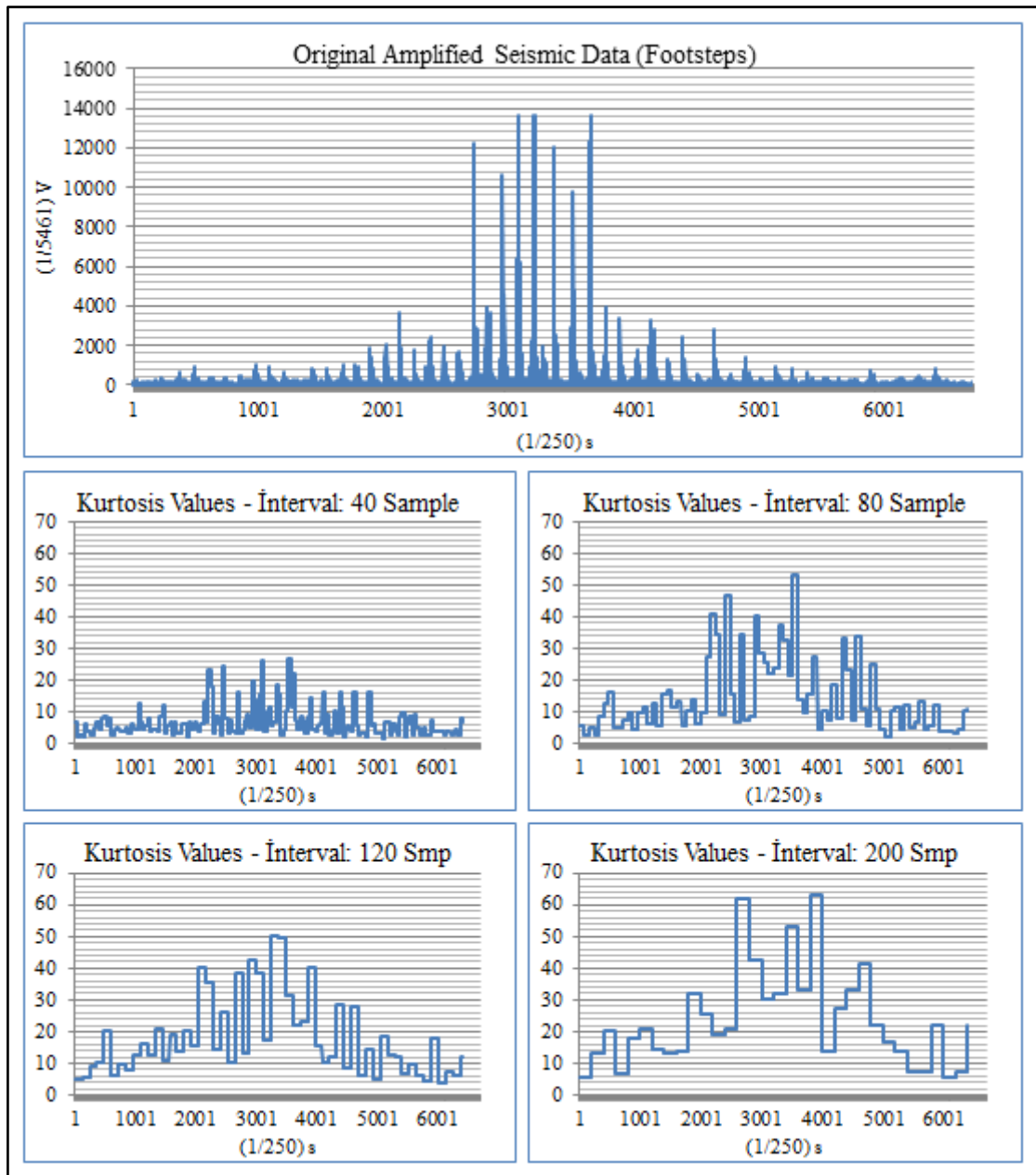


Figure 6.28. Kurtosis values of footstep data with different interval sizes.

As can be seen from the graphic, kurtosis values of footsteps are varying between 10 and 65. Kurtosis values of footsteps are intersecting with noise values but only in a small

interval. Also the kurtosis values of footstep are increasing with the interval size. However, if the interval size grows a little more, kurtosis values will be containing several footstep signals despite single footstep. Therefore, interval should contain a number of samples between 80 and 120.

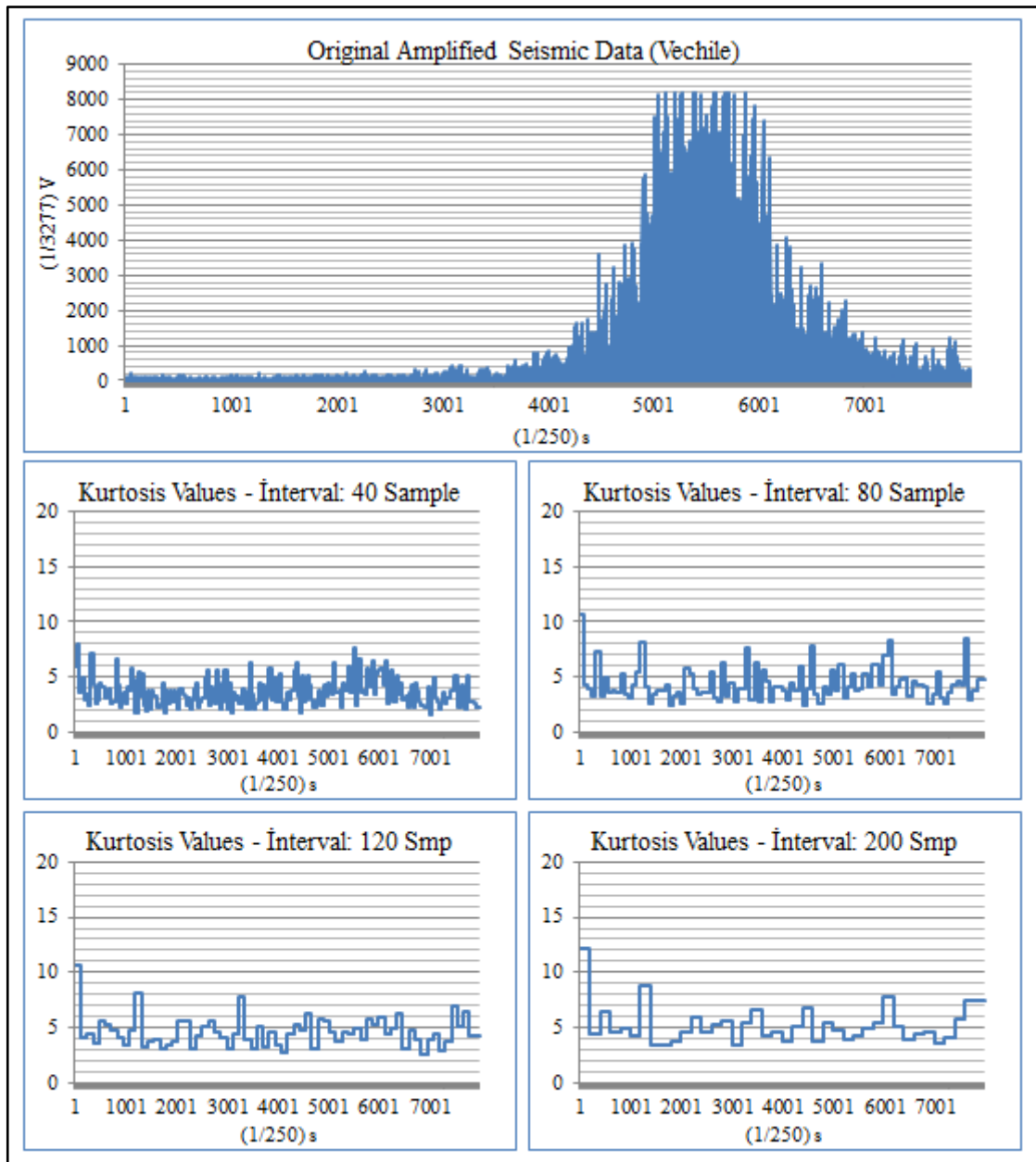


Figure 6.29. Kurtosis values of vehicle data with different interval sizes.

As mentioned in the previous pages, kurtosis equation is more sensitive to quick changes. As can be seen from the graph, the noise and vehicle kurtosis values are completely overlapped.

If the interval size enlarged very much, kurtosis values of vehicle could be differing from the noise. However, this will prevent footstep and rain detection also increased memory usage will decrease the operation life of the product.

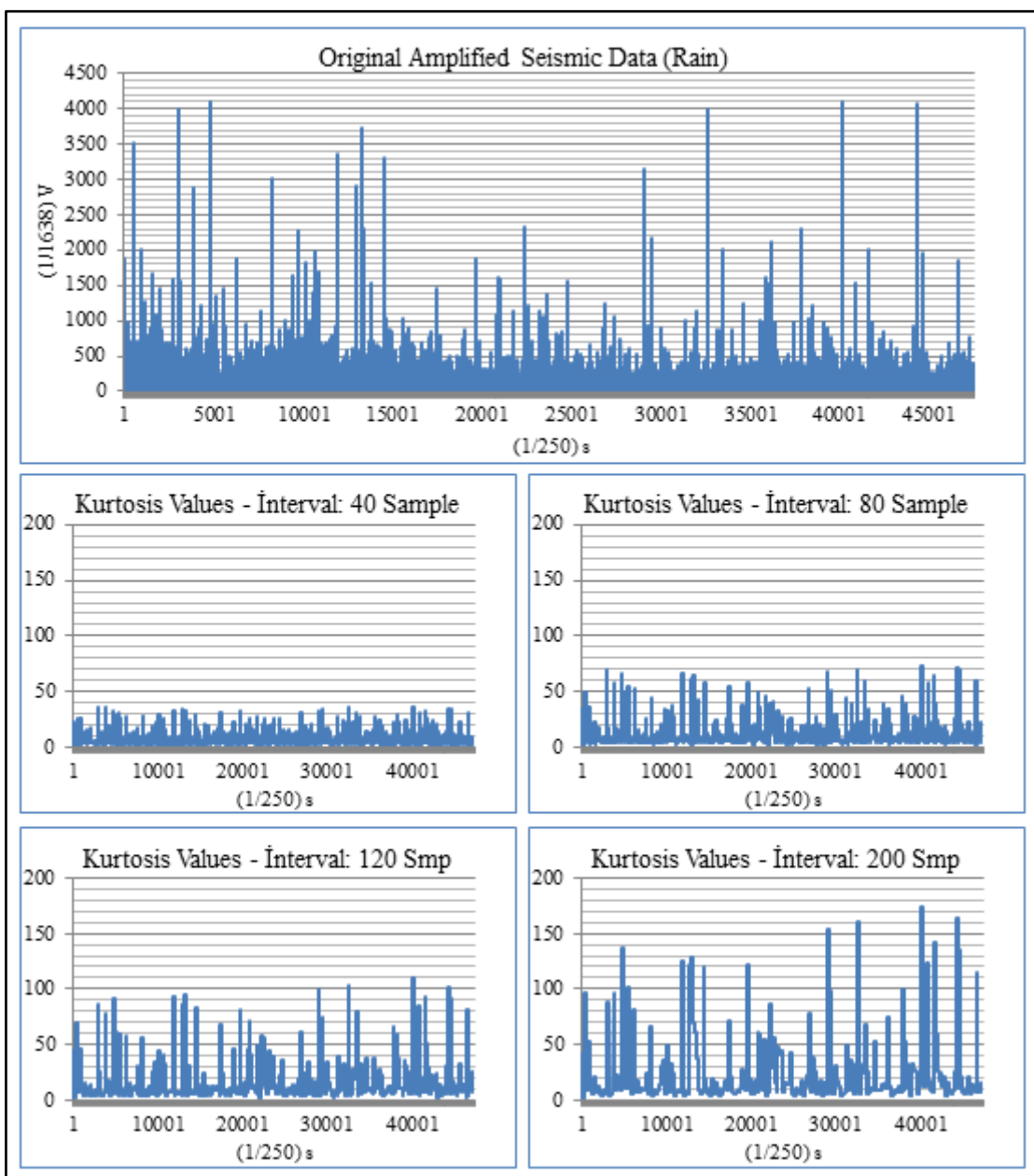


Figure 6.30. Kurtosis values of vehicle data with different interval sizes.

As can be seen in the graphics, the highest kurtosis values were obtained on rain data. Kurtosis values of rain signals can easily reach to 170. Because of this feature, rain and footstep signals could be easily separated from each other. As with the other tests, kurtosis values are growing with the interval size.

As a result of all analyses, kurtosis is successful at detecting footsteps and rain; however for vehicle detection; kurtosis is not a suitable equation without any additional properties.

## 7. PROBABILITY OF DETECTION AND FALSE ALARM

In this section, the signal processing code's PD and PFA performances are measured in detail. The behavior of signal processing code under different conditions will be analyzed with four different types of field test.

In first test, only noise data is collected from ground with different gain values. Signal processing code should not produce any alarm to these noise data to have a clear "Correct Rejection in Detection" performance. Then, a large number of footstep tests will be executed to measure the footstep detection performance. In the next phase, vehicle tests will be evaluated and after that, vehicle and footstep vibrations will be executed together.

Table 7.1. General test properties

General Test Properties	Value
Test Location	Yeditepe University Kayışdağı Campus
Weather Condition	Dry
Air Temperature	9 °C
Soil moisture status	Wet
Sampling Frequency	250 sample/second
Amplification Gain	Different in each Test
Vehicle	Kia Rio GSL EX 1.4
Person A Weight	60 kg
Person B Weight	120 kg

Table 7.2. General detection performance criteria

	Detection is present	Detection is Absent
Signal is present	True Detection (Hit)	Missed Detection (Missed)
Signal is absent	False Detection (False Detection)	Correct Rejection in Detection

Table 7.3. General classification performance criteria

	Classification is present	Classification is Absent
Signal is present	True Classification (Hit)	Missed Classification (Missed)
Signal is absent	False Classification (False Alarm)	Correct Rejection in Classification

“True detection” means; signal type is detected correctly. “Missed detection” means; signal is not detected. “False detection” means; signal type is detected incorrectly, for example; if a vehicle signal has detected in footstep test, this detection is called “False detection” because there is not any vehicle movement in the area that means signal is absent but detection is present. “Correct Rejection in Detection” condition occurs only if there is not any signal and also any detection.

“True Classification” means; intruder type is classified correctly. “Missed classification” means; intruder type is not classified. “False classification” means; signal type is classified incorrectly, for example; if a vehicle signal has classified in footstep test, this classification is called “False classification” because there is not any vehicle movement in the area that means signal is absent but classification is present. “Correct Rejection in Classification” condition occurs only if there is not any intruder and also any alarm.

From table 7.2, it could be easily seen that correct rejection is %100 in both detection and classification when there is not any intruder. So, the probabilities of true, false and missed detections/classifications are calculated by the formulas in the figure 7.1..

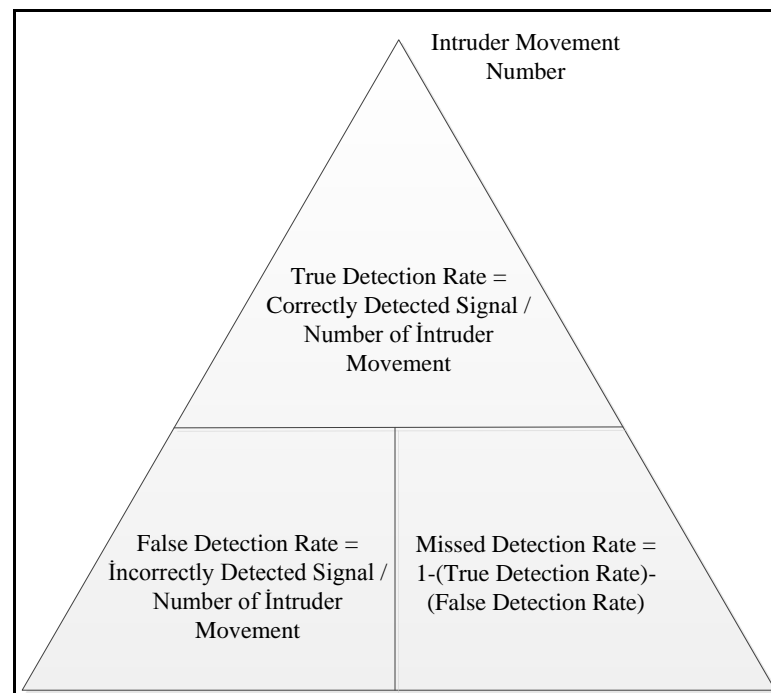


Figure 7.1. Detection rate calculation criteria

## 7.1. NOISE ANALYSES

In noise tests, environment is listened with 20 different gain values while there is no mobility. Then, collected data were processed with the signal processing code.

As is known, the output of the signal processing code is classification. However, this classification is determined after determining the types of vibrations which are detected. Thus, in the table 7.4., both classification results vibration detection results are given.

Related gain values are; 500, 1k, 1.5k, 2k, 2.5k, 3k, 3.5k, 4k, 4.5k, 5k, 5.5k, 6k, 6.5k, 7k, 7.5k, 8k, 8.5k, 9k, 9.5k, 10k.

Table 7.4. Noise performance of signal processing code in field

Gain Values	Vibration Type Detection			Classification		
	Footstep	Rain	Vehicle	Footstep	Rain	Vehicle
500	0	0	0	-	-	-
1000	0	0	0	-	-	-
1500	0	0	0	-	-	-
2000	0	0	0	-	-	-
2500	0	0	0	-	-	-
3000	0	0	0	-	-	-
3500	0	0	0	-	-	-
4000	0	0	0	-	-	-
4500	0	0	0	-	-	-
5000	0	0	0	-	-	-
5500	0	0	0	-	-	-
6000	0	0	0	-	-	-
6500	0	0	0	-	-	-
7000	0	0	0	-	-	-
7500	0	0	0	-	-	-
8000	0	0	0	-	-	-
8500	0	0	0	-	-	-
9000	0	0	0	-	-	-
9500	0	0	0	-	-	-
10000	0	0	0	-	-	-

As can be seen in the table above, the signal processing algorithm did not produce any alarm or any vibration type detection in all amplification gain values.

In environment without any mobility, the algorithm should not produce any type of alarm and it could be easily seen from the table 7.2., signal processing algorithm is successful in this condition.

## 7.2. FOOTSTEP ANALYSES

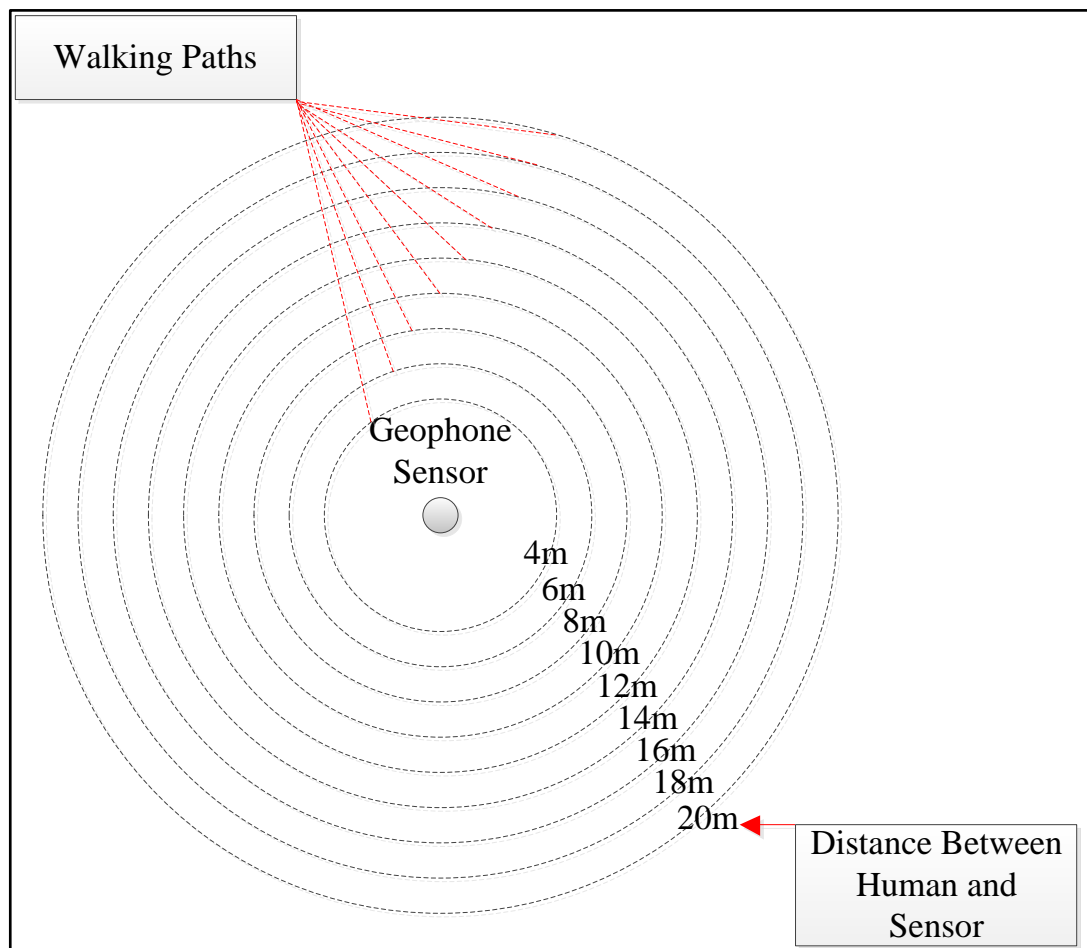


Figure 7.2. Footstep test paths

As shown in the graph above, footstep tests are executed on a circle with a certain radius around the geophone sensor. In each test, 60 footsteps have been taken.



Table 7.5. Footstep test pool

Distance	Person A				Person B			
	Gain 1k	Gain 2.5k	Gain5k	Gain7.5k	Gain 1k	Gain 2.5k	Gain5k	Gain7.5k
4m	A-1k-4m	A-2.5k-4m	A-5k-4m	A-7.5k-4m	B-1k-4m	B-2.5k-4m	B-5k-4m	B-7.5k-4m
6m	A-1k-6m	A-2.5k-6m	A-5k-6m	A-7.5k-6m	B-1k-6m	B-2.5k-6m	B-5k-6m	B-7.5k-6m
8m	A-1k-8m	A-2.5k-8m	A-5k-8m	A-7.5k-8m	B-1k-8m	B-2.5k-8m	B-5k-8m	B-7.5k-8m
10m	A-1k-10m	A-2.5k-10m	A-5k-10m	A-7.5k-10m	B-1k-10m	B-2.5k-10m	B-5k-10m	B-7.5k-10m
12m	A-1k-12m	A-2.5k-12m	A-5k-12m	A-7.5k-12m	B-1k-12m	B-2.5k-12m	B-5k-12m	B-7.5k-12m
14m	A-1k-14m	A-2.5k-14m	A-5k-14m	A-7.5k-14m	B-1k-14m	B-2.5k-14m	B-5k-14m	B-7.5k-14m
16m	A-1k-16m	A-2.5k-16m	A-5k-16m	A-7.5k-16m	B-1k-16m	B-2.5k-16m	B-5k-16m	B-7.5k-16m
18m	A-1k-18m	A-2.5k-18m	A-5k-18m	A-7.5k-18m	B-1k-18m	B-2.5k-18m	B-5k-18m	B-7.5k-18m
20m	A-1k-20m	A-2.5k-20m	A-5k-20m	A-7.5k-20m	B-1k-20m	B-2.5k-20m	B-5k-20m	B-7.5k-20m

As can be seen in the table 7.5., there are three features that separates the footstep tests such as walking person, amplification gain and radius of footstep path.

### 7.2.1. Vibration Type Detection Performances

First, signal processing algorithm will be executed on the data and signal type detection performances in all footstep tests will be measured. True footstep detection rate means; x percentage of 60 footsteps are detected as a footstep signal. False footstep detection rate means; x percentage of 60 footsteps are detected as a vehicle or rain signal. Missed footstep detection rate means; x percentage of 60 footsteps are not detected as a footstep or vehicle or rain.

After measuring detection performances, classification performance will be calculated.

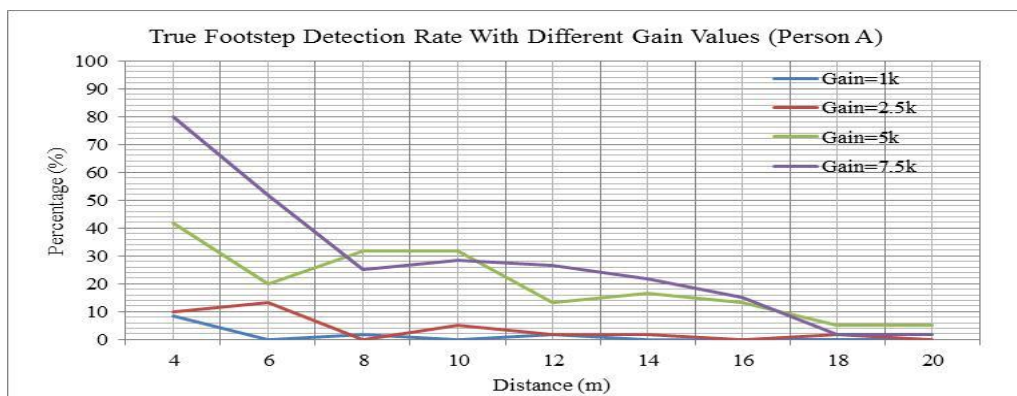


Figure 7.3. True footstep detection rate with different gain values (Person A)

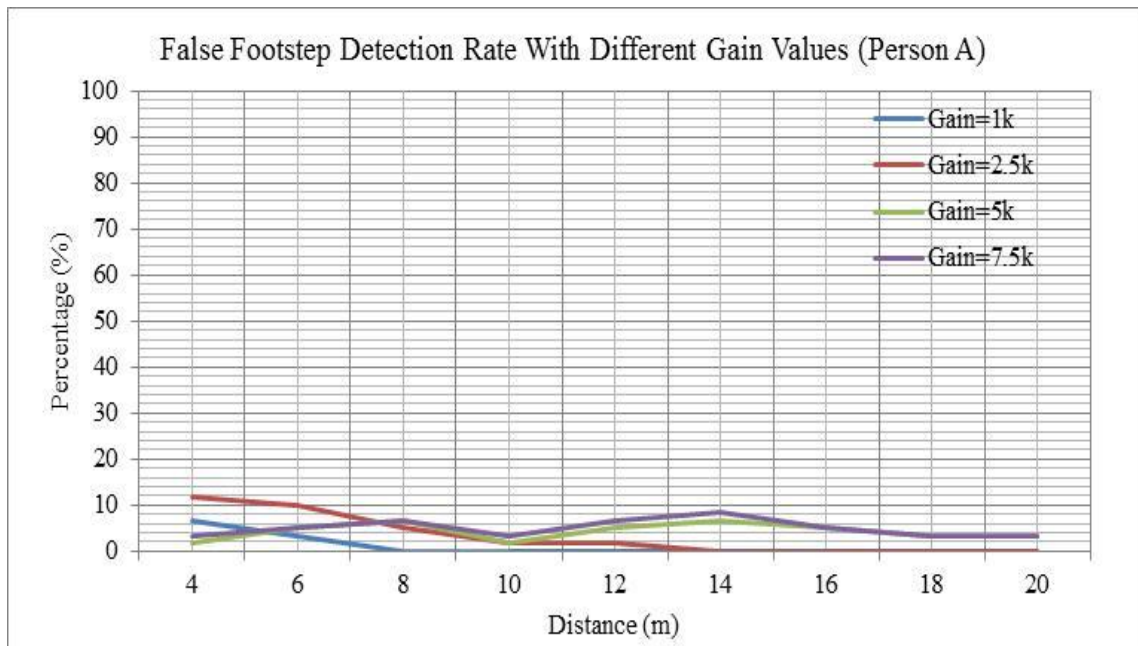


Figure 7.4. False footstep detection rate with different gain values (Person A)

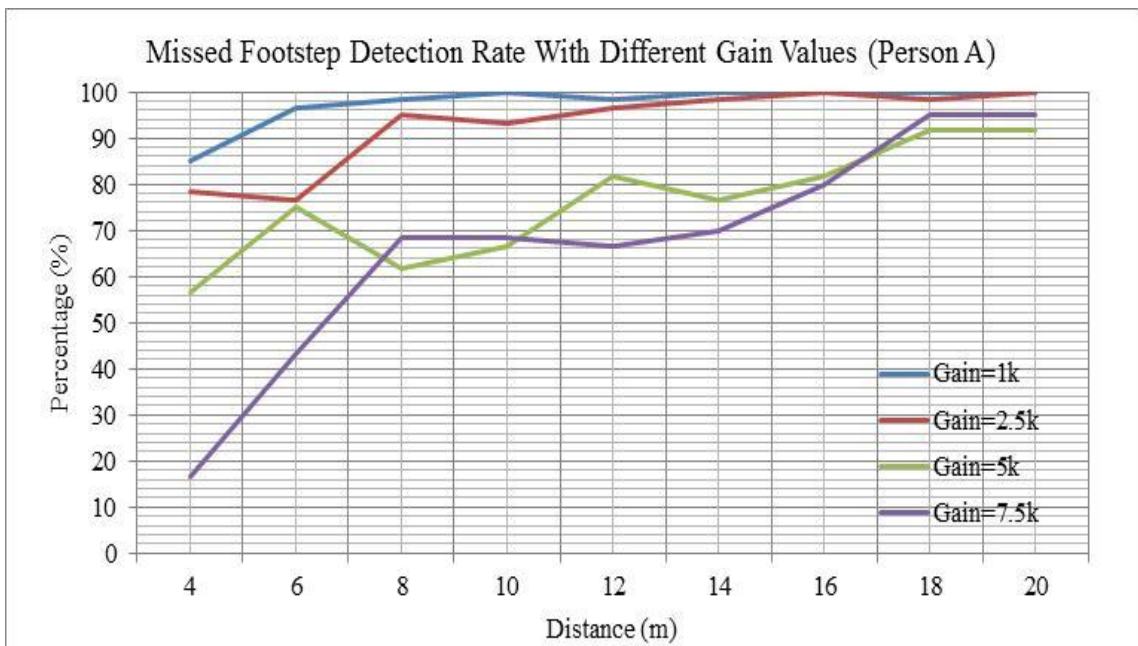


Figure 7.5. Missed footstep detection rate with different gain values (Person A)

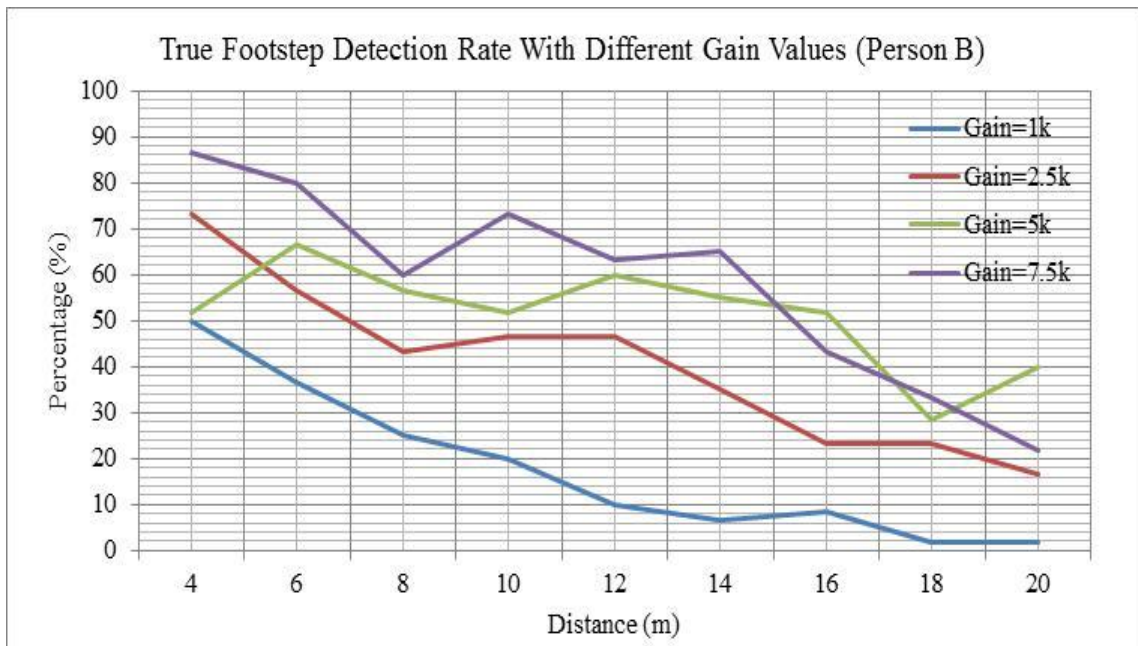


Figure 7.6. True footstep detection rate with different gain values (Person B)

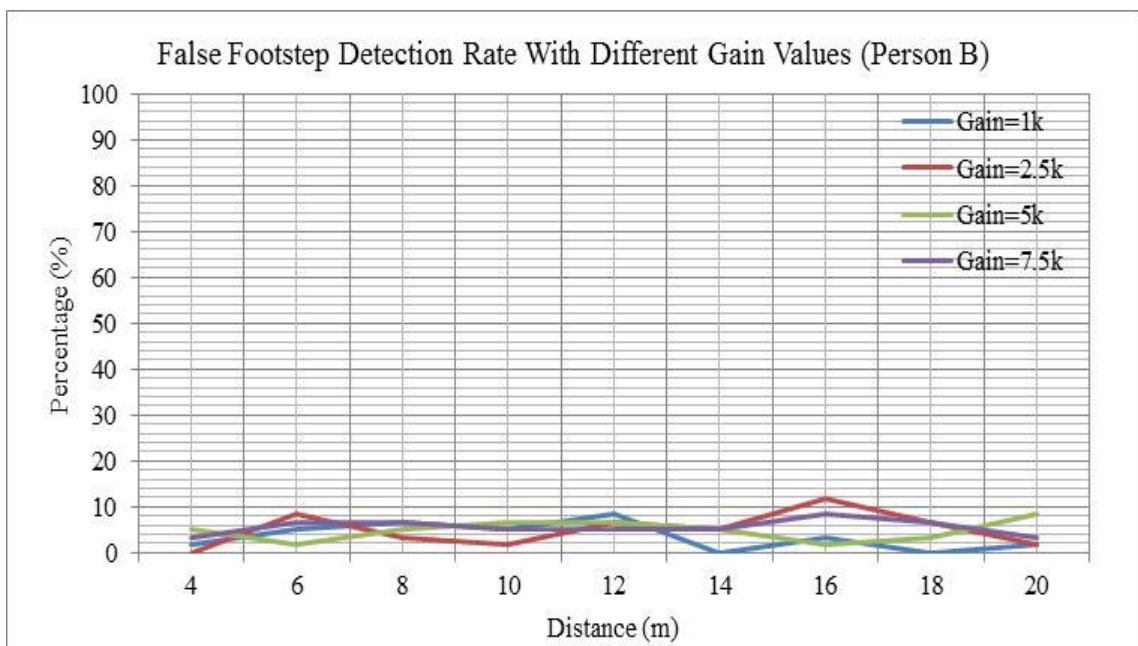


Figure 7.7. False footstep detection rate with different gain values (Person B)

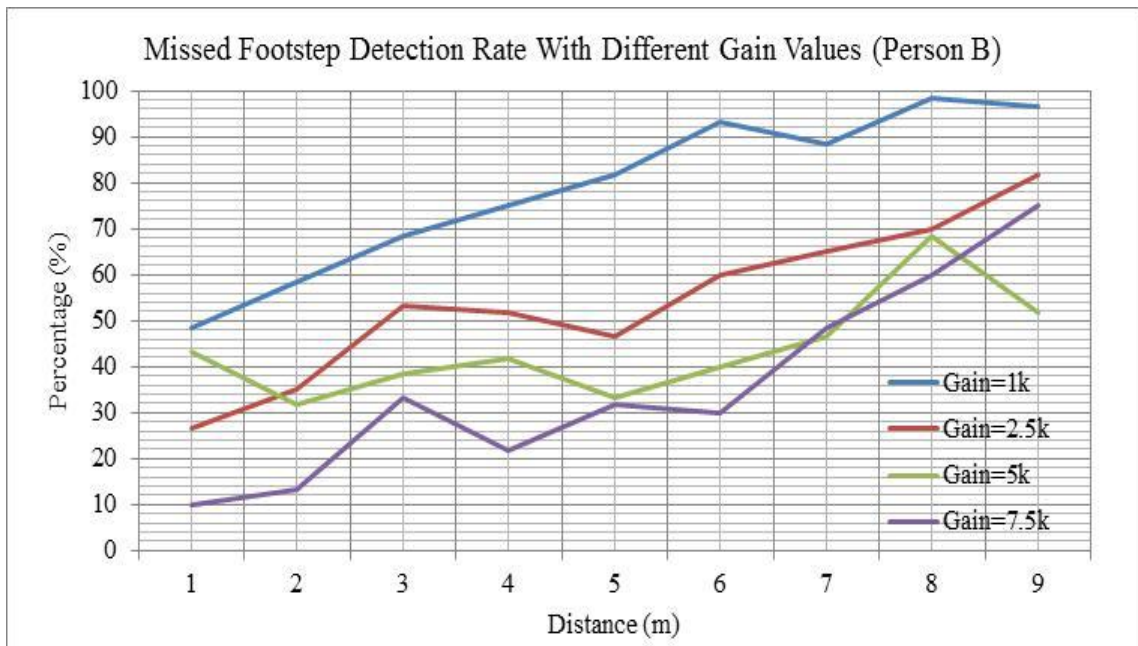


Figure 7.8. Missed footstep detection rate with different gain values (Person B)

By the above detection performance charts, signal processing algorithms performance much depends on the weight of the person who executed footsteps. 120-pound Person B's footsteps can be detected with higher accuracy and also from further distances.

From the same graphics, it can be easily seen that detection performance of footstep is decreasing with increasing distance.

The most important point of attention in graphics is high missed detection rates and low false detection rates. Nevertheless, in close proximity, true footstep detection rates can go up to 80%. Detection distance measurements will be considered in the classification part. Another remarkable point of the analyses that the change in the amplification gain is affecting the detection performance of footstep signals. Better detection performances obtained with higher amplification gain values.

### 7.2.2. Classification Performances

First, to evaluate the classification results, a classification performance criterion must be determined. Table 7.6. has the details of the criteria.

Table 7.6. Classification performance criteria of footstep tests

Classification Result	Conditions
TRUE	Only footstep alarm occurs.
FALSE	If rain or vehicle alarm occurs.
MISSED	No alarm occurs

Table 7.7. Footstep classification results with 1k gain value

Distance (m)	Footstep Classification Results With 1k Gain							
	Person A				Person B			
	Footstep	Rain	Vehicle	Result	Footstep	Rain	Vehicle	Result
4	-	-	-	MISSED	+	-	-	TRUE
6	-	-	-	MISSED	+	-	-	TRUE
8	-	-	-	MISSED	+	-	-	TRUE
10	-	-	-	MISSED	+	-	-	TRUE
12	-	-	-	MISSED	+	+	-	FALSE
14	-	-	-	MISSED	-	-	-	MISSED
16	-	-	-	MISSED	-	-	-	MISSED
18	-	-	-	MISSED	-	-	-	MISSED
20	-	-	-	MISSED	-	-	-	MISSED

Table 7.8. Footstep classification results with 2.5k gain value

Distance (m)	Footstep Classification Results With 2.5k Gain							
	Person A				Person B			
	Footstep	Rain	Vehicle	Result	Footstep	Rain	Vehicle	Result
4	-	+	-	FALSE	+	-	-	TRUE
6	+	+	-	FALSE	+	+	-	FALSE
8	-	-	-	MISSED	+	-	-	TRUE
10	-	-	-	MISSED	+	-	-	TRUE
12	-	-	-	MISSED	+	-	-	TRUE
14	-	-	-	MISSED	+	-	-	TRUE
16	-	-	-	MISSED	+	+	-	FALSE
18	-	-	-	MISSED	+	-	-	TRUE
20	-	-	-	MISSED	+	-	-	TRUE

Table 7.9. Footstep classification results with 5k gain value

Distance (m)	Footstep Classification Results With 5k Gain							
	Person A				Person B			
	Footstep	Rain	Vehicle	Result	Footstep	Rain	Vehicle	Result
4	+	-	-	TRUE	+	-	+	FALSE
6	+	-	-	TRUE	+	-	-	TRUE
8	+	-	-	TRUE	+	-	-	TRUE
10	+	-	-	TRUE	+	-	-	TRUE
12	-	-	-	MISSED	+	-	-	TRUE
14	-	-	-	MISSED	+	-	-	TRUE
16	-	-	-	MISSED	+	-	-	TRUE
18	-	-	-	MISSED	+	-	+	FALSE
20	-	-	-	MISSED	+	+	-	FALSE

Table 7.10. Footstep classification results with 7.5k gain value

Distance (m)	Footstep Classification Results With 7.5k Gain							
	Person A				Person B			
	Footstep	Rain	Vehicle	Result	Footstep	Rain	Vehicle	Result
4	+	-	-	TRUE	+	-	-	TRUE
6	+	-	-	TRUE	+	-	-	TRUE
8	+	-	-	TRUE	+	-	-	TRUE
10	+	-	-	TRUE	+	-	-	TRUE
12	+	-	-	TRUE	+	-	-	TRUE
14	+	+	-	FALSE	+	-	-	TRUE
16	+	-	-	TRUE	+	+	-	FALSE
18	-	-	-	MISSED	+	-	-	TRUE
20	-	-	-	MISSED	+	-	-	TRUE

As seen from the above tables, classification distance varies depending on the walking person's weight and amplification gain value.

Each of the above tests is listed in a single condition at the following figures. The probability of each classification results according to the different conditions are evaluated by summing Person A and Person B conditions. Thus, average of two different human weight types will be represented by the following figures. Graph points are calculated with tests which have the distance value equal or smaller than the "range" value.

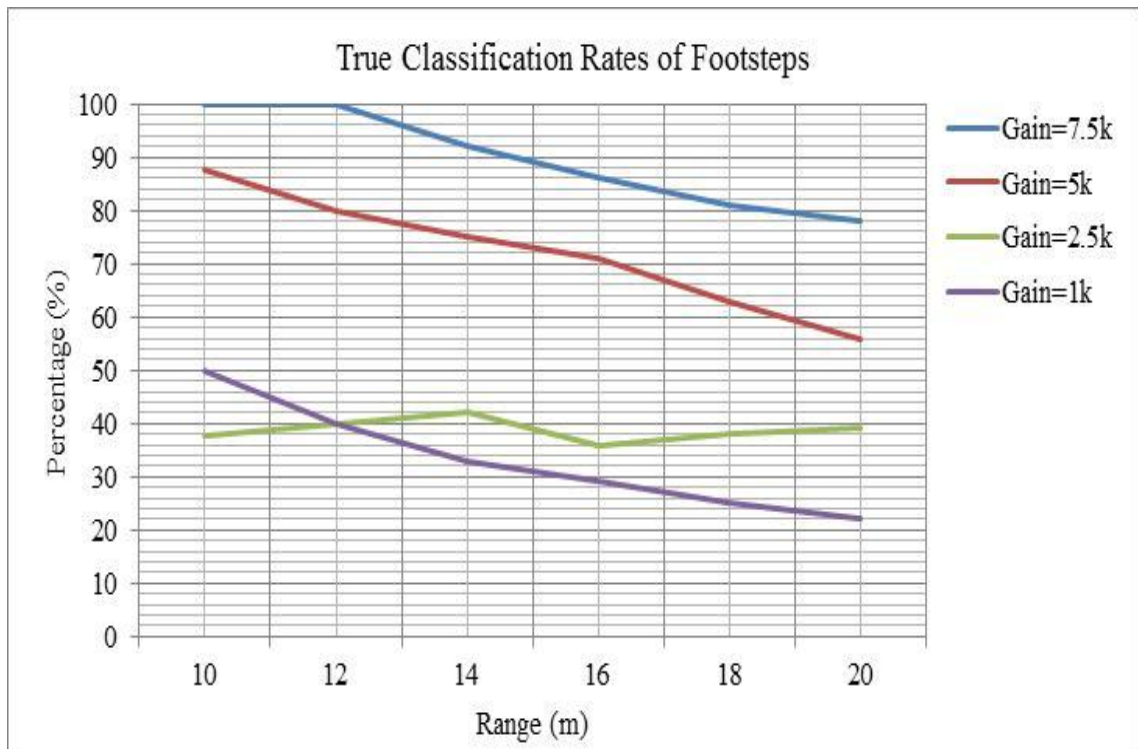


Figure 7.9. True classification rates of footsteps with different gain and range values

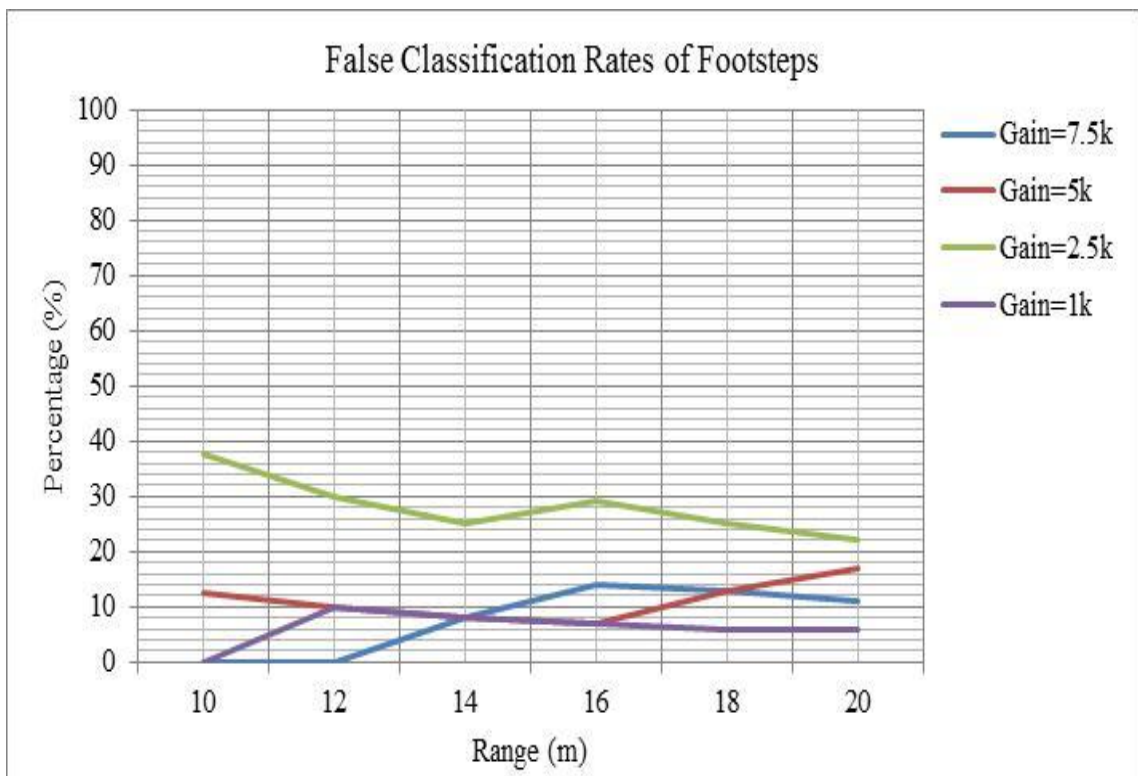


Figure 7.10. False classification rates of footsteps with different gain and range values

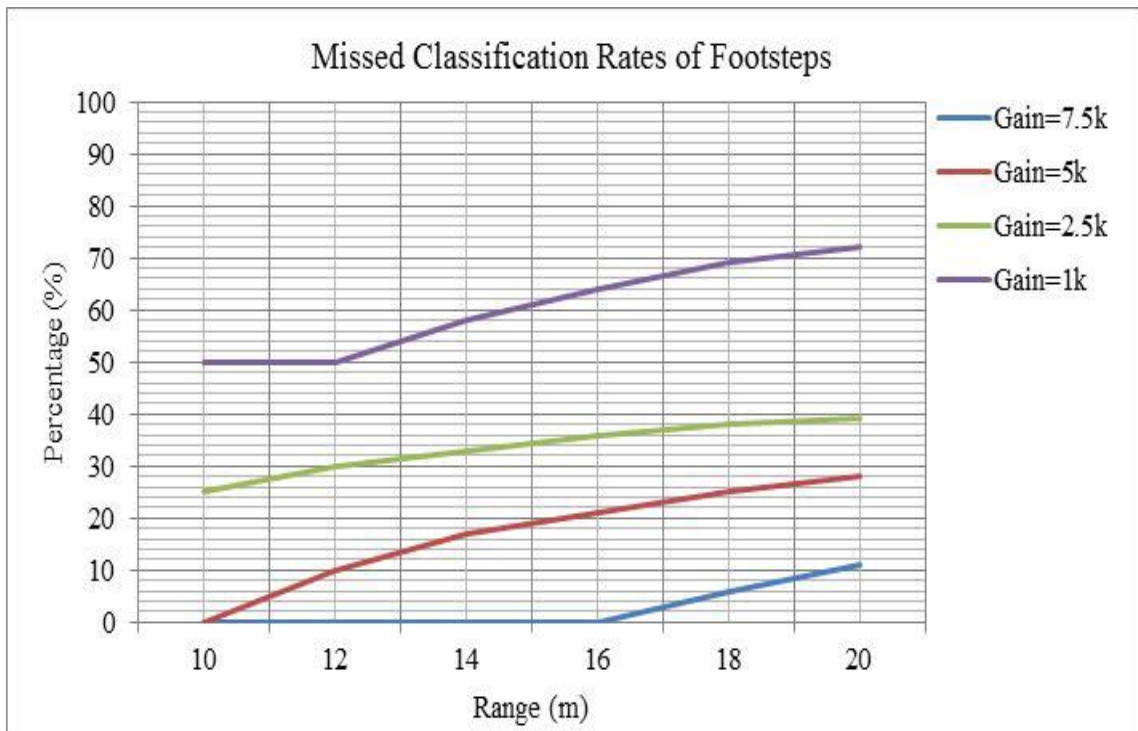


Figure 7.11. Missed classification rates of footsteps with different gain and range values

As seen in the above graphs, classification performance can vary a lot depending on several parameters such as gain, distance. However, with the appropriate gain value and at 15 meter range, system is capable of detecting and classifying footsteps with 90% accuracy can be easily said.

False alarm rates are lower than 40% in each condition. Also true alarm rates are bigger with higher gain values. Missed classification rates are lower with lower amplification gain values.



### 7.3. VEHICLE ANALYSES

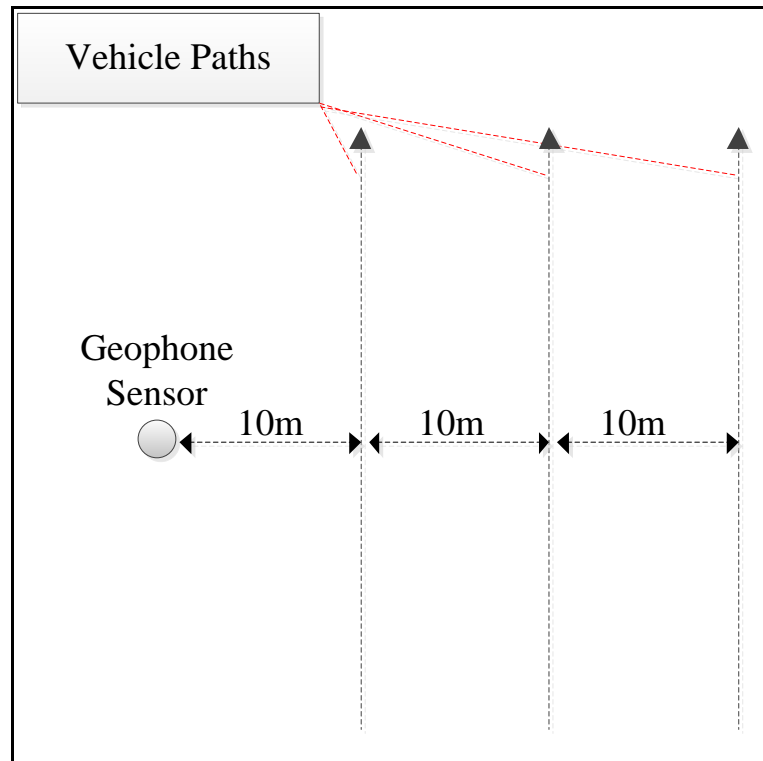


Figure 7.12. Vehicle test paths

As shown in the graph above, vehicle tests are executed on a line with distances from geophone sensor; 10 meters, 20 meters and 30 meters. All lines are passed with two different vehicle speed such as; 20km/h and 40 km/h.

Table 7.11. Vehicle test pool

Distance (m)	Gain=1k		Gain=5k	
	Speed=20km/h	Speed=40km/h	Speed=20km/h	Speed=40km/h
10	G1000S20D10	G1000S40D10	G5000S20D10	G5000S40D10
20	G1000S20D20	G1000S40D20	G5000S20D20	G5000S40D20
30	G1000S20D30	G1000S40D30	G5000S20D30	G5000S40D30

As can be seen in the table 7.11., there are three features that separates the vehicle tests such as vehicle speeds, amplification gains and distances between vehicle movement line and sensor.

First, to evaluate the classification results, a classification performance criterion must be determined. Table 7.12. has the details of the criteria.

Table 7.12. Classification performance criteria of vehicle tests

<b>Classification Result</b>	<b>Conditions</b>
TRUE	Only Vehicle alarm occurs.
FALSE	If rain or footstep alarm occurs.
MISSED	No alarm occurs

Table 7.13. Vehicle classification results with different test parameters

<b>Test ID</b>	<b>Vibration Type Detection</b>			<b>Classification</b>
	<b>Footstep</b>	<b>Rain</b>	<b>Vehicle</b>	
G1000S20D10	3	1	1	TRUE
G1000S20D20	0	0	0	MISSED
G1000S20D30	0	0	0	MISSED
G1000S40D10	1	2	1	TRUE
G1000S40D20	3	0	0	MISSED
G1000S40D30	1	0	0	MISSED
G5000S20D10	8	0	1	TRUE
G5000S20D20	9	0	0	FALSE
G5000S20D30	0	0	0	MISSED
G5000S40D10	3	2	1	TRUE
G5000S40D20	4	2	1	TRUE
G5000S40D30	1	1	0	MISSED

As can be seen in the table above, there are false vibration type detections are evaluated. However, these false vibration type detections are filtered in classification processes. Only 1 false classification has executed in 12 tests.

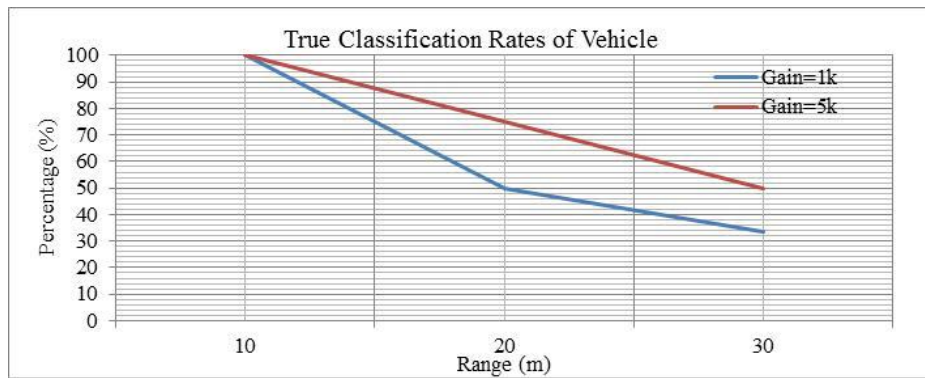


Figure 7.13. True classification rates of vehicle with different gain and range values

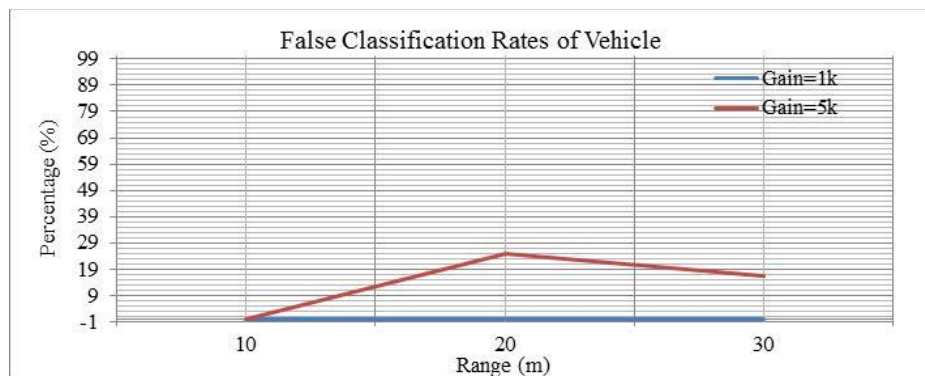


Figure 7.14. False classification rates of vehicle with different gain and range values

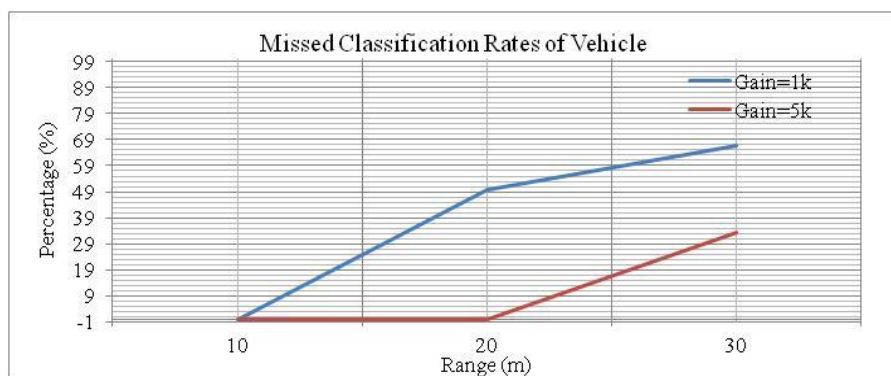


Figure 7.15. Missed classification rates of vehicle with different gain and range values

The above tests, the 20 km / h and 40 km / h data are combined so the results are representing the average model of that two speeds. Classification rate is 100% in 10 meters

range and with higher amplification gain values; higher vehicle classification rates could be evaluated.

#### 7.4. VEHICLE AND FOOTSTEP COMBINED ANALYSES

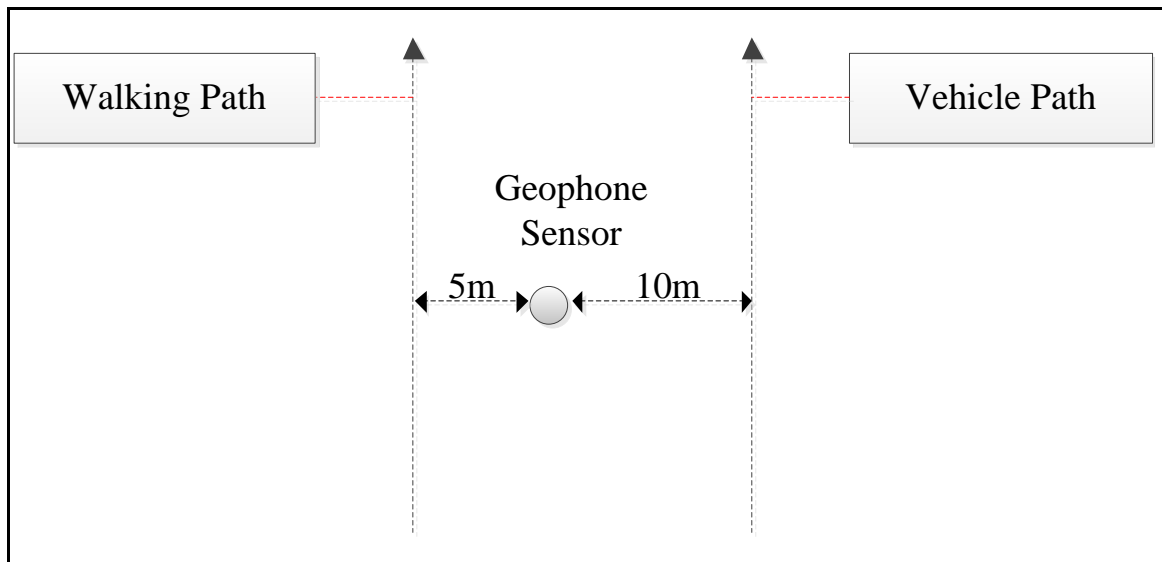


Figure 7.16. Vehicle and footstep together test paths

As shown in the graph above, vehicle with footstep tests are executed on two different line at the same moment. Walking path distance with geophone sensor is 5 meter and vehicle path distance is 10 meter. In vehicle path, vehicle is passed with two different vehicle speed such as; 20km/h and 40 km/h. And all tests were repeated twice.

Table 7.14. Vehicle and footstep together test pool

Test Repeat	Gain=1k		Gain=5k	
	Speed=20km/h	Speed=40km/h	Speed=20km/h	Speed=40km/h
First Test	G1000S20T1	G1000S40T1	G5000S20T1	G5000S40T1
Second Test	G1000S20T2	G1000S40T2	G5000S20T2	G5000S40T2

As can be seen in the table 7.14., there are three features that separates the vehicle and footstep together tests such as vehicle speeds, amplification gains and repeating number.

First, to evaluate the classification results, a classification performance criterion must be determined. Table 7.15. has the details of the criteria.

Table 7.15. Classification performance criteria of vehicle tests

Classification Result	Conditions
TRUE	Vehicle and footstep alarm occurs together
FALSE	If rain alarm occurs
MISSED	If one or two alarm type of vehicle and footstep alarm is missed.

Table 7.16. Vehicle and footstep together classification results

Test ID	Vibration Type Detection			Classification
	Footstep	Rain	Vehicle	
G1000S20T1	10	1	1	TRUE
G1000S20T2	8	0	1	TRUE
G1000S40T1	7	0	1	TRUE
G1000S40T2	14	1	1	TRUE
G5000S20T1	9	1	1	TRUE
G5000S20T2	7	1	1	FALSE
G5000S40T1	19	0	1	TRUE
G5000S40T2	11	2	1	TRUE

As can be seen in the table above, there are false vibration type detections are evaluated. However, these false vibration type detections are filtered in classification processes. Only one false classification has executed in eight tests.

Under these test conditions, classification rate of vehicle and footsteps together is %87.5 in specified ranges.

There is no need to draw any graphic about that calculation because not any missed alarm situation has occurred. Results are successful.

## 7.5. QAT AND SAT ANALYSES

In this section, detection performance of the change in the QAT and SAT memory size were investigated.

Data are used in the analyses at this chapter is taken from the Person A,B-7.5k-Gain-Footstep-Tests. The reason of preferring these data; best performance was obtained with this data in previous sections.

As seen in the following charts, best true footstep detection rates are achieved while the QAT memory size is 30 samples and SAT memory size is 20000 samples.

Lower or higher than 30 sample QAT memory sizes prevents detection of footsteps due to the oscillations in the footstep vibrations.

As mentioned earlier in this thesis, the larger SAT memory sizes provide stability at the intruder movement moments. However, due to the limitations of WSN, SAT memory size cannot be enlarged as desired.

As mentioned earlier in this thesis, the SAT, the larger the memory size, markings moments that occurred remains stable.



Figure 7.17. True footstep detection rate with different QAT memory sizes (Person B)

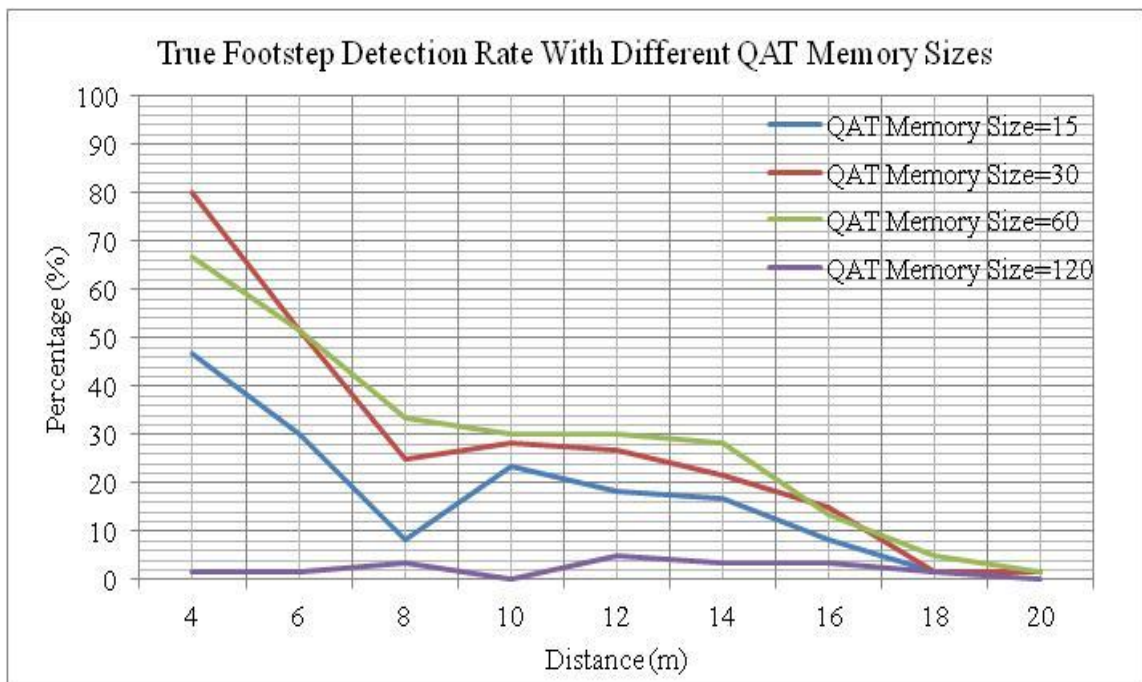


Figure 7.18. True footstep detection rate with different QAT memory sizes (Person A)

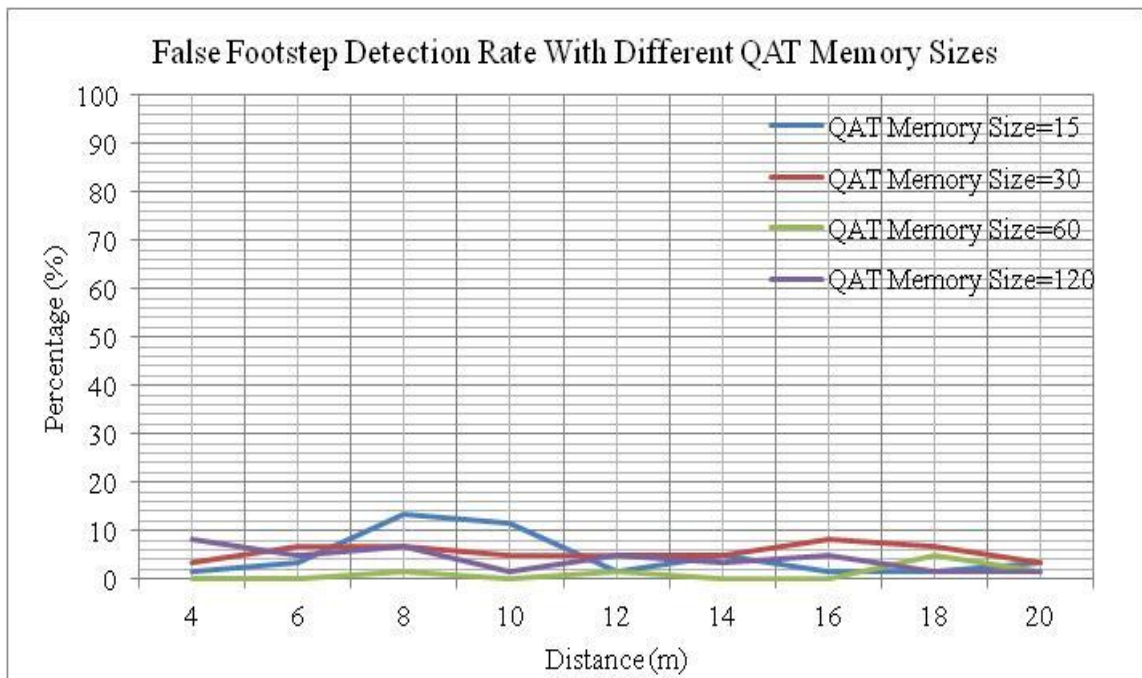


Figure 7.19. False footstep detection rate with different QAT memory sizes (Person B)

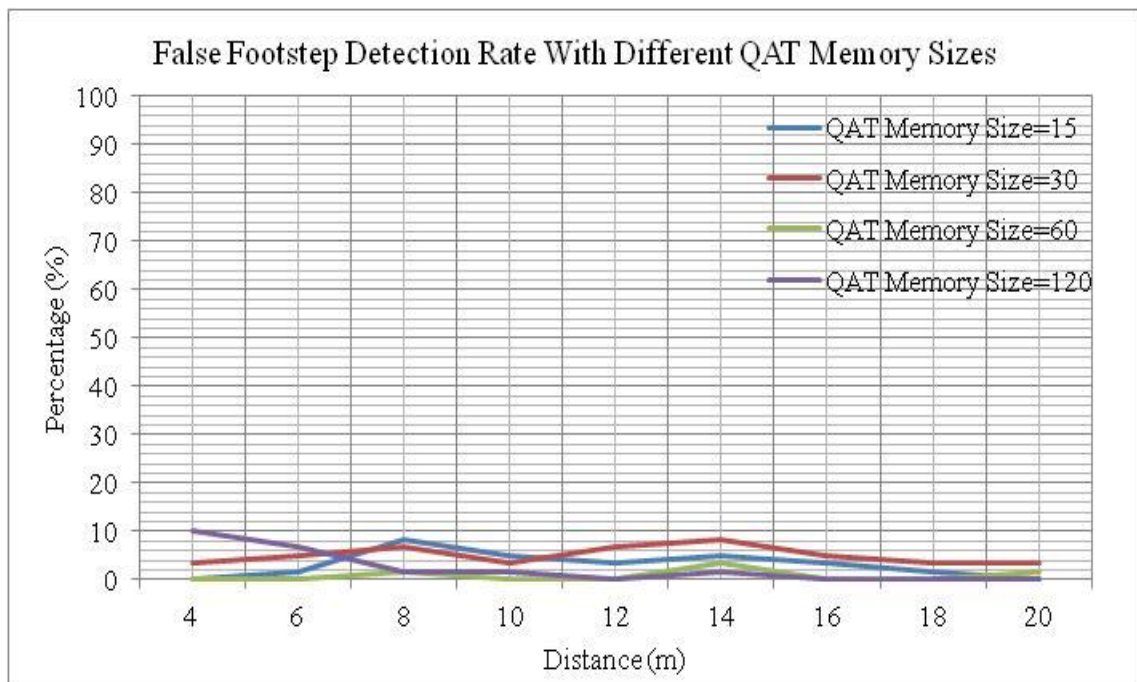


Figure 7.20. False footstep detection rate with different QAT memory sizes (Person A)

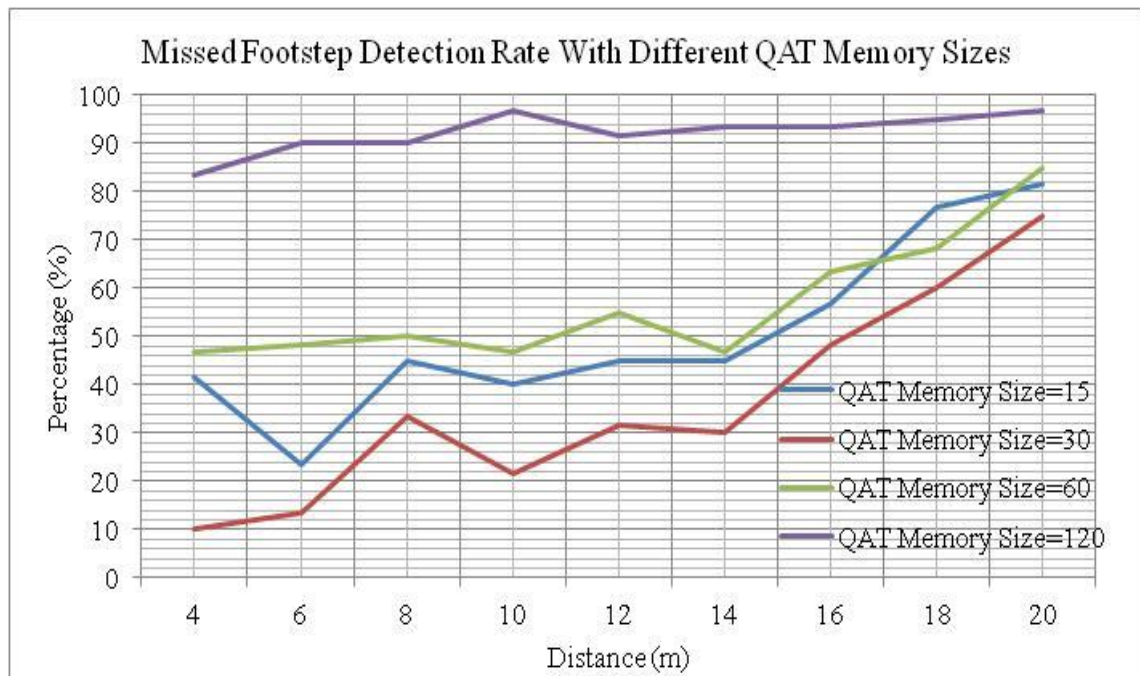


Figure 7.21. Missed footstep detection rate with different QAT memory sizes (Person B)



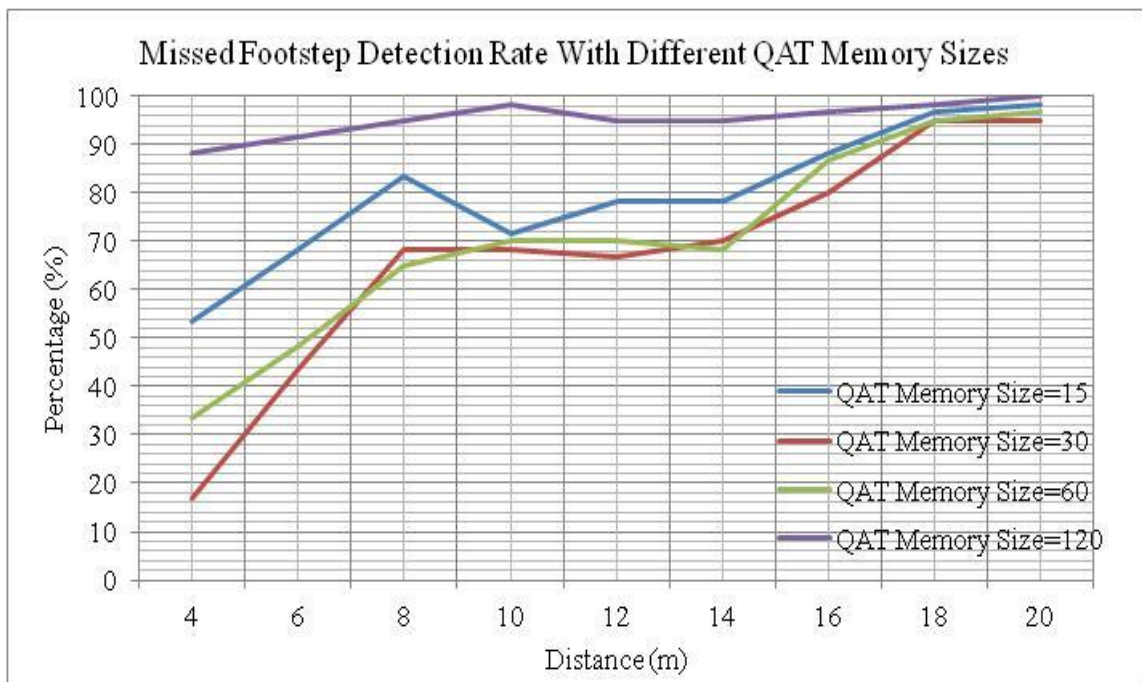


Figure 7.22. Missed footstep detection rate with different QAT memory sizes (Person A)

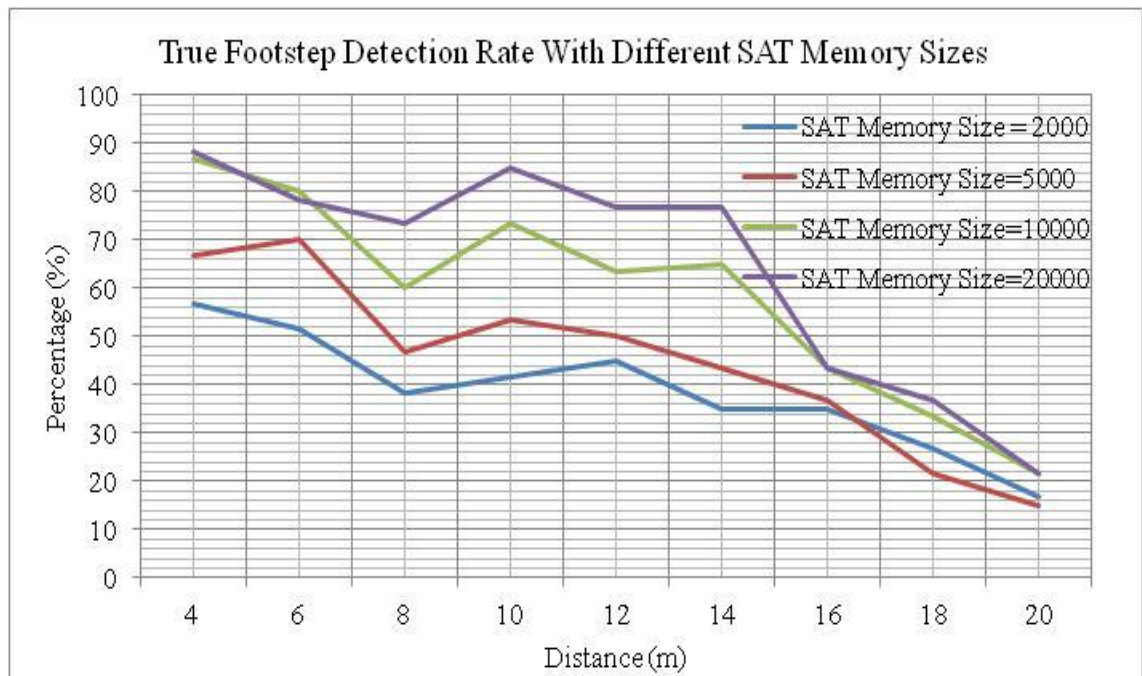


Figure 7.23. True footstep detection rate with different SAT memory sizes (Person B)

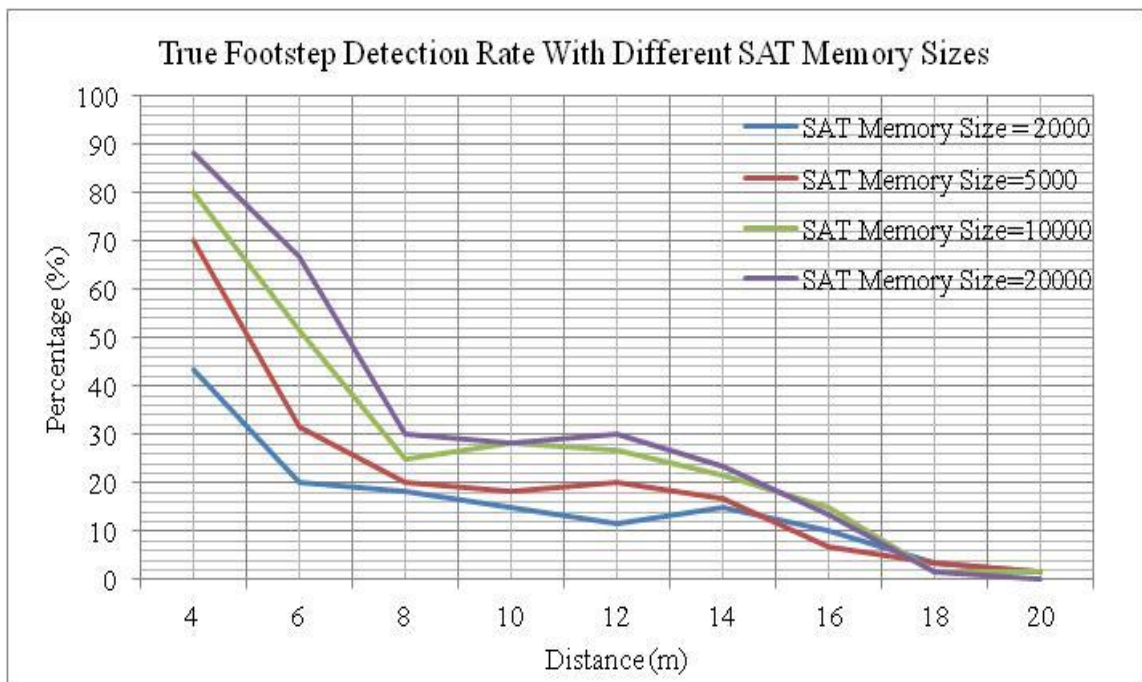


Figure 7.24. True footstep detection rate with different SAT memory sizes (Person A)

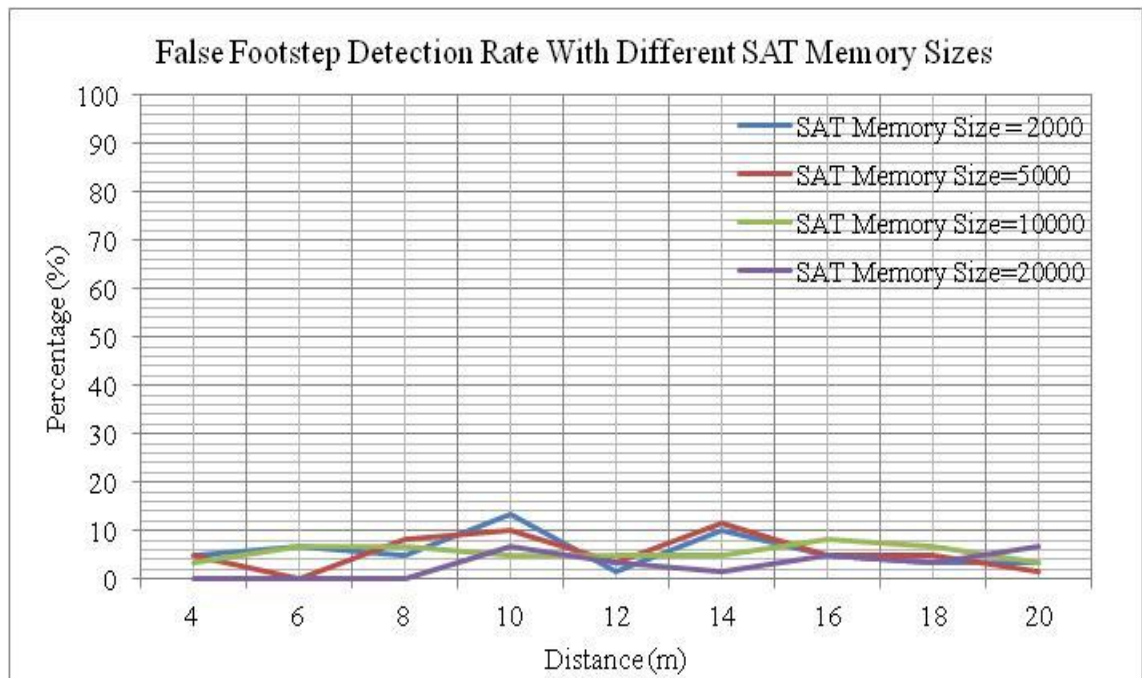


Figure 7.25. False footstep detection rate with different SAT memory sizes (Person B)

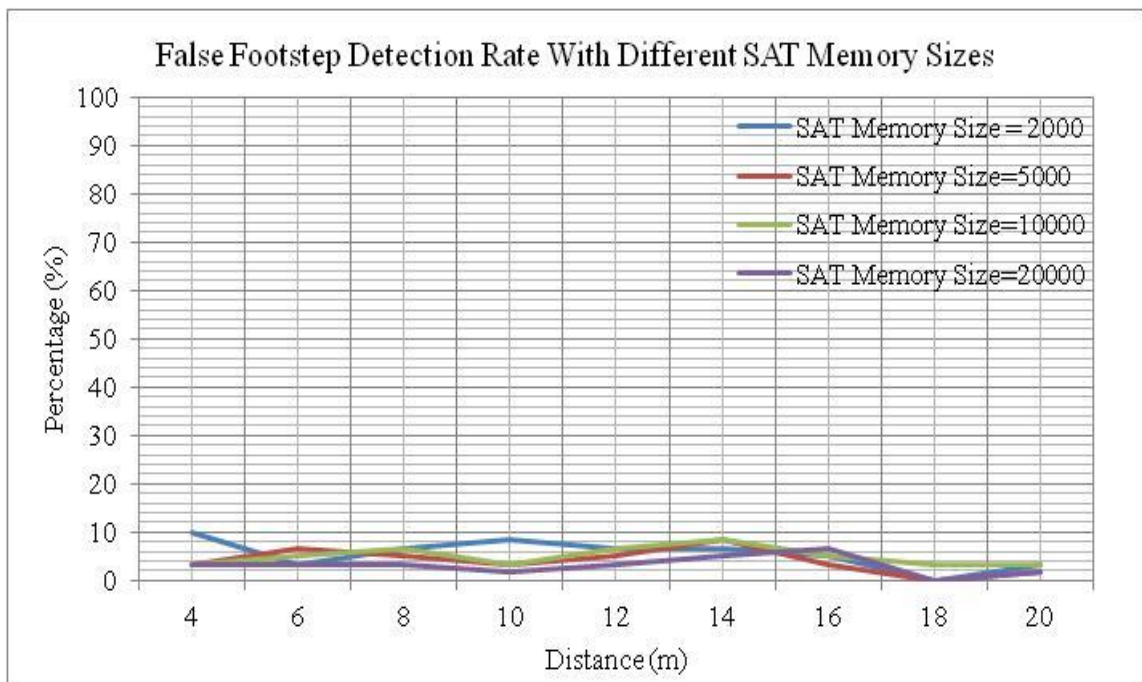


Figure 7.26. False footstep detection rate with different SAT memory sizes (Person A)

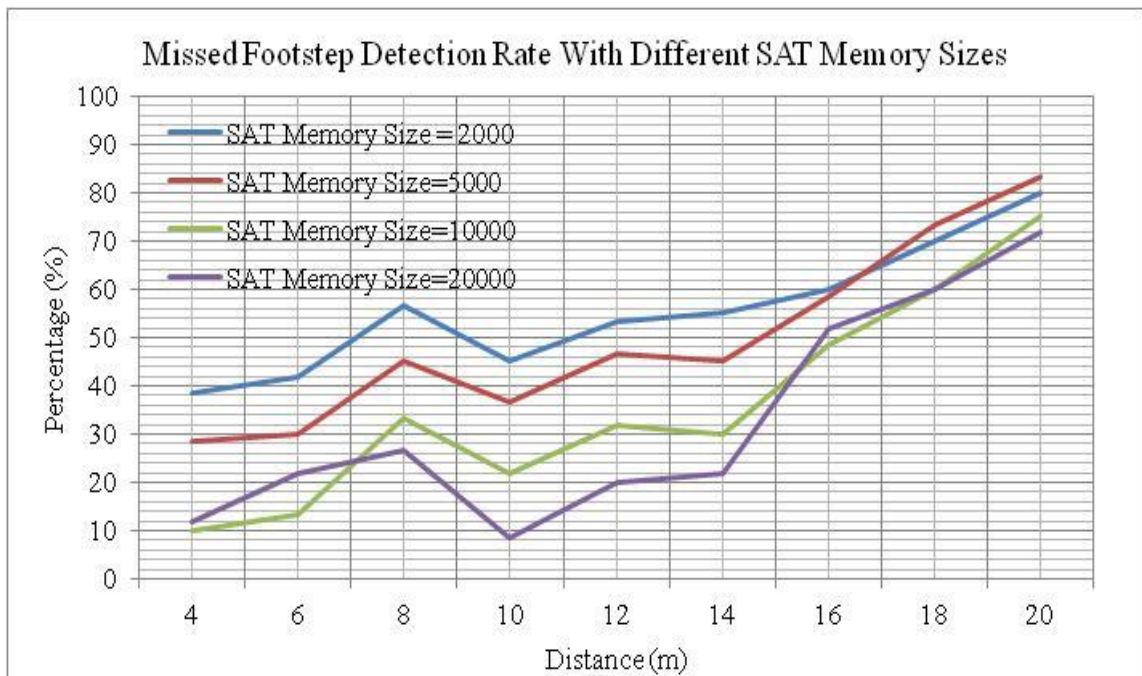


Figure 7.27. Missed footstep detection rate with different SAT memory sizes (Person B)

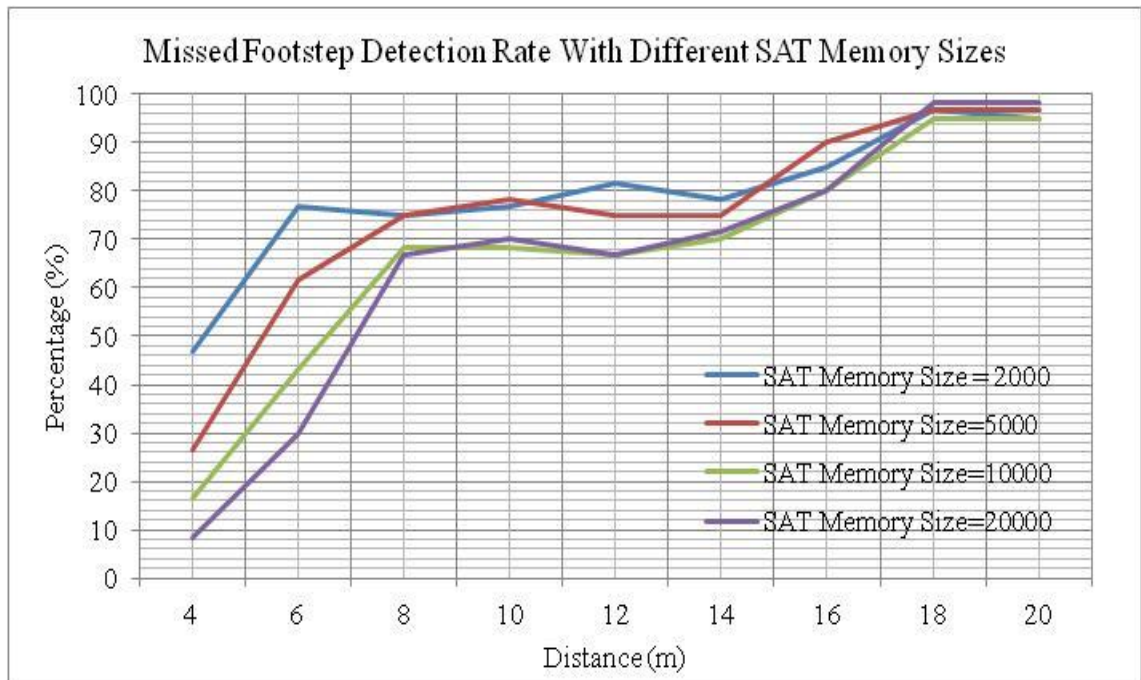


Figure 7.28. Missed footstep detection rate with different SAT memory sizes (Person A)



Figure 7.29. Test area photos-1



Figure 7.30. Test area photos-2

## 7.6. COMPARISON WITH SIMILAR PRODUCTS

Similar versions of the product designed in this thesis are available at the market, which are called unattended ground sensor systems. However, specifications and prices of these products are mostly not shared on the internet because they are generally used in military applications.

The name of some similar products and the producers are; Falcon Watch RF 5400VH Remote Surveillance System- Harris Corporation, Scorpion Unattended Target Recognition Systems-Northrop Grumman Corporation, Unattended Ground Sensors-Trident System Inc., Tactical Unattended Ground Sensors-Textron Defense Systems.

In the product datasheets, it is mentioned that detection range values are depending on the type of the soil [41-42]. In addition, the false alarm rates are not mentioned in the products user manual.

Table 7.17. Technical specifications of similar products [41-42]

<b>Properties</b>	<b>Thesis Sensor Node</b>	<b>Harris RF-5400VH-SS Mini-Sensor Node</b>	<b>Trident System Inc. Recce Node</b>
Frequency Band	2400-2484 MHz (16 Channel)	138-174 MHz (Full Mhz Band)	900 MHz
Transmit Output	39.8mW	1.5W	Unknown
Operational Life	3 month	6 month	1 month
Power Sources	3xD-Size Duracell MN1300	2xLithium 9-Volt Batteries	2xD-Size
Power Capacity	72WH	Unknown	Unknown
False Alarm Rate for Human Detection	%10 Probability in 15m range with 7.5k gain	Unknown	Unknown
False Alarm Rate for Vehicle Detection	%25 Probability in 20m range with 5k gain	Unknown	Unknown
Human Classification Range	%90 Probability in 15m range with 7.5k gain	15m	30m
Vehicle Classification Range	%75 Probability in 20 m range with 5k gain	50m	100m
Size	14.8L x 10.8W x 7.5H cm	9.2L x 7.9W x 5.1H cm	10.2D x 19.05H cm
Weight	0.32 kg	0.36 kg	1.6 kg

## **8. CONCLUSIONS**

Two distinct intruder detection methods have been proposed and implemented in this thesis. One of them is based on communication using power line that feed the sensor network which is stated as stand-alone architecture (SAA) and the other is based on WSN and termed as WCA. Signal processing algorithm is based on time signal samples and is simple as opposed to server based complicated algorithms that rely on frequency spectrum of the received sensor signals.

Hardware design of the sensor board is discussed in detail and many aspects of this design have been elaborated. All electrical parameters of each circuit blocks such as filters, buffers and amplifiers were analyzed in both directions at the transmission line. Also power and alarm generator stages are designed especially for both WCA and SAA requirements.

Geophone sensor and soil characteristics are examined in detail to determine the hardware and signal processing algorithm requirements.

Performance evaluation of the hardware and signal processing algorithm were performed on realistic scenarios and high detection and classification rates were achieved. Also the pd and pfa graphics of signal processing algorithm are executed with several different type of intruder data and the achievements in all corners are measured. In addition, the signal processing algorithm performance is compared with kurtosis equation. The change in time threshold sizes affects on performance were also calculated.

### **8.1. FUTURE WORK**

The algorithm may be improved to detect intruder in harsh environments. Another area that would be interesting to explore is to explore communication possibilities over other RF devices. In addition, the use of solar panels for WCA seem to be suitable due to low power consumption. Also one of the major issues is the modularity between the nodes which is achieved in SAA but not in WCA.

12-Bit internal ADC used in this study was troublesome because low resolution in ADC require high amplification rate which is increasing the ambient noise value. With an external ADC, higher resolution can be achieved. However, new ADC's power consumption rates should be discussed during the ADC selection period. Noise reduction in analog circuits is one of the most important issues in these types of systems. In addition to filtering methods, studies on amplifiers which are less affected by system noise could improve the performance of intruder detection.

Another important research topic may be usage of different type of sensors in a single node.

The implantation of sensors to the ground can cause some differences on signal reading. This situation must be analyzed and the optimum implantation type needs to be determined.

The designed signal processing algorithm does not include complex functions to be suitable for WSN applications. In addition, the irregularities of ground based noises are minimized with using adaptive threshold methods. However, static and dynamic offsets could be optimized with a different research work. Also, another optimization could be done on classification parameters. To achieve these improvements, large-scale data pools are required. In addition to rain, other natural noise sources, such as wind behavior on ground can be examined. To execute this study, geophone responses on wind-based acoustic signals should be further studied.



## REFERENCES

1. Schmidl, T. M. and D. C. Cox, "Robust frequency and timing synchronization for OFDM", *Proceedings of the IEEE*, Vol. 45, pp. 1613-1621, 2007.
2. Huang, P., M. H. Johnson and T. Damarla, Exemplar Selection Methods to Distinguish Human from Animal Footsteps, *ARO Muri No:2009-31*, 2009.
3. Van de Beek, J. J., M. Sandell and P. O. Borjesson, "ML Estimation of Time And Frequency Offset in Ofdm Systems", *IEEE Transactions on Signal Processing*, Vol. 45, 1997.
4. Tufvesson, F., O. Edfors and M. Faulkner, "Time and Frequency Synchronization For OFDM Using PN-Sequencepreambles", *Proc. IEEE Vehicular Technology Conference*, Vol. 4, pp. 2203-2207, 1999.
5. Paajanen, M., J. Lekkala and K. Kirjavainen, "Electronical Film – a New Multipurpose Electret Material", *Sensors and Actuators*, 2000.
6. Rodriguez, R. V., J. S. D. Mason, J. Fierrez and J. O. Garcia, Analysis of Time Domain Information for Footstep Recognition, *International Symposium on Visual Computing 2010*, pp. 489-498, Berlin, 2010.
7. F. Succi, G. Frado, R. Gampert, T. Pedersen, H. Dhaliwal. "Problems in Seismic Detection and Tracking", *Proc. SPIE*, vol. 4040, p. 165, 2000.
8. Chen, J. *Multimodal Wireless Networks: Communication and Surveillance on the Same Infrastructure*, M.S. Report, IT University of Copenhagen, 2007.
9. G. Succi, D. Clapp, R. Gampert, G. Prado, "Footstep Detection and Tracking", *Proc. SPIE*, vol. 4393, 2001, p. 22.

10. H. Amick. "A Frequency-Dependent Soil Propagation Model". *SPIE Conference on Current Developments in Vibration Control for Optomechanical Systems*, July 1999.
11. Peck, L., Gagnon, J. and Lacombe, J, "Seismic Detection of Personnel: Field Trials with REMBASS-II and Qual-Tron Sensors", *ERDC/CRREL TR-06-4*, 2006.
12. Xing, H., L. Fang and J. L. Liu, "Wavelet Denoising and Feature Extraction of Seismic Signal For Footstep Detection", *International Conference on Wavelet Analysis and Pattern Recognition*, pp. 218-223, Beijing, 2007.
13. Richman, M. S., D. S. Deadrick, R. J. Nation and S. L. Whitney, "Personnel Tracking Using Seismic Sensors", *The International Society For Optics and Photonics*, Vol. 4393, pp. 14-21, 2001.
14. Lacombe, J., L. Peck, T. Anderson and D. Fisk, "Seismic Detection Algorithm and Sensor Deployment Recommendations for Perimeter Security", *The International Society For Optics and Photonics*, Vol. 6231, pp. 1-10, 2006.
15. Pakhomov, A. and T. Goldburt, "Seismic Systems for Unconventional Target Detection and Identification", *The International Society For Optics and Photonics*, Vol. 6201, pp. 1-12, 2006.
16. Pakhomov, A., A. Sicignano, M. Sandy and T. Goldburt, "Single and Three Axis Geophone: Footstep Detection with Bearing Estimation, Localization and Tracking", *The International Society For Optics and Photonics*, Vol. 5090, pp. 155-161, 2003.
17. Audette, W. E., D. B. Kynor, J. C. Wilbur, J. R. Gagne and L. Peck, "Improved Intruder Detection Using Seismic Sensors and Adaptive Noise Cancellation", *Human, Light Vehicle, and Tunnel Detection Workshop*, pp. 1-14, Hanover, 16-17 June 2009.
18. Peck, L., J. Lacombe and T. Anderson, *Seismic Detection of Personnel: Field Trials and Signatures Database*, *Army Engineer Research and Development Center*, Hanover, 2007.

19. Blum, R. S. And S. A. Kassam, "Optimal Distributed Detection of Weak Signals in Dependent Sensors", *IEEE Transactions on Information Theory*, Vol. 38, pp. 1066-1079, 1992.
20. Kay, S. M., *Fundamentals of Statistical Signal Processing: Detection Theory*, Prentice-Hall, NJ USA, 1998.
21. Succi, G., G. Prado, R. Gampert, T. Pedersen and H. Dhaliwal, "Problems in Seismic Detection and Tracking", *Unattended Ground Sensor Technologies and Applications II*, pp. 165-173, SenTech, Stoneham, 1999.
22. Sundaresan, A., A. Subramanian, P. K. Varshney and T. Damarla, A Copula Based Semi-parametric Approach for Footstep Detection Using Seismic Sensor Networks, *Army Research Laboratory No: W911NF-07-2-0007*, Adelphi, 2009.
23. Eskikale, T. And T. Kara, "Uzaktan İnsan Algılama ve Verilerin İşlenmesi", *6th International Advanced Technologies Symposium*, pp. 391-394 Elazığ, 16-18 May 2011.
24. Chen, J. *Multimodal Wireless Networks: Communication and Surveillance on the Same Infrastructure*, M.S. Report, IT University of Copenhagen, 2007.
25. Jin, X., S. Gupta, A. Ray and T. Damarla, "Multimodal Sensor Fusion for Personnel Detection", *14th International Conference on Information Fusion*, pp. 437-444, Chicago, Illinois, 2011.
26. Reddy, V. V., V. Divya, A. W. H. Khong and B. P. Ng, "Footstep Detection and Denoising using a Single Triaxial Geophone", *Institute of Electrical and Electronics Engineers*, pp. 1171-1174, 2010.
27. Succi, G., D. Clapp, R. Gampert and G. Prado, "Footstep Detection and Tracking", *The International Society For Optics and Photonics*, Vol. 4393, pp. 22-29, 2001.

28. Qu, L., H. Chen, Y. Tu, Nonparametric Copula Density Estimation in Sensor Networks, *Mathematics Faculty Publications and Presentations*, Boise, 2011.
29. Varshney, P. K., Personnel Detection via Fusion of Heterogeneous Sensor Data, *OMB NO. 0704-0188*, Syracuse, 2009.
30. Houston, K. M. and D. P. McGaffian, "Spectrum Analysis Techniques for Personnel Detection Using Seismic Sensors", *The International Society For Optics and Photonics*, Vol. 5090, pp. 162-173, 2003.
31. Libby, R., A simple method for reliable footstep detection on embedded sensor platforms, 2009.
32. Goodman, G. L., Detection and Classification for Unattended Ground Sensors, *Land Operations Division*, Salisbury, 1999.
33. Goodman, G. L., "Detection and Classification For Unattended Ground Sensors", *In Proceedings of Information Decision and Control 99*, pp. 419-424, 1999.
34. Wong, D. L., Y. H. Hu and A. Sayeed, "Detection, Classification, and Tracking of Targets", *IEEE Signal Processing Magazine*, Vol. 19, pp. 17-29, 2002.
35. Pakhomov, A. and T. Goldburt, "Seismic Signals and Noise Assessment for Footstep Detection Range", *The International Society For Optics and Photonics*, Vol. 5417, pp. 87-98, 2004.
36. Input/Output. Inc., "SM-24 ST Upright Geophone", Vol.1, No:1, 2006, <http://www.geophone.com/techpapers/SM-24%20ST%20Brochure.pdf>
37. Texas Instruments, "MSP430F15x, MSP430F16x, MSP430F161x, MIXED SIGNAL MICROCONTROLLER", Vol.1, No:1, 2002, <http://www.ti.com/lit/ds/symlink/msp430f1611.pdf> [retrieved 11 march 2011]

38. ST electronics, "8 Mbit, Low Voltage, Serial Flash Memory With 25 MHz SPI Bus Interface", Vol:1, No:1, 2002,  
<http://www.datasheetcatalog.org/datasheet/stmicroelectronics/8495.pdf> [retrieved 13 December 2002]
39. Chipcon Inc., "2.4 GHz IEEE 802.15.4 / ZigBee-ready RF Transceiver", Vol:1, No:1, 2003, <http://pdf1.alldatasheet.com/datasheet-pdf/view/125399/ETC1/CC2420.html> [retrieved 09 July 2004]
40. Texas Instruments, "2.4-GHz RF Front End", Vol:1, No:1, 2008,  
<http://www.ti.com/lit/ds/symlink/cc2591.pdf>, [retrieved 16 March 2008]
41. Trident, "Unattended Ground Sensor Nodes", Vol:1, No:1, 2008,  
<http://www.tridsys.com> [retrieved 09 July 2009]
42. Harris, "Falcon Watch RF-5400VH Remote Surveillance System", Vol:1, No:1, 2008,  
<http://www.harris.com> [retrieved 18 May 2009]